Sajid Ahammed

Hydrogen-Argon Power Cycle (HAPC) on a Wartsila medium-speed engine: an Investigation using 1D-Simulation

Wärtsilä Finland Oy

School of Technology and Innovations

Master's thesis in Energy Technology

Master of Science in Technology, Industrial Systems Analytics (ISA)

Vaasa, 2025

Acknowledgments

The research for this master's thesis was concluded in collaboration with Wärtsilä Finland Oy and the EPS team at the University of Vaasa as part of my Master of Science in Technology Studies in Industrial System Analytics (ISA) at the Faculty of Technology and Innovation, University of Vaasa. I am truly grateful to Allah for giving me the strength and determination to complete this thesis.

I want to express my profound gratitude to my supervisor, Professor Dr. Maciej Mikulski, for his invaluable direction, encouragement, and expert guidance throughout this journey. His insights and assistance have been invaluable in concluding this thesis. I would also like to thank Dr. Jari Hyvönen of Wärtsilä Finland Oy for his advice, encouragement, and confidence in my abilities. I also want to convey my gratitude to the second evaluator, Dr. Emmanuel Ndzibah, for his intelligent remarks.

I would like to thank my instructors, Dr. Zeeshan Ahmad from Wärtsilä Finland Oy and Mr. Aneesh Vasudev (M.Sc.) from the University of Vaasa, for their proper guidance throughout this research. Their advice was pivotal in shaping this work, which I hope will contribute to the iHAPC project and future studies in this field.

My profound gratitude goes to my parents, Saad Ahammed and Parul Ahammed, and my brother, Shahriar Ahammed, for their unconditional love and encouragement, which have been a continual source of inspiration. I am also deeply grateful to my friends, especially Md. Yeasin Arafat and Fatama Sultana, for their support during challenging times. My appreciation extends to the EPS Team at the University of Vaasa for their flexibility and encouragement, and to Amir Solemani for his guidance throughout this journey.

Finally, I am grateful to my colleagues at Wärtsilä Finland Oy, particularly those in the Advanced Concepts and Research & Technology team, for their cooperation. This thesis forms part of Work Package 1 (WP1) of the **iHAPC-Integrated Hydrogen-Argon Power Cycle** project, co-funded by Business Finland. I hope this research lays the groundwork for future opportunities and endeavours.

In closing, I reflect on my favourite verse from the Quran: *"So, which of the favours of your Lord would you deny?" (Quran, 55:13).*

Sincerely,
Sajid Ahammed

UNIVERSITY OF VAASA

School of Technology and Innovations

Author:	Sajid Ahammed
Title of the Thesis:	Hydrogen-Argon Power Cycle (HAPC) on a Wartsila medium-speed engine: an Investigation using 1D-Simulation
Degree:	Master of Science in Technology
Programme:	Industrial Systems Analytics (ISA)
Supervisors:	Prof. Dr. Maciej Mikulski, Dr. Jari Hyvönen
Instructors:	Dr. Zeeshan Ahmad, Aneesh Vasudev (M.Sc.)
Involved partners:	Wärtsilä, and EPS University of Vaasa
Year: 2024	**Pages:** 160

ABSTRACT:

The hydrogen argon power cycle (HAPC) is the next big thing for the energy sector. It offers a groundbreaking approach to achieving zero-emission and high-efficiency power generation by leveraging hydrogen's clean burning properties and argons' superior thermodynamic characteristics. This study investigates the integration of HAPC into a medium-speed Wärtsilä (W6L20-2STC) engine, utilizing one-dimensional modelling in GT Suite software to analyse and investigate the engine performance across a range of operating conditions.

The thesis investigates critical parameters influencing combustion dynamics, efficiency, and emissions in the closed-loop W6L20-2STC engine model. These parameters include variation in Argon to Oxygen ratios (mixture composition), the use of alternative inert gases (e.g., argon, helium) as diluents, compression ratios (CRs), exhaust back pressure, oxygen to fuel ratios, and hydrogen fuel impurities. The study combines a comprehensive literature review on the Argon power cycle (APC) with a detailed W20 engine model simulation. A six-cylinder closed-loop simulation model was developed in GT-Suite for HAPC operations based on a fully functional and rigorously validated W6L20-2STC engine model obtained from Wärtsilä. The turbocharger was removed, and a new condenser was introduced to separate H_2O from the HAPC Cycle, for a controlled environment evaluation. The simulations were conducted across various parameter sweeps to systematically examine their impact on HAPC engine and system performance. This thesis provides critical insight into optimizing HAPC-based engine systems to improve its performance and environmental impacts. The integration of a valued simulation model with literature findings offers a robust framework for advancing sustainable engine technology.

Results reveal that replacing air with an argon and oxygen mixture in a closed-loop configuration enhances thermal efficiency compared to state-of-the-art marine engines. The simulations depict an optimized efficiency reaching 58.04% while eliminating NO_x emissions completely due to the absence of atmospheric nitrogen. The integration of essential components such as water

condensers and an ejector, oxidizers, and fuel injectors ensure a closed-loop operation that conserves argon and maintains high system efficiency. These system-level simulation outcomes were critically analysed with the design constraints of the closed-loop HAPC system for the W20 engine while considering real-world implementation scenarios. An optimal argon-to-oxygen mixture composition for the closed-loop HAPC was identified as 90% to 88% argon with 10% to 12% oxygen, achieving an effective balance between power output, efficiency, and engine durability. A compression ratio of 11.90 was found to maximize the engine efficiency while stoichiometric mixtures (λ=1) with an exhaust back pressure after the condenser of 3.23 bar enhanced combustion performance with rather than borderline thermal load levels. Furthermore, impurities in hydrogen, such as dilution with 2% nitrogen, have been shown to significantly reduce in-cylinder pressure and combustion efficiency over time in consecutive simulation cycles, indicating a miserable decline in HAPC efficiency gains over conventional air cycles.

This study highlights HAPC as a sustainable energy solution, offering superior efficiency and environmental benefits over conventional air cycles. HAPC has the potential to bridge the gap between renewable energy storage and flexible power generation while supporting global decarbonization and clean energy goals. The findings from this thesis work contribute towards the development of system-level understanding of the HAPC power systems.

KEYWORDS: ZEM, Integrated Hydrogen–Argon Power Cycle (iHAPC), Closed-loop system, Wärtsilä W20 engine, GT-Suite 1D-simulation, Clean energy, Zero exhaust

Contents

1 Introduction 15

1.1 Background 17

1.1.1 Integrated Hydrogen-Argon Power Cycle (iHAPC): An Innovative Energy System of the Future 17

1.2 Problem Formulation and Scope of Thesis 22

1.2.1 Problem Formulation 22

1.2.2 Research Question 23

1.2.3 Scope of thesis 23

1.3 Structure of the Thesis 24

2 Review of Related Literature: Analysis of State of the Art in HAPC 26

2.1 Fundamentals of APC 26

2.2 Characteristics of Relevant Fuels and Working Fluids Suitable for APC 29

2.2.1 Fuel Compatibility in APC 29

2.2.2 Characteristics Relevant Working Fluids for APC 32

2.3 State of the Art in Research on APC with fossil fuels 35

2.4 Towards APC with Hydrogen as Fuel 38

2.4.1 State of the Art in Research on APC with Hydrogen 38

2.4.2 Closed Cycle HAPC Technology 40

2.4.3 Autoignition Properties of H_2-O_2 Mixtures in Argon Atmosphere 41

2.4.4 Effects of Compression Ratio (CR) and mixture composition on HAPC 43

2.4.5 Port Fuel Injection vs. Direct Injection of Hydrogen and Oxygen 46

2.4.6 Advancements and Challenges in iHAPC 48

2.5 Developments of 1D-Engine Modelling and Simulation 50

2.5.1 General Assumptions of 1D-modeling and Governing Components Sub-models 51

2.5.2 Engine Cylinder Modelling 58

2.5.3 Heat Transfer Modelling 69

2.5.4 Argon Power Cycle in 1D-Simulation 70

3 Object and Methods 76

3.1 Reference Engine and Experimental Data for Model Validation 77
3.1.1 Technical Specifications of the W6L20-2STC Engine 77
3.1.2 Modelling Assumptions for W6L20-2STC in GT-Power 78
3.2 W20-SCRE Model Validation Methodology 81
3.3 Simulation Models 82
3.3.1 W6L20-2STC Engine: Detailed Model Configuration Description 82
3.3.2 W20-SRCE-Based Geometry Template for Model Development 83
3.4 HAPC Engine Model Development 84
3.4.1 W20-SCRE Model Adapted for Closed-Loop HAPC Implementation 84
3.4.2 Key Sub-models Utilized in HAPC Simulation 85
3.4.3 W6L20 Multicylinder Model for iHAPC Analysis 95
3.5 Post-Processing and Data Analysis Methods 97
3.6 Targeted engine design constraints 101
4 Result and discussion 103
4.1 Simulation Results of the Reference Model 103
4.2 Model Validation at Motoring Condition 105
4.2.1 Baseline Model Validation 105
4.2.2 Motoring Pressure and Temperature Comparison 107
4.3 Effect of Argon-to-Oxygen Ratio 109
4.3.1 Design of Experiments (DOE) 109
4.3.2 Mid-Load Point (50.20% Load) 111
4.3.3 75.25% Load Point 115
4.3.4 Full-Load Point (101.20%) 118
4.3.5 Discussion 120
4.4 Impact of Alternative Monatomic Gases on HAPC Performance 123
4.4.1 Design of Experiments (DOE) 123
4.4.2 Discussion 127
4.5 Effect of changing Oxygen-to-Fuel ratio (λ) 130
4.5.1 Design of Experiments (DOE) 130
4.5.2 Discussion 132

4.6 Effects of Compression Ratio and Exhaust Back Pressure 133
4.6.1 Design of Experiments and Performance Results 133
4.6.2 Compression Ratio 134
4.6.3 Exhaust Back Pressure Analysis 136
4.6.4 Discussion 139
4.7 Sweep 5: Effects of Impurities in Hydrogen Fuel on Engine Performance 143
4.7.1 Design of Experiments and results in continuing operation 143
4.7.2 Discussion 145
4.8 Summary of the Results 146
5 Conclusions 148
5.1 Specific conclusions addressing individual research questions 148
5.2 Contribution to the Field of Research 150
5.3 Outlook 150
References 152
Appendices 160
Appendix 1. GT Suite Model Development Flow Chart 160
Appendix 2. An Overview of Simulation Dashboard 160

Figures

Figure 1 The principle of closed-loop Integrated Hydrogen Argon power cycle (Van Den Brink, 2022a). 16

Figure 2 Primary Energy Growth Demand in the New Policies Scenario (Energy Agency, 2011) 17

Figure 3 An overview of the theoretical efficiency of the Otto cycle with air and argon as working fluids (Wang, Jin, et al., 2023a). 18

Figure 4 a) Realization of HAPC in recuperating engine and b) its exemplary integration to Argon-Enhanced combined energy storage or power unit (Dibble et al., 2015; Van Den Brink, 2022a). 19

Figure 5 A P-T Diagram for Adiabatic Compression Air vs Argon. Under the same compression ratio (r=12.3), argon achieves significantly higher final temperature (1611.97K) and pressure (66.09 bar) than air (828.62K and 33.56 bar, respectively), with a higher injected quantity of mass for argon than air. 27

Figure 6 Overview of the methane-argon cycle performance (Hodgson et al., 2021a) . 36

Figure 7 Overview of Closed Cycle Hydrogen Engine Technology (Pochari, 2019) 40

Figure 8 Indicated thermal efficiency versus compression ratio H_2-O_2-Ar mixtures (Killingsworth et al., 2011) 44

Figure 9 Port vs Direct vs Dual Injection (Bimmertips, 2021) 46

Figure 10 Port Injection (PI) and Direct Injection (DI) basic injection configurations for the APC (Van Den Brink, 2022b). 47

Figure 11 An Overview of 1D Engine Simulation (Grill et al., 2019) 51

Figure 12 An overview of Physics based 1 d airpath model (CA resolution) Detail airpath representation including pulsations (Gamma Technologies, 2024d). 53

Figure 13 The Schematic of staggered grid approach: scalars calculated at centroid, vector quantities at boundaries (Gamma Technologies, 2024a) 54

Figure 14 Fluid Properties Applicable to Combustion Systems Overview (Gamma Technologies, 2024a) 62

Figure 15 Combustion and heat transfer methodology employed for the calculations (Margot et al., 2021). 69

Figure 16 An overview of Ar-H_2 Closed Cycle Engine Model Configuration in GT-suite (Tingting, 2022) 71
Figure 17 An expanded detailed model diagram of the air separation unit by using Aspen Plus (Sierra Aznar, 2018a) 72
Figure 18 Model overview with Contour plot showing the temperature (Van Den Brink, 2022a) 73
Figure 19 Schematic of the architecture of the Split-cycle engine model (Dong et al., 2022). 75
Figure 20 Research design and methodology flow chart. 76
Figure 21 Methodology Flow chart of Integration. 80
Figure 22 Model Validation Flow chart. 81
Figure 23 Overview of the 1-D model representing the Wärtsilä 6L20-2STC research engine. 82
Figure 24 Overview of W20-DF SCRE model geometry. 84
Figure 25 A 1D closed loop GTP Model of W20-SCRE layout for HAPC. 85
Figure 26 Conceptualization view of the combustion object. 86
Figure 27 The imposed burn rate and start of combustion for 50 %, 75.25%, and 101.2% load. 87
Figure 28 Condenser configuration and Intercooler Efficiency sub-model connection. 88
Figure 29 An overview of condenser effectiveness visualization. 91
Figure 30 An overview of water ejector sub-model. 92
Figure 31 An overview of O2 and H2 Injection Control subassembly. 93
Figure 32 An overview of Additional controller units of sub-models. 95
Figure 33 A 1D closed loop multi-cylinder HAPC GT-Suite Model of Wärtsilä 20 layout. 96
Figure 34 Reference GTP simulated data of engine performance metrics of W6L20-2STC model. 103
Figure 35 In-cylinder pressure comparison for validation (Experimental data vs W6L20-2STC model vs SCRE) 106
Figure 36 Motored Pressure vs Crank Angle plot for Argon-Oxygen Mixture vs. Air ... 107

Figure 37 Motored Temperature vs Crank Angle plot for Argon-Oxygen Mixture vs. Air. 108

Figure 38 Performance Metrics Analysis of Closed-Loop HAPC at 50% Load for Different Diluted Mixture Compositions. 111

Figure 39 In Cylinder Pressure Analysis of 50% Load for different mixture compositions. 113

Figure 40 In Cylinder Temperature Analysis of 50% Load for different mixture compositions. 114

Figure 41 Performance Metrics Analysis of Closed-Loop HAPC at 75.20% Load for Different Diluted Mixture Compositions. 115

Figure 42 In Cylinder Pressure Analysis of 75.25% Load for different mixture compositions. 116

Figure 43 In Cylinder Temperature Analysis of 75.25% Load for different mixture compositions. 117

Figure 44 Performance Metrics Analysis of Closed-Loop HAPC at 101.1% Load for Different Diluted Mixture Compositions. 118

Figure 45 In-Cylinder Pressure Analysis of 101.20% Load for different mixture compositions. 119

Figure 46 In Cylinder Temperature Analysis of 101.20% Load for different mixture compositions. 120

Figure 47 Comparison of Mixture Composition for Targeted Engine Design Constraint. 123

Figure 48 Performance analysis of inert gases configurations in a six-cylinder W20 engine. 125

Figure 49 Comparison of In-Cylinder Pressure for Different Inert Gas Configurations. 126

Figure 50 Comparison of In-Cylinder Temperature for Different Inert Gas Configurations. 127

Figure 51 Influence of oxygen to fuel ratio on combustion dynamics and exhaust gas accumulation. 131

Figure 52 Effects of Compression Ratio Variation for Engine Performance Metrics in GTP Simulation. 135

Figure 53 Exhaust Back Pressure Analysis on Combustion Dynamics and Efficiency. .. 136

Figure 54 In-cylinder pressure curves for different exhaust back pressure simulations. 138

Figure 55 In-cylinder Temperature curves for different exhaust back pressure simulations. 139

Figure 56 Engine performance vs. effect of impurities of hydrogen as fuel in the system. 144

Tables

Table 1 Main advantages of HAPC in an integrated argon-enhanced combined energy storage/power unit vs. state-of-the-art peaking power plant technology. Adapted from (Mikulski, 2024). 21

Table 2 Theoretical comparison of Poisson Relations and their Impact on Pressure, Temperature, and Efficiency. 27

Table 3 Fuel properties used in APC (Martinez, 2020) 30

Table 4 Comparison of fuel types in APC according to literature. 31

Table 5 Properties: Argon (Ar) vs Air (N_2) vs Helium (He) and other monatomic gases (Bich et al., 1990) 33

Table 6 Injection Method Comparison (Kim et al., 2015; Van Den Brink, 2022a; Xinyu et al., 2020) 48

Table 7 An overview of the general Assumption in 1D airpath modelling (Gamma Technologies, 2024c) 52

Table 8 Combustion Models Overview for SI, Diesel, and HCCI Systems (Gamma Technologies, 2024a) 63

Table 9 Specification of the research engine 77

Table 10 An overview of Targeted engine design constraints 102

Table 11 Baseline operating points and initial values for simulation. 105

Table 12 Comparison of experimental and simulated data for validation 107

Table 13 Constant combustion Parameters for different loads 110

Table 14 Inputs and Initial values of DOE 124

Table 15 Reference inputs for the initial conditions of the simulation. 130

Table 16 The parameters defined for the design of the experiment. 134

Table 17 The design of experiment inputs. 143

Table 18 Thesis Summary and Key Parameters Influence on Engine Performance Metrics 147

Abbreviations

Abbreviation	Full Form
APC	Argon Power Cycle
Ar	Argon
ASCE	Argon Split Cycle Engine
BDC	Bottom Dead Centre
BMEP	Brake Mean Effective Pressure
BSFC	Brake-Specific Fuel Consumption
CA	Crank-Angle
CFD	Computational Fluid Dynamics
CHT	Conjugate Heat Transfer
CI	Compression-Ignition
CR	Compression Ratio
CVCC	Constant Volume Combustion Chamber
DF	Dual Fuel
DI	Direct Injection
DuI	Dual Injection
EVO	Exhaust Valve Opens
EGT	Exhaust Gas Temperature
FVM	Finite Volume Method
GTP	GT Power
H_2	Hydrogen
HAPC	Hydrogen-Argon Power Cycle
He	Helium
HCCI	Homogeneous Charged Compression Ignition
ICEs	Internal Combustion Engines
iHAPC	Integrated Hydrogen-Argon Power Cycle
IEA	International Energy Agency
IMEP	Indicated Mean Effective Pressure
IRENA	International Renewable Energy Agency

LHV	Lower Heating Value
MDO	Marine Diesel Oil
MFB	Mass Fraction Burned
MFR	Mass Flow Rates
NO_x	Nitrogen Oxide
PFI	Port Fuel Injection
PM	Particulate Matter
RCEM	Rapid Compression Expansion Machine
RICE	Reciprocate Internal Combustion Engine
RQ	Research Question
SACI	Spark Assisted Compression Ignition
SCRE	Single Cylinder Research Engine
SI	Spark Ignition
SL	Laminar Flame Speed
TDC	Top Dead Centre
TDCF	Top Dead Centre Firing
TPA	Three-Pressure Analysis
VVT	Variable Valve Timing
W6L20-2STC	Wärtsilä Six-Cylinder Two Stage Turbocharged Engine
RCEM	Rapid Compression Expansion Machine
EGT	Exhaust Gas Temperature

1 Introduction

The Argon Power Cycle (APC) presents an innovative thermodynamic framework designed to enhance the Reciprocate Internal Combustion Engine (RICE) performance while enabling the integration of post-combustion carbon capture. By optimizing thermal efficiency and mass transfer processes, APC offers a promising, cost-effective solution to advance the adoption of renewable energy sources (Sierra Aznar, 2018a). The process of APC uses Argon (Ar) as a working fluid and oxygen as the oxidizer, and it has the ability to adopt any fuel as an energy source. The reason behind choosing Ar is its natural abundance, accounting for 0.93% of the atmosphere. As the third most abundant gas, Ar is significantly more abundant than other noble gases. Although APC has no fuel limitation, hydrogen's high gravimetric energy density, efficient heat transfer, and clean combustion make it useful for APC to be used as fuel in Internal Combustion Engines (ICEs) by providing rapid power output (Van Oijen, 2019a). This combination of APC with hydrogen (H_2) introduces the Hydrogen-Argon Power Cycle (HAPC) as, an efficient, eco-friendly power cycle that leverages argon's abundance and hydrogen's favourable characteristics of fuel combustion.

The HAPC marks a significant advancement in the energy sector, achieving full valorization of H_2 as a fuel by achieving unprecedented levels of power generation. By replacing air with monoatomic gas such as Ar, this approach revolutionizes combustion technology in ICEs. Wherein, increased thermodynamic efficiency by 10%-20% along with zero tail-pipe emissions and closed-loop recirculation of Ar. To put it briefly, HAPC offers similar benefits as fuel-cell technology but at a far lower mass, volume, and cost (Pröll et al., 2010). Furthermore, the integration of hydrogen energy storage and generation with various production processes, including methane reforming, biomass gasification, and coal gasification through chemical looping, offers additional benefits for system integration (Ahlström, 2020; Lee et al., 2021). The idea of the Integrated Hydrogen-Argon Power Cycle (iHAPC) aims to bring HAPC to technology readiness level 6 (TRL-6, which indicates that the technology has a fully functional prototype or representational model) by demonstrating sustainable operations.

The iHAPC process, represented schematically in Figure 1, operates as a closed-loop process. The process starts with the electrolysis unit, where excess renewable energy is utilized to split water into hydrogen (H_2) and oxygen (O_2). These two gases are then compressed in two separate streams to the necessary pressure levels and injected into the combustion chamber. Where hydrogen combusts with oxygen, producing high-temperature, high-pressure exhaust gases without nitrogen oxides due to the absence of nitrogen in the system.

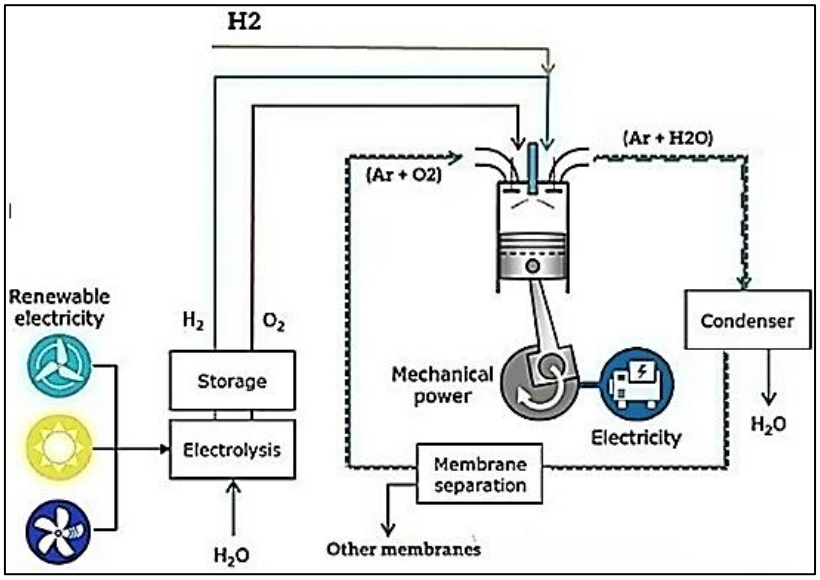

Figure 1 The principle of closed-loop Integrated Hydrogen Argon power cycle (Van Den Brink, 2022a).

Throughout the closed-loop process, argon is recirculated, maintaining the closed-loop configuration and ensuring high efficiency by conserving the working fluid and enabling continuous high-pressure operation. Usually, for a traditional power cycle, removing unwanted combustion products from exhaust requires a sophisticated combination of condensers, carbon capture, and membrane separators that could be co-optimized to secure stable concentration. However, in the case of iHAPC, it will be rather simple to separate H_2O from exhaust using a selective permeable membrane. This enables iHAPC to efficiently store and convert renewable energy into electricity, surpassing existing technologies in both efficiency and cost and providing rapid power dispatch to complement the intermittent nature of renewable energy sources.

1.1 Background

1.1.1 Integrated Hydrogen-Argon Power Cycle (iHAPC): An Innovative Energy System of the Future

As global warming concerns over climate change intensify, scalable solutions are urgently needed that mitigate greenhouse gas emissions without compromising energy security. A report by the International Energy Agency (IEA) emphasizes the necessity of reducing dependency on fossil fuels and increasing the focus on renewable energy sources by 2035. Meanwhile, IEA has identified emerging market competitors such as India, Indonesia, China, and Brazil as dominant forces in global energy demand over the next 25 years illustrated in Figure 2 (Energy Agency, 2011).

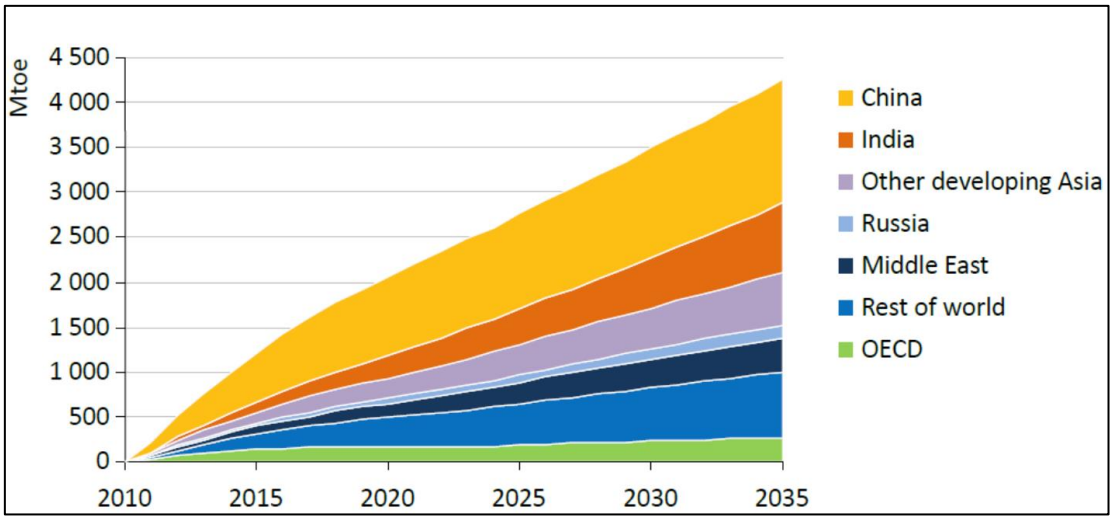

Figure 2 Primary Energy Growth Demand in the New Policies Scenario (Energy Agency, 2011)

Additionally, another report by the same agency (Energy Agency, 2024) indicates that as the world's population continues to climb and more developing countries recover from poverty, global energy consumption has been rising steadily since 1990. In 2018, the world's overall energy consumption was 9938 Mtoe, representing a 60% increase from the 1990 level I (Energy Agency, 2018). According to (Energy Information Administration (EIA), 2023), global energy consumption is projected to grow by as much as 49% by 2050. Currently, fossil fuels supply 80% of the world's energy needs. Despite decarbonization efforts, the share of renewable energy is expected to reach only 25-28% by 2050, which

is far short of the two-third range recommended by the International Renewable Energy Agency (IRENA) to significantly reduce fossil fuel dependencies (Renewable Energy Agency, 2019).

Traditional power generation reliant on fossil fuel combustion produces greenhouse gases, including CO_2, NOx, and other local pollutants, and particulate matter (PM). Industries such as heating, electricity production, construction, and transportation consume significant amounts of energy that require technology to reduce emissions from fossil fuels and utilize cleaner energy sources. Nowadays, modern ICEs have successfully lowered NOx and particulate emissions through advanced filters and after-treatment technologies, demonstrating continuous gains in efficiency and effectively reducing global fuel demand (Ahmad, 2022).

In this context, APC offers a promising solution by substituting air with monatomic gas such as Argon, Helium, or Neon with a higher heat capacity than air and the thermal efficiency of ICEs can be significantly improved. This thermodynamic advantage is governed by the specific heat ratio (γ), which is a key factor determining the efficiency of thermodynamic cycles.

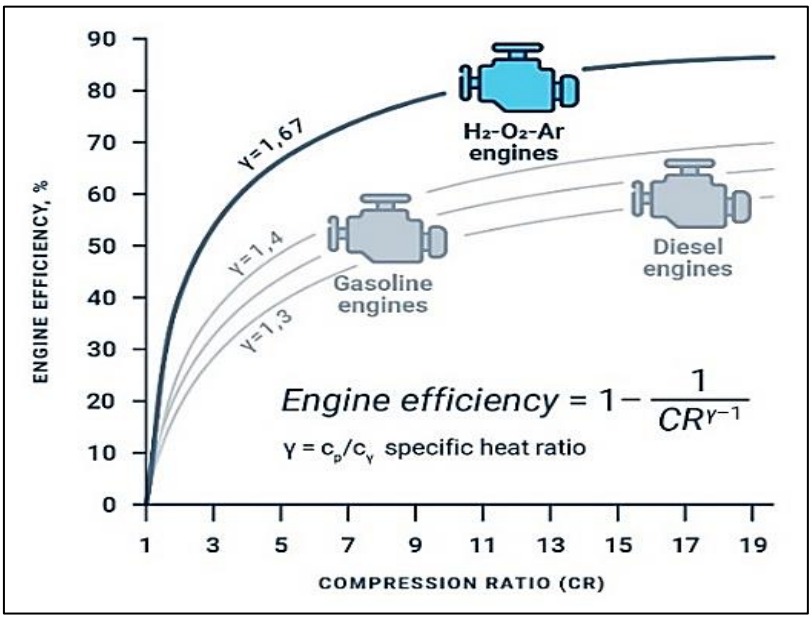

Figure 3 An overview of the theoretical efficiency of the Otto cycle with air and argon as working fluids (Wang, Jin, et al., 2023a).

Morden lean burn gasoline engines where γ = 1.4, operating with approximately 50% adiabatic efficiency (Wang, Jin, et al., 2023a). By utilizing an argon-fuel-oxidizer mixture, it is possible to augment thermal efficiency by 15% to 22%. The theoretical efficiency of APC approaches 90% in Figure 3 (Wang, Jin, et al., 2023a). Experiments conducted by the University of Berkeley (Shi et al., 2021) and Toyota (Rentaro et al., 2010) demonstrated that APC could be more efficient in small-scale operations with closed-loop recycling of argon, which could be an admissible pathway to bring the APC concept into practice. These advancements in APC efficiency provided a strong foundation for the development and implementation of HAPC, further enhancing its potential as a leading sustainable energy technology.

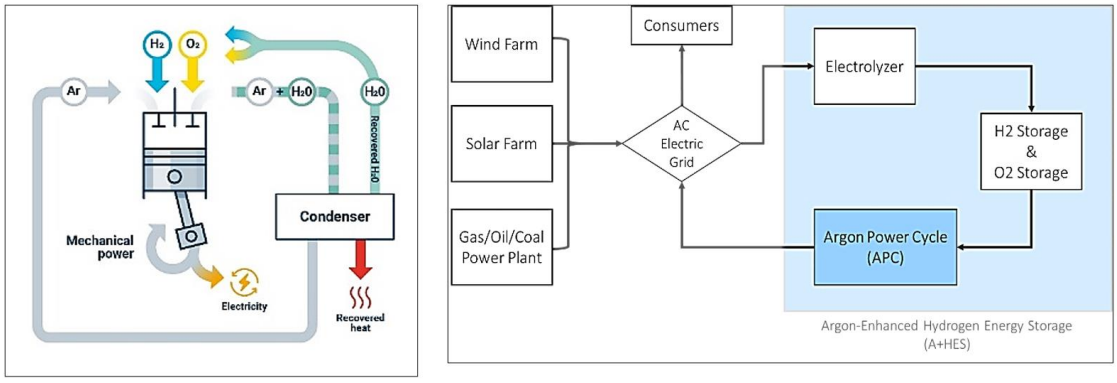

(a (b

Figure 4 a) Realization of HAPC in recuperating engine and b) its exemplary integration to Argon-Enhanced combined energy storage or power unit (Dibble et al., 2015; Van Den Brink, 2022a).

The rapid expansion of green hydrogen production requires a re-evaluation of APC's feasibility. Utilizing clean hydrogen and oxygen from electrolysis, the HAPC engine airpath can be realized with a single high-efficiency condenser for water separation, as depicted in Figure 4(a). Various turbo-compounding solutions can be incorporated to recover additional efficiency from the system (Dibble et al., 2015). HAPC primarily serves as a grid peaking plant, complementing hydrogen energy storage and generation, as depicted in Figure 4(b).

From that perspective, HAPC represents an innovative advancement in energy technology. Its potential to generate power with great efficiency and zero emissions is expected

to transform the energy sector. By leveraging the unique properties of hydrogen and argon, the HAPC creates closed-loop power systems that maximize thermal efficiency and minimize environmental impact. Firstly, the standard Argon power cycle (APC) utilizing methane as fuel achieves an efficiency of approximately 51.7%.(Wang et al., 2024). When hydrogen is used as fuel, the efficiency typically improves by around 10% compared to the standard APC. Furthermore, incorporating modifications such as condenser, water ejector, and controllers can substantially enhance efficiency, potentially reaching up to 64% (Van Oijen, 2019a). Secondly, when coupled with H_2 and O_2 produced by electrolysis, HAPC can generate flexible electric power with zero exhaust gas emissions, making it an ideal solution for sustainable power generation without contributing to air pollution.

Furthermore, hydrogen which can be produced massively from renewable energy sources such as solar, wind, biomass, and water can be converted to electricity or fuel with only heat and water vapor as emissions. This positions hydrogen as a crucial element in linking renewable energy resources with zero-emission energy conversion technologies. Eventually, the hydrogen economy supports a transition from large, centralized power plants to smaller, decentralized facilities located near the point of use. This shift enhances energy security and reduces transmission losses making energy production more efficient and resilient.

Additionally, the solution outperforms fuel cells in terms of energy security and robustness because iHAPC can be operated as a normal engine if hydrogen or argon is unavailable. Typically, highly discretized energy systems require fast response to balance the grid and compensate for the unpredictable nature of renewable energy. Conventional Peaker plants, typically gas turbine or generator set plants, often operate on the principle of utilizing waste heat in co-generation to improve overall efficiency. However, these plants traditionally do not incorporate excess energy storage solutions, as their primary function is to operate only during peak hours or for grid stabilization when additional power generation is required.

Table 1 Main advantages of HAPC in an integrated argon-enhanced combined energy storage/power unit vs. state-of-the-art peaking power plant technology. Adapted from (Mikulski, 2024).

Advantage/Impact	Economical	Environmental	Societal
Superior power generation efficiency: up to 15 percentage points higher than conventional engine plant	**+++**	**++**	**+**
True zero emissions: no exhaust - only trace elements from lubricating oil and blow-by gases	**+**	**+++**	**++**
Space and material conservation: stack-less concept – no intake or exhaust ducts; no after-treatment; heat recovery incorporated into the condenser cooling circuit and optional turbo-compounding	**++**	**+**	**+**
Full valorization of off-streams: accommodating oxygen from electrolysis	**++**	**+++**	**+**
Complying with the circular economy: The condensed water can be reused for electrolysis; argon can be recovered from air to offset blow-by losses	**+**	**++**	**++**
+++ Superior advantage; ++ Significant direct advantage; + Indirect advantage			

The HAPC addresses this limitation by integrating hydrogen energy storage. When there is excess solar or wind power, it can be stored as hydrogen. This stored hydrogen can then be utilized by HAPC during periods of high demand or when greed stabilization is necessary. By incorporating hydrogen energy storage, the HAPC provides a more flexible and sustainable solution for managing energy supply and demand. In this integrated concept, hydrogen is generated via electrolysis as mentioned before when an excess of cheap electricity is available. Changing the conventional engine to one operating on the HAPC offers significant benefits in this configuration.

In the light of Table 1, illustrates the multiple benefits of the HAPC. Superior power generation efficiency results in a 15% increase compared to conventional e-plants, providing

significant economic and environmental advantages. True zero emission ensures no exhaust apart from the trace elements, which significantly benefits the environment. Space and material conservation through a stack-less concept and the elimination of intake or exhaust ducts provide indirect economic, environmental, and societal advantages. The full valorisations of off-streams, such as the on-site accommodation of oxygen produced from electrolysis, provide significant economic and environmental benefits. This approach facilitates a closed-loop system, eliminating exhaust gas emissions and allowing excess oxygen to be re-recirculated within the system. Additionally, the HAPC cycle is fully compliant with the circular economy, as condescend water is reused for electrolysis and Argon can be recovered from the air, thus enhancing environmental and social impacts.

For all these reasons iHAPC will present a game-changing solution for combined energy generation and storage in plants. There is no other technology in this prospect that is equally economically attractive in both capital and operational cost right now while providing a clear advantage to the environment and society in such an elegant manner (Hodgson et al., 2021a). Scientifically, this development further benefits several complementary ecosystem endeavours. Furthermore, its support for decentralized energy generation could reshape the global energy landscape, ensuring flexibility, sustainability, and accessibility in power generation using ICEs.

1.2 Problem Formulation and Scope of Thesis

1.2.1 Problem Formulation

This thesis work hypothesizes that the integration of HAPC into the medium-speed Wärtsilä W6L20-2STC engine can potentially enable a yield of 65% thermal efficiency with zero exhaust emissions. Leveraging Argon as the working fluid, the research addresses critical challenges in closed-loop engine design by analysing gas mixture compositions, hydrogen injection strategies, pressure drop analysis, and combustion dynamics. The stated hypothesis is validated through 1-dimensional simulations using GT-Suite

(Gamma Technologies, 2024c) software. The thesis on the simulation basis addresses necessary modifications to the real engine to optimize the efficiency of HAPC, fostering a way towards its potential implications for next-generation power plants.

1.2.2 Research Question

- *RQ1: What is the optimal noble gas (argon)-to-oxygen or fuel ratio for maximizing combustion efficiency?*
- *RQ2: How do alternative monatomic gases or gas mixtures, such as helium or neon, affect the Hydrogen Argon Power Cycle (HAPC) performance under controlled conditions?*
- *RQ3: How do variations in stoichiometric oxygen ratios influence combustion efficiency and exhaust gas temperatures in HAPC?*
- *RQ4: How do compression ratio and exhaust back pressure impact combustion dynamics, and efficiency?*
- *RQ5: How do impurities in hydrogen fuel affect engine performance, and how quickly do they cause a noticeable drop in efficiency?*

1.2.3 Scope of thesis

The scope of the thesis is to develop a specialized system-level one-dimensional simulation model of the HAPC for the Wärtsilä (W20) engine. The tool is further used to address the stated research questions. To this end, the thesis entails comprehensive performance analysis and model validation under diverse operational conditions. By focusing on HAPC, the study seeks to enhance the understanding and application of this cycle in optimizing engine design.

Wärtsilä provided the baseline GT-Suite models of the Wärtsilä 20DF multicylinder research engine and its production version W6L20 DF-2STC working on Natural gas and Marine Diesel Oil (MDO). The baseline models have been thoroughly calibrated with engine test run experimental data, to accurately represent the real system. The models

were rebuilt to use argon as a working fluid in a closed-loop manner including modelling of crucial APC subsystems like water condenser, oxygen, and hydrogen injectors while respecting the geometrical constraints of the system.

The analytical part of the study focuses on how specific gas mixtures, combustion dynamics, compression ratio, excess oxygen, and back pressure affect engine performance in this hydrogen-powered engine concept. Through the analysis of engine performance under verifying conditions, this research work provides an understanding of the Argon power cycle potential in real-world applications and guides the direction toward building a prototype of such a system.

1.3 Structure of the Thesis

This thesis uses a structured approach to examine the Hydrogen Argon power cycle (HAPC) in seven key chapters. The Hydrogen Argon power cycle is introduced in Chapter 1, with a focus on its potential in the energy sector. It is contextualized within the national and international innovation framework of the internal combustion engine.

In Chapter 2, a thorough literature review is conducted. The characteristics of the fuel and working fluid are examined concerning the development of argon power cycles (APC) and current trends are reviewed, with an emphasis on identifying gaps in systems that rely on hydrogen and fossil fuels. Additionally, it examines a one-dimensional simulation method particularly used with the APC and hydrogen as fuel.

The methods employed, including the model development and validation procedures that are essential for scaling the hydrogen argon power cycle concept, are covered in detail in Chapter 3. It illustrates the modelling assumption and goes through the models that have been used as a tool in a methodical manner. Additionally, it gives a thorough explanation of mathematical concepts, such as how efficiency is determined concerning the argon power cycle and other quantities that are relevant to the quantitative data post-processing in the result section, as well as all other angles that are discussed in

general terms. In Chapter 4, results are discussed for both the experimental and simulation parts that validate the model under various conditions involving the ratios of argon, hydrogen, and oxygen with other monatomic gases.

The findings are discussed in Chapter 5 in the context of argon power cycle research and development, with an emphasis on possible applications and implications. The main contributions are outlined in Chapter 6 along with their importance in advancing the Argon power cycle. Furthermore, an extensive foundation for future study and application in the field of hydrogen argon power cycle is provided by the appendix, which includes all cited sources, additional materials, and detailed modelling data.

2 Review of Related Literature: Analysis of State of the Art in HAPC

2.1 Fundamentals of APC

The Argon Power Cycle (APC) uses argon as a working fluid, a mono-atomic gas that makes up about 1% of the atmospheric air. Unlike conventional engines burning hydro-carbon fuels and emitting pollutant exhaust gases, the APC operates in a closed-loop system, that recirculates Agron with no loss after an initial intake (Van Den Brink, 2022a). The specific heat ratio (γ) for Argon is 1.67 as a characteristic of monatomic gases, and significantly higher than air's ratio of 1.40. The theoretical efficiency of an ideal Otto cycle is given by equation 2.1.

In the equation, η_{th} is theoretical efficiency and r is the compression ratio. The high value of γ for argon significantly improves cyclic efficiency, making it more efficient than other gases (Saidu Arah & Audu, 2020).

$$\eta_{th} = 1 - \frac{1}{r^{\gamma-1}} \qquad 2.1$$

Following (Van Den Brink, 2022a) equation 2.2 and 2.3, derived from the Poisson relation, described how Argon-specific heat ratio affects pressure and temperature during compression and expansion:

$$TV^{\gamma-1} = const. \rightarrow \frac{T2}{T1} = \left(\frac{V1}{V2}\right)^{\gamma-1} = r^{\gamma-1} \qquad 2.2$$

$$PV^{\gamma} = const. \rightarrow \frac{p2}{p1} = \left(\frac{V1}{V2}\right)^{\gamma} = r^{\gamma} \qquad 2.3$$

These equations illustrated the thermodynamic behaviour within the APC. For the isentropic process, these provide a theoretical assessment of cycle efficiency. By using the equation above and the same compression ratio (r =12.3) of the Wartsila 20 (DF) engine, the efficiency and thermodynamic properties of argon and air can be compared by theoretical analysis. For Air γ =1.4 and Argon γ =1.67 illustrated in Table 2.

Table 2 Theoretical comparison of Poisson Relations and their Impact on Pressure, Temperature, and Efficiency.

Property	Air	Argon
Molar Mass (g/mol)	28.97	39.95
Mass Required (g)	1.16	1.61
$P_{initial}$ (bar)	1.00	1.00
$T_{initial}$ (K)	300	300
T_{Final} (K)	818.62	1611.97
P_{Final} (bar)	33.56	66.09
η_{th} (%)	63.40	81.40
$T_{increased}$ (%)	96.90	
$P_{increased}$ (%)	96.90	

The data presented in Table 2 are calculated from the above equations, assuming identical initial conditions of pressure and temperature. The comparison between air and argon as working fluids in thermodynamic cycles is depicted in Figure 5.

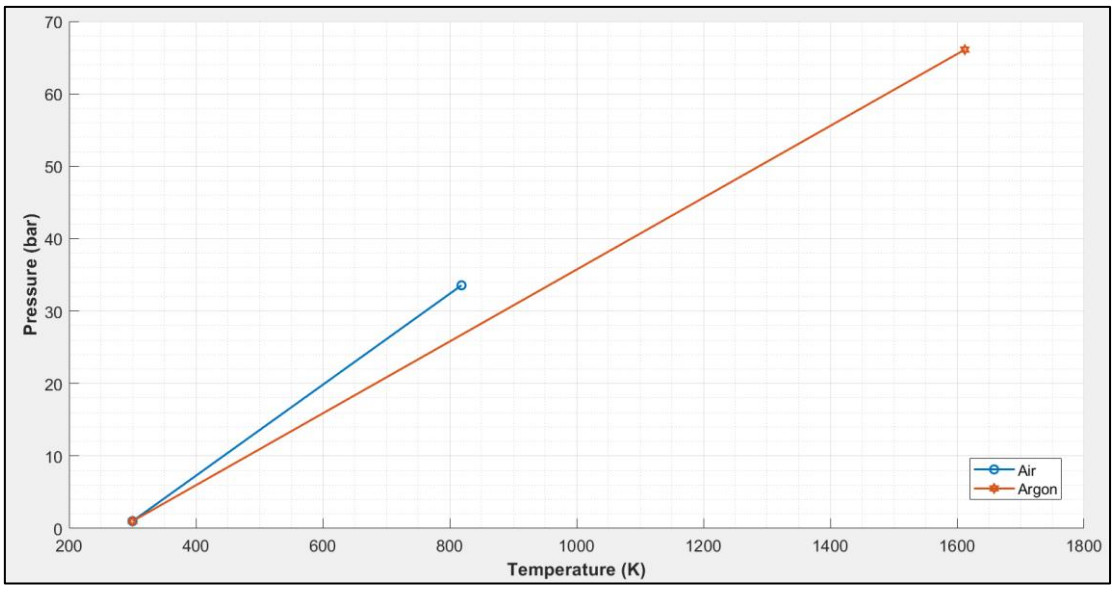

Figure 5 A P-T Diagram for Adiabatic Compression Air vs Argon. Under the same compression ratio (r=12.3), argon achieves significantly higher final temperature (1611.97K) and pressure (66.09 bar) than air (818.62K and 33.56 bar, respectively), with a higher injected quantity of mass for argon than air.

In Figure 5, it underscores the clear theoretical advantage of argon, primarily due to its higher specific heat ratio relative to air. For the reference compression ratio (r=12.3), argon reaches significantly higher final temperature (1611.97 K) and pressure (66.09 bar) compared to air, which attains final values of 828.62 K and 33.56 bar, respectively. Moreover, the required mass of air is calculated to be 1.16 grams, while for argon, it is 1.61 grams.

This substantial increase in temperature and pressure leads to a notable improvement in thermal efficiency of 81.4% for argon compared to 63.40% for air. This can be attributed to the thermodynamic principle that a higher γ allows for more effective energy conservation during the compression and expansion phases of the engine cycle, thus maximizing work output. However, while Argon's thermodynamic properties present clear benefits, these improvements come with significant technical challenges that must be critically addressed. The theoretical increase in operating temperatures increases the risk of pre-ignition, a phenomenon where the air-fuel mixture ignites prematurely due to excessive heat in the combustion chamber (J. Kim et al., 2024). Pre-ignition disrupts the control timing of combustion, often leading to engines knocking a destructive process that damages internal components such as pistons and cylinder walls. The elevated risk of pre-ignition with argon requires complete control over combustion timing and advanced thermal management strategies to prevent engine failures (Xie et al., 2021).

In addition, higher pressure and temperature cause substantial thermal stress on engine components. Over the duration of these extreme conditions can wear out materials faster, leading to early failure of critical components like valves and cylinder heads. To deal with these issues, research by (Q. Zhang et al., 2013) suggested that engine components would need to use specific materials that can handle high temperatures, such as ceramic composite or a better cooling system to keep things from overheating. While Argon can improve engine efficiency, it also brings challenges like pre-ignition and thermal stress that must be addressed with advanced analysis. To fully take advantage of Argon's benefits combined with better heat management, stronger materials, and

precise control of the combustion process to balance the gains in efficiency with the need to protect engine components is crucial. Strategies like optimizing the compression ratio, using spark-assisted compression ignition, and modifying additional components such as controllers can help to mitigate these issues and enhance overall performance (Shi et al., 2021).

2.2 Characteristics of Relevant Fuels and Working Fluids Suitable for APC

2.2.1 Fuel Compatibility in APC

In recent years the APC has become an advanced ICE technology designed to improve performance by using argon as a working fluid, Oxygen as the oxidizer, and other fuels. As APC enhances thermal efficiency, particularly when fuelled by natural gas, extending the lean burn limit and minimizing nitrogen oxide (NO_x) and unburned hydrocarbon emissions (Shi et al., 2021). This emission reduction makes it a promising alternative to conventional combustion engines, especially when integrated with different fuels such as natural gas, hydrogen, or methane.

Given the significance of fuels in APC, the research found that the performance of hydrogen-fuelled engines is sensitive to oxygen concentration, with the optimal combustion occurring around 15% oxygen and 85% Ar (L. Li et al., 2018a; Shahsavan et al., 2018b). To further improve efficiency, technologies like spark-assisted compression ignition, and membrane separators can increase overall system performance (Wang, Jin, Deng, Ding, et al., 2023a) (Wu et al., 2021b). Moreover, the APC's closed-loop design enables carbon capture, offering a solution to greenhouse gas emissions and reducing the need for extensive exhaust treatment systems (L. Li et al., 2018b).

i. Fuel properties

To ensure performance in APC, several studies have been conducted for natural gas, hydrogen, and methane. Comparison of these key fuel properties is crucial to understanding how these fuels behave in the APC. These properties, such as heating value, density,

and flame temperature, directly influence combustion dynamics and overall engine performance. The fuel properties are listed in Table 5. In the context of the APC, comparing hydrogen, methane, and natural gas as fuel reveals significant implications for engine performance and optimization.

Among all the fuels presented in Table 3, hydrogen, with a lower heating value (LHV) Of 120 MJ/Kg, making it ideal for maximizing power output and efficiency. Its higher adiabatic flame temperature (~2045°C compared to methane's ~1950°C) suggests improved thermal efficiency, especially in cycles that leverage the heat-retaining properties of argon (Falfari et al., 2023).

Table 3 Fuel properties used in APC (Martinez, 2020)

Property	Natural Gas (CH_4 + Other Alkanes)	Methane (CH_4)	Hydrogen (H_2)
Atomic/Molecular Mass [g/mol]	~16-18	16.04	2.016
Boiling Point [° C]	~-161.5	-161.5	-252.87
Density [kg/m^3] @ 20° C	0.68-0.84	0.717	0.08988
Lower Heating Value (LHV) [MJ/kg]	~45-50	50	120
Adiabatic Flame Temperature [° C]	1950-1980	~1950	~2045

Hydrogen's lower density (0.08988 kg/m3 at 20°C) contrasts with methane (0.717 kg/m3) and natural gas (0.68-0.84 kg/m3), implying higher volumetric flow rates are required for the same mass flow rate. Its low viscosity (0.0084 cP at 20°C) facilitates faster air-fuel mixing, enhancing combustion efficiency (Stępień, 2021). Meanwhile, its high thermal conductivity (186.9 mW/mK) contrasts with lower values for methane and natural gas (34.4 mW/mK), indicating a greater tendency for heat transfer during combustion. Hydrogen's broad flammability limits (4-75% in air) allow more flexibility in air-fuel mixtures compared to the narrower range of methane and natural gas (5-15%) (Jin, Deng, Xie, et al., 2023).

Both hydrogen and methane have similar ignition temperatures (~580°C), so combustion initiation occurs under comparable conditions. However, hydrogen's higher specific heat ratio compared to methane and natural gas implies a more expansive combustion process, resulting in more efficient energy conservation in the thermodynamic cycle in APC. Overall, hydrogen stands out due to its superior energy density, higher flame temperature, and more efficient combustion dynamics, while methane and natural gas provide comparable performance with lower volumetric flow requirements and narrower flammability limits.

ii. Comparison of Fuel types

Table 4 below summarizes how natural gas hydrogen and methane perform in terms of efficiency, emission, anti-knock properties, and operational challenge in the argon power cycle according to recent research by (Shi et al., 2021) (Wang, Jin, Deng, Ding, et al., 2023a) (Wu et al., 2021b).

Table 4 Comparison of fuel types in APC according to literature.

Fuel Type	Thermal Efficiency	Emissions	Anti-Knock Properties	Challenges
Natural Gas	Higher efficiency with direct injection into an Ar-O_2 mixture (Shi et al., 2021).	Reduced NO_x and unburned hydrocarbons.	Moderate anti-knock properties, enabling higher compression ratios.	Requires CO_2 absorption to achieve zero emissions (Li et al., 2018).
Methane	Significant thermal efficiency, especially with direct injection (Wang et al., 2023).	Lower emissions compared to traditional cycles.	Superior anti-knock properties, enhancing stability and thermal efficiency.	Few operational challenges; highly efficient in lean-burn conditions.

Hydrogen	High efficiency and potential for zero CO_2 emissions (Li et al., 2018).	Zero CO_2 emissions, but NOx may form at high temperatures.	Lower anti-knock resistance, leading to potential knocking.	Requires advanced strategies like lean combustion and water injection to suppress knock (Wang et al., 2023).

iii. Challenges in Fuel Adaptability

The APC incorporates several challenges in fuel adaptability, variation in thermal efficiency arises due to fluctuations in the equivalence ratio and oxygen content, complicating the optimization of engine performance under different operating conditions (Shahsavan et al., 2018b). Natural gas and hydrogen are both feasible fuel choices, each comes with limitations. Natural gas requires efficient carbon capture technologies to reach zero-emission operation (L. Li et al., 2018b), while hydrogen, despite Its high efficiency, thanks is associated with higher operational costs and increased risk of pre-ignition or knock (Wu et al., 2021b).

The careful selection of fuel and combination of working fluids based on respective properties are essential for optimizing the performance of ICEs. Additionally, stable combustion requires precise control over spark timing, pressure, and temperature to achieve optimal performance and minimize emissions (Wang, Jin, Deng, Ding, et al., 2023a). Addressing these issues is critical to fully realizing the APC's potential for efficient and sustainable power generation.

2.2.2 Characteristics Relevant Working Fluids for APC

In the context of internal combustion engines, the selection of appropriate working fluid is crucial for optimizing performance, efficiency, and reliability. Table 5 presents the key properties of various monoatomic gases, highlighting their impact on engine operation. These gases exhibit a range of densities, significantly influencing energy content per unit volume and, consequently, the efficiency of the combustion process. For instance,

helium has a low density whereas Xenon has a significantly higher density, and the variation affects both energy density and engine efficiency during combustion (Shahsavan et al., 2018b).

Table 5 Properties: Argon (Ar) vs Air (N_2) vs Helium (He) and other monatomic gases (Bich et al., 1990)

Property	Nitrogen (N_2)	Argon (Ar)	Helium (He)	Neon (Ne)	Xenon (Xe)
Atomic Mass [g/mol]	28.02	39.948	4.0026	20.1797	131.293
Natural State [-]	Gas	Gas	Gas	Gas	Gas
Boiling Point [°C]	-195.8	-185.7	-268.9	-246	-108
Density [kg/m³] @ 20°C	1.16	1.664	0.1634	0.9	5.851
Viscosity [cP] @ 20°C	0.0176	0.0223	0.0196	0.0313	0.00565
Ionization Energy [kJ/mol]	1402	1520	2372	2080	1170
Natural Abundance in Air [%]	78	0.93	0.005	0.0018	N/A
Specific Heat Ratio (γ)	1.4	1.67	1.67	1.67	1.67
Thermal Conductivity [mW/mK] @ 20 °C	25.83	17.72	155.91	49.4	5.57
Molar Weight [g/mol]	14.01 x 2	39.948	4.0026	20.1797	131.293
Diffusivity in Air (cm²/s)	0.177	0.138	125.3	0.45	0.067
Initial Temperature (K)	N/A	300	310 – 340	500	1000
Initial Pressure (bar)	N/A	1.05	1.05	6	20

The stability of these gases under engine operating conditions is determined by their boiling points. It indicates the temperature at which a substance transitions from a liquid to a gas. In engine operations, especially under extreme temperature conditions, the stability of the gas is essential for maintaining consistent pressure and overall engine efficiency (Bich et al., 1990). Gases with lower boiling points, like helium, are more prone to face changes, which can lead to fluctuations in performance. In contrast, gases with higher boiling points, such as Xenon, offer greater stability across a broader temperature

range, ensuring reliable and efficient engine operation. Helium, with an extremely low boiling point of-268.9 °C, contrasts sharply with xenon, which has a higher boiling point of -108°C. This property is crucial for maintaining gas stability and ensuring consistent engine performance.

Moreover, the densities of monatomic gases as working fluids directly impact thermal efficiency, system performance, engine design, and fuel aspiration. It also plays a crucial role in determining the necessary adjustments in mass flow rate and boost pressure to maintain the same trap mass as the reference engine (Wang, Yue, et al., 2023). Argon, with a density of 1.664 kg/m^3, is 1.43 times denser, allowing for a mass flow rate and reduced boost pressure to achieve equivalent trapped mass than nitrogen. In contrast, helium with a much lower density of 0.1634 kg/m^3, requires approximately seven times the mass flow rate and significantly higher boost pressure to compensate for its low density. Similarly, neon with a density of 0.9 kg/m^3, is 22% less dense than nitrogen, requiring a moderately higher mass flow rate and boost pressure. (W. Li et al., 2015) mentioned that the density variation of working fluid underscores the importance of calibrating engine parameters to the specific properties of each working fluid to optimize the performance effectively.

Additionally, (Gracki et al., 1969) mentioned that viscosity also plays a pivotal role, in affecting the fuel-air mixture and lubrication efficiency. Helium's low viscosity of 0.0196 cP at 20 °C aids in efficient mixing and smooth engine operation. In contrast, argon and nitrogen, with a viscosity of 0.0223 CP and 0.0176 cP respectively, offer different advantages in terms of lubrication and dynamic mixing. Ionization energy is another crucial factor, as it influences the ease of ignition and stability of combustion (Clements & Smy, 1976). Xenon’s high ionization energy of 1170 KJ/mol indicates a higher energy requirement for ignition, which could impact ignition stability under various operating conditions. Thermal conductivity significantly impacts heat transfer and engine cooling efficiency (Peterson et al., 1971). Argon, with a thermal conductivity of 17.9 mW/ (m.K), and helium, with a thermal conductivity of 156.7 mW/ (m.K) represent two ends in the

spectrum in terms of heat transfer capabilities. Effective heat transfer is essential for maintaining optimal engine temperatures and preventing overheating.

The APC leverages these properties to enhance engine performance. By utilizing argon, which has a higher density of 1.664kg/m^3 at 20°C, moderate boiling point of - 185.7°C, and lower thermal conductivity, the power cycle achieves fast heat transfer. Additionally, argon's specific heat (γ) ratio promotes effective energy transfer thereby increasing thermal efficiency. The careful selection and combination of working fluids based on their respective properties are essential for optimizing the performance of internal combustion engines.

2.3 State of the Art in Research on APC with fossil fuels

Argon Power Cycles (APC) offers a groundbreaking approach for fossil-fuel-based power generation systems through a closed loop in an internal combustion engine using argon or other monatomic gases. The APC can theoretically achieve up to 80% thermal efficiency, which is a significant 30% improvement over a traditional air cycle. Using natural gas as a fuel, APC can reach a minimum thermal efficiency of 41.5% under specific conditions, of low equivalence ratios at high compression ratios (L. Li et al., 2018b).

Theoretical analyses have further explored the potential of the argon cycle in various applications. A case study by (Hodgson et al., 2021b) employed a thermodynamic model to evaluate the performance of a combined Argon-Brayton cycle for power generation which helps to understand the outcome for Ar as the working fluid in the combustion model. Their result suggested that the cycle could achieve efficiencies exceeding 50%, surpassing the conventional air-based Brayton cycles. It is also highlighted by the authors that the importance of optimizing the compression and expansion stages to fully exploit argon's thermodynamic properties with less NO_x emission.

The APC eliminates NO_x by excluding N_2 from the system, thereby removing the need for costly exhaust gas after-treatment. The cycles also reduce unburnt hydrocarbon

emissions and greenhouse gas emissions due to increased efficiency and optimized combustion processes. The engine load in the APC can be controlled by adjusting the equivalence ratio and oxygen content, providing flexibility in practical applications. Spark-assisted compression ignition (SACI) can further enhance combustion stability and thermal efficiency by reducing the coefficient of variations of the indicated mean effective pressure (IMEP) by up to 84% (Hodgson et al., 2021b).

Modification to the APC with fossil fuel, such as methane as fuel in combination with argon has some major advantages over traditional gasoline engines. Argon can increase in-cylinder temperature, which may heighten the likelihood of knocking, making the engine more prone to auto-ignition. Therefore, while argon can affect combustion characteristics, it does not necessarily enable the use of higher compression rates without the risk of knock, thus enhancing engine efficiency (Hodgson et al., 2021a). Previous research work by (Jan et al., 2020) have clearly shown that the use of argon gas instead of nitrogen in the combustion process enhances in-cylinder temperature at TDC to enhance natural gas's compression ignition. This leads to enhanced combustion quality and ignition characteristics as manifested by decreased ignition delay at different operating conditions (Shahsavan et al., 2018a).

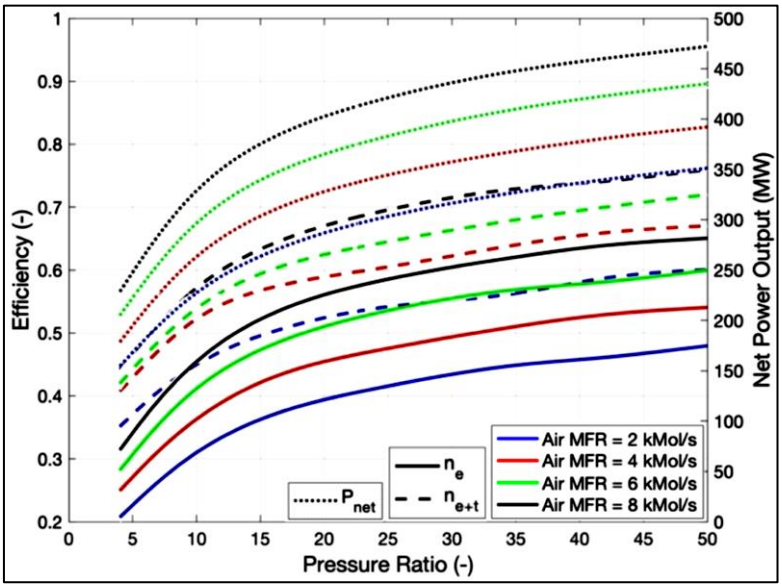

Figure 6 Overview of the methane-argon cycle performance (Hodgson et al., 2021a)

In Figure 6 the plot shows how the pressure ratio affects efficiency and net power output at different air mass flow rates (MFR). The X-axis represents the pressure ratio while at the left why exists indicates efficiency, and the right Y-axis shows net power output in megawatts (MW). The n_e (black solid line) reflex system efficiency and n_{e+t} (coloured lines) represent combined efficiency at specific air MFRs: 2 Kmol/s (blue), 6 Kmol/s (green), and 8 Kmol/s (black). The P_{net} (black dotted lines) denotes net power output. As the pressure ratio increases, efficiency improves from around 0.3 to 0.65, while net power output rises from about 50 MW to 400 MW. Higher air MFRs enhance power output but do not proportionally increase efficiency (Hodgson et al., 2021a).

Research on APC of methane direct injection engines by (Wang et al., 2024) reported a peak indicated thermal efficiency of 51.1% which is particularly significant for small bore engines, where state-of-the-art platforms typically achieve around 42%. However, this efficiency gain is a less remarked symbol for large-bore marine engines which commonly achieved similar efficiency levels. The discrepancy in thermal efficiency between large and small engines can be attributed to differences in bore size and operating speeds. Large bore engines benefit from greater displacement and lower engine speeds, naturally enhancing efficiency. In contrast, smaller engines like three-cylinder SI engines in that study (bore = 73.4 mm, 1000 rpm), face greater challenges making the reported efficiency particularly noteworthy.

The study further explored the Impact of APC quit-wearing argon ratios (Ar). At Ar= 79% significant improvements were observed while increasing AR to 85% had a more modest effect. Additionally boosting the intake pressure (P_i) in combination with a high AR- 85% proved effective in improving lean combustion and thermal efficiency. This result highlights APC's potential to further improve the performance of methane-fuelled engines, especially when combined with advanced techniques such as direct injection and intake pressure boosting. Future investigations into higher compression ratios could provide additional insights into maximizing these efficiency gains.

2.4 Towards APC with Hydrogen as Fuel

2.4.1 State of the Art in Research on APC with Hydrogen

The combustion of hydrogen in APC completely eliminates carbon dioxide emissions, an idea that, as noted by (Mohammed, 2018), probably as old as the internal combustion engine itself. (Boer et al., 1978) demonstrated the feasibility of hydrogen engines in terms of performance, highlighting their higher specific heat ratio compared to gasoline, which enhances thermodynamic efficiency.

Experimental analysis has been conducted by (Hodgson et al., 2021a) at 1000 rpm and a 9.6 compression ratio, with an IMEP of 0.1 to 0.6 MPa shows a peak efficiency of 53.5%, without water injection at argon ratio of 79%,85%, and 90% in a hydrogen-fuelled engine. However, knock intensity reached at 3.4 MPa. With 16 mg of water addition per cycle decreased efficiency to 52.4%. In this investigation, the maximum efficiency and performance with a mass flow rate (FMFR) of 8 Kmol/s of the working fluid were compared for each cycle. It is also observed that the argon cycle fuelled with methane produced water at twice the rate of the hydrogen-argon cycle, resulting in more heat being available in the condenser(Hodgson et al., 2021a). Efficiency gains are achieved when comparing argon cycle engines to air-breathing hydrogen engines. Moreover, (Morovatiyan et al., 2022) specified that adding hydrogen to methane and addition of argon to constant volume combustion chamber (CVCC) setups enhances burning velocities, flammability limits, and efficiency. Additionally, (Ding et al., 2023) stated high concentration of argon with Hydrogen enhances the lean flammability limits and combustion speeds.

The utilization of hydrogen as a fuel offers significant advancements in thermal efficiency (L. Li et al., 2018b). The high specific heat ratio of argon enhances thermodynamic efficiency, rendering APC engines more efficient than conventional internal combustion engines (Stępień, 2021; Wang, Deng, et al., 2023). Additionally, the use of an argon oxygen mixture instead of air results in higher cylinder temperature and pressure. This facilitates easier ignition and faster combustion, thereby improving thermal efficiency (Wang,

Deng, et al., 2023). Moreover, the addition of hydrogen instead of methane combustion in an argon environment extends the flammability limits, in building more flexible and efficient combustion processes. Additionally, the use of argon as a working fluid effectively eradicates NO_X emissions, which is a significant concern in the conventional combustion process (Morovatiyan et al., 2022).

In literature, (Hodgson et al., 2021a) has outlined several challenges in hydrogen-fuelled APC engines. These include premature ignition, ignition delay, knock suppression, stoichiometric combustion techniques, and water presence. APC engine knocks can occur due to high in-cylinder temperatures resulting from argon's high specific heat ratio. Knock limits the compression ratio and consequently the thermal efficiency of the engine(Jin, Deng, Wang, et al., 2023; Wang, Deng, et al., 2023; Wang, Jin, et al., 2023b). Hydrogen-fuelled engines are also prone to abnormal combustion phenomena such as pre-ignition and backfire, which exacerbated in APC engines due to elevated temperature and pressures (Falfari et al., 2023; Stępień, 2021). The use of water injections to surpass knocks introduces the challenge of managing water within the engine system. Efficient separation and collection of water from exhaust gases are necessary to minimize the impact on the specific heat ratio of working fluids (Jin, Deng, Wang, et al., 2023). Optimizing hydrogen injection and ignition strategy is crucial to prevent abnormal combustion and achieve stable and efficient combustion. The optimization includes the need for an advanced ignition system and precise control injection timing (Falfari et al., 2023; Stępień, 2021; Wu et al., 2021).

There is a need for more research on the long-term durability and reliability of hydrogen-fuelled argon power cycle engines, particularly concerning the fuel injection systems and the impact of high temperatures on engine components (Falfari et al., 2023; Stępień, 2021). More comprehensive modelling and simulation studies are required to accurately predict the behaviour of hydrogen combustion in APC engines and to develop robust control strategies for the injection and ignition process (Falfari et al., 2023). While experimental and theoretical studies show promises, there is a gap in the industrialization and

scalability of hydrogen-fuelled APC engines. Further research is needed to address the practical challenges of integrating these engines into commercial applications (Wang, Jin, et al., 2023b).

2.4.2 Closed Cycle HAPC Technology

With the unique properties of hydrogen as fuel and combining them with the principle of the APC, a new solution has been developed to improve engine efficiency and reduce emissions, known as the hydrogen argon power cycle (HAPC). By leveraging both the high thermal conductivity of argon to enter the eco-friendly, high-energy potential of hydrogen, the closed-loop HAPC creates an efficient and sustainable power cycle. The term closed loop refers to the recycling of the working fluid (Argon) Within the system, rather than releasing it into the atmosphere. This cycle is designed to operate without the intake of fresh air or expulsion of exhaust gases, which is a significant departure from traditional open-cycle internal combustion engines (Hodgson et al., 2021a; Ngwaka et al., 2021).

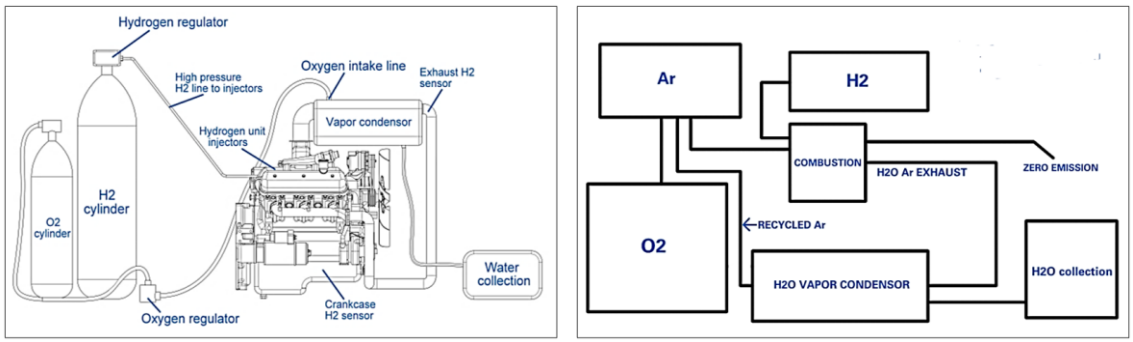

Figure 7 Overview of Closed Cycle Hydrogen Engine Technology (Pochari, 2019)

Further performance improvements were achieved by integrating additional components such as an intercooler, reheater, same source, and regenerator as illustrated in Figure 7. Second this modification has been shown to increase efficiency to 64% under comparable operational conditions (Pochari, 2019). Additionally, investigations into methane-fuelled APC cycles and the use of alternative working fluids like helium and air revealed the hydrogen cycle, although the costliest to operate, was the most efficient across various pressure ratios where HAPC is promising (Hodgson et al., 2021a).

Further research on hydrogen direct injection and intake boosting in closed-loop HAPC engines indicated that these injection strategies (DI and PFI) could significantly increase the indicated mean effective pressure and thermal efficiency. The implementation of super lean combustion and port water injection was found to be effective in mitigating knock and broadening the operational range, achieving a maximum gross indicated thermal efficiency of 59.35% (Ding et al., 2023).

Future development of closed-loop HAPC engines will likely focus on optimizing combustion strategies and addressing knock suppression. Innovations such as ultra-lean combustion, ceramic insulation coating for pistons, low friction lubricants, and an efficient argon separation system are expected to play a crucial role in advancing this technology (Wang, Jin, et al., 2023a). Continued research into the fundamental combustion characteristics and operational parameters will be essential for the successful industrialization of HAPC engines (Stępień, 2021). Alongside strategies using knock suppression and optimal combustion process, hydrogen-argon cycles are evidently energy-efficient and low-emission options to improve internal combustion engines (Van Oijen, 2019b; Wu et al., 2021).

2.4.3 Autoignition Properties of H_2-O_2 Mixtures in Argon Atmosphere

Autoignition which is also known as subsequent combustion and self-ignition of a fuel-oxidant mixture heated by a surface without the presence of an additional ignition source such as a spark or flame in the combustion chamber (Bounaceur et al., 2016). Autoignition of hydrogen poses a significant challenge in the development of the hydrogen-argon power cycle (HAPC). Uncontrolled auto-ignition can lead to knocking, reduced power output, or even engine damage. Researchers at Tongji University (Jin, Huang, et al., 2021; Wang et al., 2023) have focused on producing ultra-lean and highly diluted combustion in HAPC engines to address these issues. This approach aims to mitigate knock and improve engine efficiency.

A comprehensive study on autoignition characteristics of H2-O2 mixtures with argon and nitrogen dilutions was conducted using a rapid compression machine (Samimi-Abianeh et al., 2019). The research highlighted the sensitivity of ignition delay times to temperature, pressure, and dilution ratios. Measurements were taken at pressures of 1.0, 3.0, and 5.0 MPa and temperatures ranging from 903 K to 1042 K. The study found that the ignition delay time of hydrogen is highly sensitive to temperature, especially near the ignition limit. Additionally, the argon ratio in the diluent significantly affects the ignition delay. A higher argon ratio leads to longer delays. High pressure accelerates autoignition, while a high dilution ratio inhibits it. Key reactions sensitive to different conditions were identified, providing valuable insights for developing kinetic models of HAPC engines (Jin, Shu, et al., 2021).

Another study by (Kosarev et al., 2007) focused on the kinetics of autoignition in rich N_2O-H_2-O_2-Ar mixture at high temperatures (1000 K to 2700 K) and pressures (0.1 to 10atm). Using a shock tube experiment, researchers obtained data on ignition delay times in a mixture of 50% to 90% argon. The study proposed a mechanism to describe the kinetics of the system, specifying rate constants for ratios involving N_20, NO, and OH. This research provides valuable insights into the chemical transformations occurring in rich H_2-O_2 mixture diluted with argon (Kosarev et al., 2007). The study found that the proposed kinetic scheme accurately predicts the auto-ignition behaviour of N_20 -$N0_x$ containing mixtures diluted with argon, with experimental and calculated ignition delay times showing good agreement, supported by sensitive analysis results.

The initiation characteristics of spark-ignited (SI) premixed H_2-O_2 flames with argon, nitrogen, and carbon dioxide diluents were investigated in a constant-volume combustion vessel. The result showed that high dilution ratios and excess oxygen ratios significantly lengthened the flame initiation periods compared to nitrogen and carbon dioxide. This suggests that argon-diluted mixtures could be feasible for ultra-lean and highly diluted combustion in APC engines (Jin, Huang, et al., 2021).

Additional studies have explored the autoignition behaviour of other fuel mixtures, such as propane and syngas, with different diluents. These studies provided a broader context for understanding the role of diluents in the autoignition process. For instance, the autoignition of propane mixtures with helium and argon on nitrogen diluents was investigated, revealing the impact of diluent choice on ignition relay and radical production (Samimi-Abianeh et al., 2019). Similarly, the influence of steam dilution on the auto-ignition of hydrogen, syngas, and natural gas blends was examined, highlighting the thermal and chemical effects of diluents under various conditions. However, no chemical effect of steam edition was observed for most mixtures except for the pure carbon monoxide, where the presence of water enhanced the formation of reactive OH radicals, thereby increasing reactivity. This study underscores the importance of understanding the thermal and chemical effect of diluents in the autoignition process (Donohoe et al., 2015).

The autoignition properties of H_2-O_2 mixtures in argon diluents are influenced by several factors, including temperature, pressure, dilution ratio, and the presence of other gases. A high argon ratio and excess oxygen inhibit auto-ignition, while high pressure accelerates it. Understanding these factors is crucial for optimizing combustion processes in applications such as APC engines. Further research is needed to explore detailed kinetics and potential strategies for controlling auto-ignition in these systems for HAPC. Despite the potential, Hydrogen-Argon Power Cycle (HAPC) engines face significant challenges, including knock suppression due to high in-cylinder temperatures, abnormal combustion phenomena, and limitations in increasing the compression ratio. Effective knock mitigation strategies, such as port water injection, are essential to expanding the operational range and improving overall engine reliability.

2.4.4 Effects of Compression Ratio (CR) and mixture composition on HAPC

A recent study by Livermore National Laboratory (Killingsworth et al., 2011) and UC Berkeley (Sierra Aznar, 2018b) investigated H_2 with air and oxygen mixture across a compression ratio between 4.5 to 7, identifying knock as a limiting factor beyond CR 7.

Another examination was done at a constant engine speed of 900 rpm and a coolant temperature of 75°C, with argon concentrations of 84%, 86%, and 88% which have been illustrated in Figure 8.

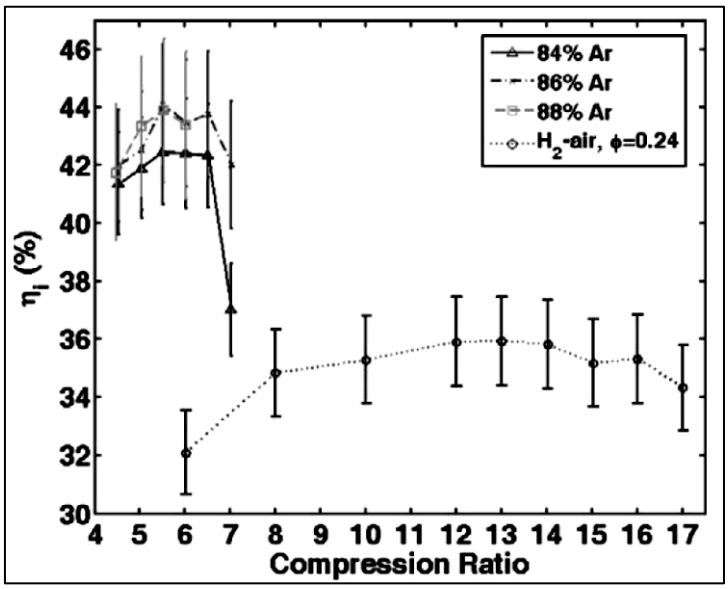

Figure 8 Indicated thermal efficiency versus compression ratio H_2-O_2-Ar mixtures (Killingsworth et al., 2011)

The result indicated that advanced spark timing increases engine torque, however, it also highlighted the risk of knocking. CR 5.5 was highlighted as the most efficient, especially underload operation with high argon concentration. A critical finding was the motor temperature at TDC for the compression of 6 H_2-O_2-Ar mixture Was comparable to that of a CR 16 H_2-air mixture highlighting the efficiency gains due to reduced heat transfer, faster burn rates, and less unburnt fuel (Killingsworth et al., 2011). (Wang, Jin, Deng, Ding, et al., 2023c) extended the findings of compression ratio by testing hydrogen-fuelled APC engines with argon ratio from 71% to 99% and across the compression ratio of 5 to 19. At CR 7 and with 91% argon a remarkable 70% thermal efficiency was achieved significantly higher than the 52% efficiency of the hydrogen-air cycle. However, argon's high specific heat ratio elevated compression temperatures which raise the pre-ignition. Split-cycle engines and direct hydrogen injection were proposed as mitigation strategies for this (Jin et al., 2021).

(De Boer & Hulet, 1980) investigated H_2-O_2-Ar combustion over a wider range of compression ratios 5.5 to 12, identified challenges at higher compression ratios included power loss and unstable operation at CR 12. Although efficiency gains of over 70% were reported, the knocking was observed particularly at CR 7. Autoignition occurred before spark timing, in addition, technological developments have targeted these challenges. (Robert et al., 2017) reported that air-recirculating noble gas in internal combustion engines that integrated variable valve timing (VVT) and a closed loop argon recycling system optimized combustion while reducing pre-ignition. Moreover, (Sierra Aznar, 2023), in collaboration with Japanese researchers, explored Natural Gas (NG)/O_2/Ar mixtures in spark ignition engines, and found that APC extended lean limits and produced higher efficiency compared to air-based cycles. At CR of 8 had achieved 42% efficiency, while knocking limited operation at CR 12.5. In another study, (Aznar et al., 2017) examined those CH_4/O_2/Ar mixtures with direct injection (DI) concept. DI of fuel a 15% O_2 + 85% Ar mixture achieved a 44% efficiency at 7.3 bar IMEP, highlighting its potential to mitigate knocking and support a higher compression ratio compared to port-injected (PFI) systems.

(Rapp, 2011) investigated mixtures of H_2-O_2-Ar, at CRs between 4.5 and 5.5 achieved stable operation at lower CRs. However, at CR 7, knocking became excessive, demonstrating the limitations of hydrogen-argon combustion at higher CRs. Moreover, (Ikegami et al., 1982) investigated H_2-O_2-Ar in conventional compression ignition engines with DI. At CR 12.3, an IMEP of 8.4 bar and an improvement of 16% efficiency over air-based combustion, showcased the potential benefit of argon to enhance thermal efficiency. While argon-enhanced hydrogen combustion cycles can achieve efficiency improvements of over 70%, challenges such as knocking and pre-ignition persist. Advanced engine designs and optimized combustion control will be crucial for fully realizing the potential of these systems (Jeroen, 2019; Sierra Aznar, 2023).

2.4.5 Port Fuel Injection vs. Direct Injection of Hydrogen and Oxygen

Hydrogen Argon Power Cycle (HAPC) has limited research on injection methods that are very vital in enhancing combustion process efficiency and stability. Port Fuel Injection (PFI), Dual Injection (DuI), and Direct Injection (DI) are basically three major classes of fuel injection patterns shown in Figure 9 with their benefits and drawbacks (Van Den Brink, 2022b).

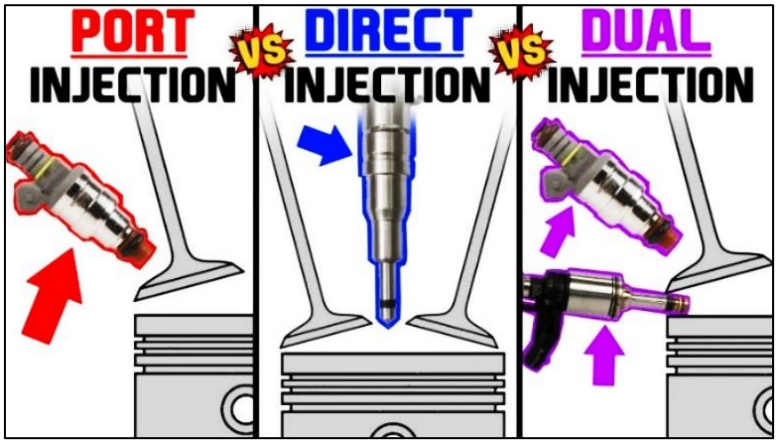

Figure 9 Port vs Direct vs Dual Injection (Bimmertips, 2021)

This section gives a comparative analysis of these strategies examining combustion stability, efficiency, lean limit, volumetric efficiency, and techno challenges. Based on the existing literature review and the development of novel research directions that will be discussed further, the following objectives are set to strive to clarify the way toward enhancing HAPC for future energy systems. The injection strategy of H_2 and O_2 into the cycle can be viewed as both a difficult and an opportunity to improve the performance of the APC since it provides the system with an additional degree of freedom. (Van Den Brink, 2022b) illustrated that the injection of both hydrogen and oxygen into an internal combustion engine can be accomplished using four potential strategies shown in Figure 10: port injection (PI) or direct injection (DI) for each gas. The investigation by (Van Den Brink, 2022a) focused exclusively on two specific configurations, which are the direct injection of oxygen (DI-O_2) and the direct injection of hydrogen (DI-H_2) into the

combustion chamber. The alternative configurations, PI-H_2-O_2 and DI-H_2-O_2 were outside the scope of the investigation.

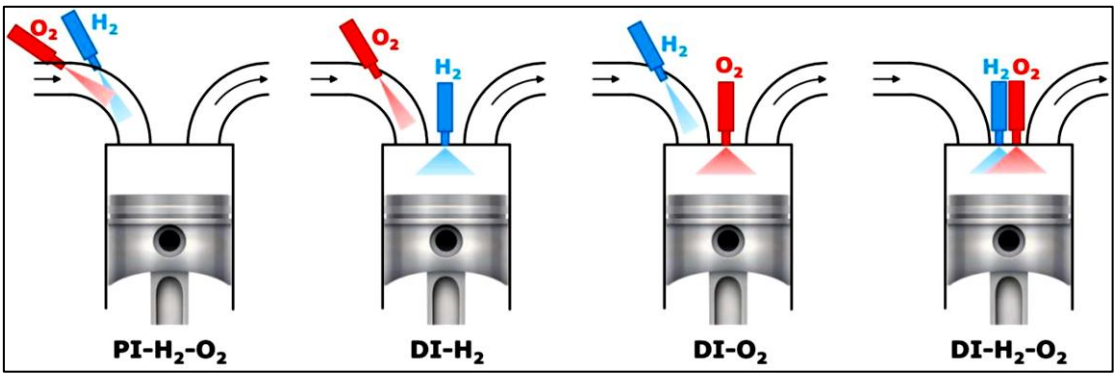

Figure 10 Port Injection (PI) and Direct Injection (DI) basic injection configurations for the APC (Van Den Brink, 2022b).

The study of these injection strategies represents a relatively novel area of research. While the combustion of hydrogen in ICEs has been previously examined, high-pressure direct injection in compression ignition (CI) engines, particularly in argon environments, remains largely unexplored. Nevertheless, the direct injection of hydrogen may encounter challenges due to the low penetration of the light hydrogen gas, which can hinder the effective mixing process. Conversely, the denser nature of oxygen in DI-O_2 could potentially address these issues by enhancing the mixing and reaction process. Therefore, it is essential to investigate the gaseous injection of hydrogen and oxygen and their respective impacts on mixing and reaction dynamics within the combustion chamber.

Table 6 aims to contribute to the understanding of these injection strategies and their potential benefits and drawbacks in ICEs. The following table obtained from the literature (N. Kim et al., 2015; Van Den Brink, 2022a; Xinyu et al., 2020) present a comparison of Port Fuel Injection (PFI) and Direct Injection (DI) systems: Combustion stability and efficiency; Extension of lean limit; Volumetric efficiency and boosting requirement; and technical challenges.

Table 6 Injection Method Comparison (N. Kim et al., 2015; Van Den Brink, 2022a; Xinyu et al., 2020)

Aspect	Port Fuel Injection (PFI)	Direct Injection (DI)
Combustion Stability and Efficiency	Enhanced stability with hydrogen-methane blends due to accelerated chemical kinetics.	Superior volumetric efficiency and reduced backfire risk. Better control over the fuel-air mixture enhances combustion efficiency.
Lean Limit Extension	Extends lean limit, enhancing efficiency at lower fuel-to-air ratios.	Achieves lean limit extension by injecting small amounts of hydrogen directly into the combustion chamber, improving turbulence and charge stratification.
Volumetric Efficiency and Boosting Requirements	Typically, lower volumetric efficiency is compared to DI due to fuel displacing intake air.	Significantly improves volumetric efficiency by injecting fuel directly into the combustion chamber, without displacing intake air. Requires robust injectors and higher injection pressures.
Technical Challenges	Risk of backfire, particularly with hydrogen fuelling. Requires precise control of fuel-air mixture.	Demands high-pressure and high-temperature-resistant injectors. Injection systems must deliver fuel at high flow rates.

2.4.6 Advancements and Challenges in iHAPC

The integration of HAPC introduces greater flexibility and better control over combustion. Despite their potential advantages, HAPC faces significant challenges such as knock suppression due to high in-cylinder temperatures, abnormal combustion phenomena, and limitations in increasing the compression ratio (Mansor et al., 2022; Van Oijen, 2019a). Several studies have focused on enhancing the thermal efficiency of HAPC engines. For

instance, the implementation of hydrogen direct injection and intake boosting has been shown to significantly increase the indicated mean effective pressure and thermal efficiency (Ding et al., 2023). Specifically, hydrogen direct injection at 1000 rpm increases the indicated mean effective pressure from 0.39 MPa to 0.72 MPa, achieving a maximum gross indicated thermal efficiency of 57.89%. Additionally, For the water injection in HAPC, under intake boosted conditions further increased the maximum gross indicated thermal efficiency to 59.35% to showdown operational flexibility (Ding et al., 2023).

Operational flexibility is crucial for the practical application of HAPC engines. The use of the Miller cycle in turbocharged hydrogen engines has been shown to increase power density and reduce brake-specific fuel consumption (BSFC). The Miller cycle achieved a 37.7% higher brake power (BP) and a 16% lower BSFC compared to lean burn and stoichiometric equivalent ratio burn methods (Luo & Sun, 2016). This indicates that the Miller cycle can effectively enhance the operational flexibility of HAPC engines. Moreover, the application of coaxial injection technology in hydrogen-fuelled argon engines has improved the mixing process and combustion performance. This technology allows for better control of the flame characteristics, which is essential for maintaining operational flexibility under varying conditions (Wu et al., 2021).

Despite the promising efficiency and flexibility metrics, the high in-cylinder temperatures associated with argon cycles can lead to knocking, which impeded the argumentation of compression ratio and practical efficiency. Studies have shown that port water injections can effectively mitigate knocks, thereby broadening the operational range of intake-boosted conditions (Ding et al., 2023). Comparative studies have also been conducted to evaluate the performance of HAPC engines against other configurations. For example, a study by (Hodgson et al., 2021a) on closed-loop oxy-hydrogen Brayton power cycle found that modifying the cycles with an intercooler, reheater and regenerator could increase efficiency under typical operating conditions (Hodgson et al., 2021a). This highlights the potential for further optimization of HAPC engines through innovative cycle modifications.

These studies indicate that significant advancements have been made in enhancing the efficiency and operational flexibility of hydrogen argon power cycle engines. Techniques such as hydrogen direct injection, intake boosting, and the Miller cycle have shown substantial improvements in performance metrics. However, challenges such as knock separation and abnormal combustion remain, necessitating ongoing research and development to fully realize the potential of HAPC engines.

2.5 Developments of 1D-Engine Modelling and Simulation

Numerical studies of 1D simulation have played a crucial role in advancing the understanding of APC. Computational fluid dynamics (CFD) simulations and thermodynamic models have provided insights into the optimal conditions for Argon (Ar) utilization. For example, (E. Zhang et al., 2017) conducted a series of CFD simulations to analyze the combustion characteristics of an argon-hydrogen mixture on a 0.402 L, single-cylinder diesel engine that has been modified into a spark ignition engine with a port fuel injection system. The study demonstrates that combustion stability, which refers to the consistency and uniformity of the combustion process with minimal fluctuation in pressure and energy release, was significantly improved by the addition of argon. This enhancement in instability led to a notable reduction in peak temperature and the corresponding decrease in NOx emissions. Moreover, it found that there was a very strong correlation between P_{max} and its corresponding crank angle, and the absolute value of the correlation coefficient between the two was up to 0.926 for the operation with Ar-O_2-H_2 mixtures. Figure 11 represents a structural framework of engine simulation, combining combustion and system-level analysis at multiple scales (0D/1D, 3D and CFD). It demonstrates the interaction between advanced combustion technology and predictive models for knock, misfire and combustion stability, underscoring the importance of turbulence, frame geometry, and end-cycle variability in enhancing engine performance.

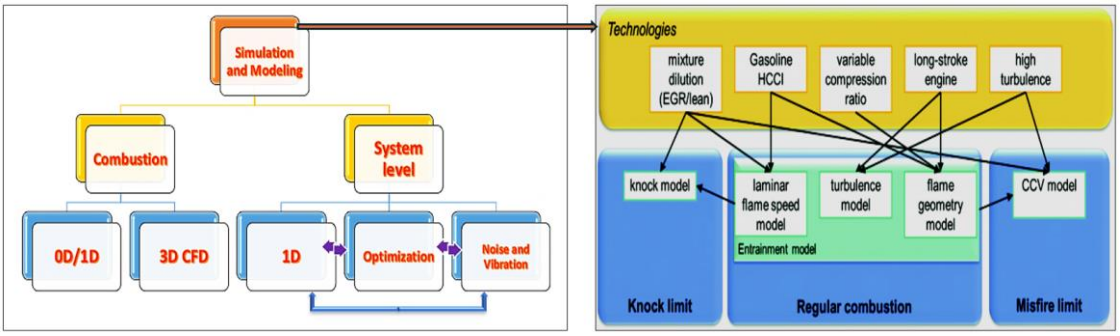

Figure 11 An Overview of 1D Engine Simulation (Grill et al., 2019)

In 1D engine simulation modelling technology becomes a crucial part of finding out the heating, and thermal aspects of combustion engine models and determining their performance and emission rate. Integrating the existing 1D models where Finite element analysis (FEM) is employed for the calculation of heat distribution and its dissemination through an element at a node can be considered as an alternative to Computational fluid dynamics (CFD) to Conjugate Heat Transfer (CHT) full-scale scenarios (Stefano Alberto Malan Loris Ventura, 2023). The transient 1D engine model considers the full engine setup, including the boosting system, the air and exhaust channel, the EGR path (both high and low pressure), and the combustion chamber. 1D simulation is the process of modelling the dynamics and integration of numerous components within complex systems using empirical data and physics equations.

2.5.1 General Assumptions of 1D-modeling and Governing Components Sub-models

In the modelling of airpath systems and sub-models GT suite software is widely employed to simulate the dynamic behaviour of air intake and exhaust gases. To maintain computational efficiency while accurately capturing critical flow phenomena, A 1-dimensional modelling approach is adopted. The method assumes the flow properties such as pressure temperature and velocity very only along the primary flow direction, the negligible variation across other dimensions. The simplification enables models of complex airport geometries efficiently while preserving the essential dynamics required for optimizing engine performance (Kulkarni et al., 2019).

a) General Assumptions in 1D Airpath Modelling

Several key assumptions underpinning the only modelling approach, allowing for a streamlined but effective representation of the airpath have been illustrated in Table 7.

Table 7 An overview of the general Assumption in 1D airpath modelling (Gamma Technologies, 2024c)

Assumption	Description
One-Dimensional Flow	Flow variables (pressure, temperature, velocity) are assumed to vary only along the axial direction, neglecting radial and transverse variations. This simplifies flow dynamics in components like pipes and manifolds.
Quasi-Steady Flow	Though engine operations are transient, flow is treated as quasi-steady at each time step. Variations are gradual, allowing for steady-state assumptions in computations.
Compressible Flow	Gases, including intake air and exhaust, are treated as compressible, governed by the ideal gas law ($p = \rho RT$), linking pressure, density, and temperature.
Component-Specific Sub-Models	Each component (compressor, turbine, intercooler, etc.) is modelled individually using empirical data and fluid dynamic principles, capturing performance under varying conditions.
Thermodynamic Equilibrium	Each control volume assumes uniform thermodynamic properties, simplifying temperature and pressure calculations.
Heat Transfer and Frictional Losses	Heat exchange with surrounding walls and friction losses are included, as they impact airpath efficiency.

b) Fluid Dynamics Governing Equations

The 1D-air path model employs several key assumptions to streamline the representation of flow dynamics. First, it assumes 1D flow, meaning that flow variables vary exclusively along the axial direction while neglecting radial and transverse variations. This simplification is particularly beneficial for analysing components such as pipes, manifolds, and turbochargers. Second, the model treats the flow as quasi-steady, allowing for gradual changes in flow parameters at each time step, despite the transient nature of engine operations.

Additionally, the gases, including air intake and exhaust illustrated in Figure 12, are considered compressible fluids and are modelled using the ideal gas law, expressed as $p = \rho RT$, where p denotes pressure, ρ represents density and T signifies temperature. Each component with the airport, such as compressors, turbines and intercoolers, is characterized by component-specific sub-models derived from empirical data and fundamental fluid dynamics principles, ensuring accurate performance representation across varying conditions.

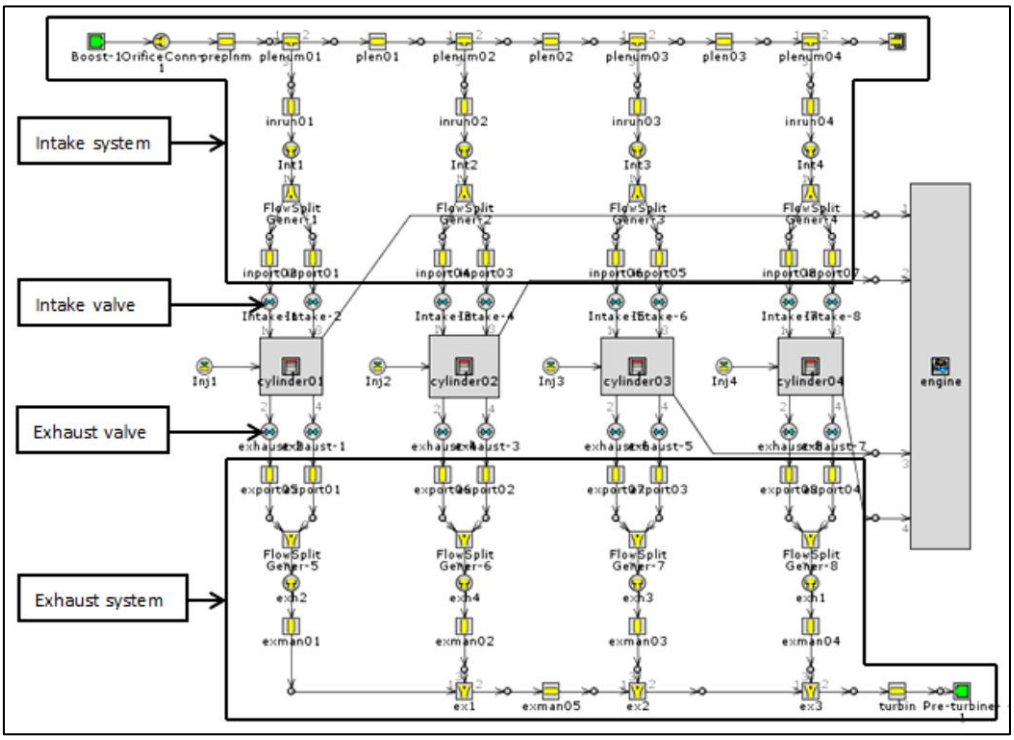

Figure 12 An overview of Physics based 1 d airpath model (CA resolution) Detail airpath representation including pulsations (Gamma Technologies, 2024d).

The model also presumes thermodynamic equilibrium within each control volume, suggesting that state variables such as temperature and pressure are uniform and do not vary significantly within a single volume. Finally, it incorporates heat transfer and frictional losses which are critical factors influencing the overall efficiency and the engine path by accounting for interactions between the gas and component surfaces.

To facilitate the analysis, the entire system is discretized into multiple volumes, with each flow split represented by a single volume and each pipe divided into one or more volumes. These volumes are interconnected by boundaries. Within each volume, scalar variables such as pressure, temperature, density, internal energy, enthalpy, and species concentrations are assumed to be uniform shown in Figure 13. In contrast, vector variables including mass flux velocity and mass fraction fluxes are calculated at boundaries. This approach to discretization is known as a staggered grid.

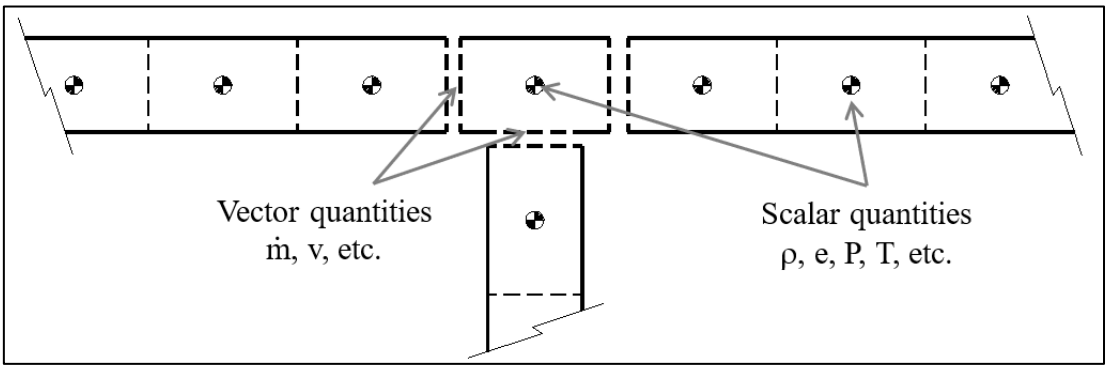

Figure 13 The Schematic of staggered grid approach: scalars calculated at centroid, vector quantities at boundaries (Gamma Technologies, 2024a)

The conservation equations solved by GT-Suite are shown below with proper elaboration in equation 2.4 to 2.12 (Gamma Technologies, 2024a). The left-hand side represents the derivatives of the primary variables. The methods to calculate the secondary variables, such as pressure and temperature, are discussed below in the discussion of the explicit solvers in equation 2.5 and implicit solvers in equation 2.6.

$$\textbf{Continuity: } \frac{\mathrm{dm}}{\mathrm{dt}} = \sum_{\mathrm{boundaries}} \dot{\mathrm{m}} \qquad 2.4$$

$$\textbf{Energy: } \frac{d(me)}{dt} = -\rho\frac{dv}{dt} + \sum_{boundaries}(\dot{m}H) - hA_s(T_{fluid}\text{-}T_{wall}) \text{ (explicit solver)} \quad 2.5$$

$$\textbf{Enthalpy: } \frac{d(\rho HV)}{dt} = \sum_{boundaries}(\dot{m}H + V\frac{dp}{dt} - hA_s(T_{fluid}\text{-}T_{wall}) \text{ (implicit solver)} \quad 2.6$$

$$\textbf{Momentum: } \frac{d\dot{m}}{dt} = \frac{d\rho A + \sum_{boundaries}(\dot{m}u) - 4Cf\frac{pu|u|dxA}{2\ D} - Kp(\frac{1}{2}pu|u|)A}{dx} \quad 2.7$$

In equations 2.4 to 2.12 the used variables are interpreted as follows:

$\dot{m}$	boundary mass flow rate into volume
m	mass correspondent to a specific volume
V	volume
P	pressure
ρ	density
A	cross-sectional flow area
As	heat transfer surface area
E	total internal energy (internal energy and kinetic energy per unit mass)
H	total specific enthalpy
h	heat transfer coefficient
T_{fluid}	the temperature of the fluid
T_{wall}	wall temperature
u	velocity at the boundary
Cf	Fanning friction factor
Kp	pressure loss coefficient (commonly due to bend, taper or restriction)
D	equivalent diameter
Dx	length of the mass element in the flow direction (discretization length)
dp	pressure differential acting across

c) Component Sub-Models in 1D Airpath Modelling

To accurately represent complex engine components in the airport, 1D modelling uses a specialized sub-model for different parts of the system (Gamma Technologies, 2024b):

Pipes and Ducts: The flow in pipes is discretized into control volumes, and pressure losses due to the friction are calculated using empirical formulas like the fanning friction factor. Heat transferred through the pipe walls is also accounted for, which can significantly affect gas temperatures.

Valves and orifice: flow through valves is modelled using the discharge coefficient and pressure drop across the valve. The mass flow rate is determined by the following equation 2.8 (Gamma Technologies, 2024d). Where C_d is the discharge coefficient, A is the valve area, and ΔP is the pressure differential.

$$\dot{m} = CdA\sqrt{2\rho\Delta p} \qquad 2.8$$

Turbochargers: Turbocharger modelling involves both the compressor and turbine. These are represented by performance maps, which describe the relationship between pressure ratio, mass flow rate, and efficiency as a function of shaft speed. These allows the model to capture how the turbocharger affects intake air density and exhaust flow which can be illustrated in the following equation 2.9 (Gamma Technologies, 2024a). In the following equation Πc refers to the pressure ratio across the system while N is the rotational speed of the turbocharger.

$$\dot{m} = f(\Pi c, N) \qquad 2.9$$

Intercoolers: modelled using the effectiveness-NTU method, intercoolers reduce the temperature of compressed air before it enters the engine. The heat transfer is given by equation 2.10 where E is the heat exchanger's effectiveness, C_{min} is the minimum heat capacity rate, and Tair and T coolant temperature of the air and coolant respectively.

$$\dot{Q} = \in Cmin\,(Tair - Tcoolant) \qquad 2.10$$

Workflow Solution and Crank-Angle Resolution: To achieve accurate modelling of transient phenomena, particularly valve events and combustion dynamics, the flow and

thermodynamics properties are resolved using crank-angle (CA) resolution. Instead of conventional time steps, each time step corresponds to a small increment of crankshaft rotation which can be denoted by equation 2.11.

$$\Delta t = \frac{\Delta\theta}{\omega} \qquad 2.11$$

In the equation, Δt is the time step, $\Delta\theta$ is the crankshaft angle increment, and ω is the crankshaft's angular velocity. The fine resolution allows for high-precision modelling of flow pulsations, backpressure, and valve interactions crucial for optimizing engine breathing dynamics and combustion efficiency.

Pulsation Effect and Airpath Dynamics: In high-performance or turbocharged engines, pressure waves from valve events create pulsation in the intake and exhaust systems. This pulsation can alter air density, influencing the engine's air-to-fuel ratio, combustion efficiency, and turbine performance in the turbine-charged system. The only model captures this pulsation by solving the compressible flow Navier Stokes equation 2.12.

$$\frac{\partial(\rho u)}{\partial t} + \frac{\partial(\rho u + p)}{\partial x} = -\tau, \omega A \qquad 2.12$$

In equation, incompressible flow $\frac{\partial(\rho u)}{\partial t}$ represents time derivation of momentum density, $\frac{\partial(\rho u+p)}{\partial x}$ presents convective and pressure terms**.**

Pulsation, especially in turbocharged engines, plays a critical role in affecting air density and turbine performance, influencing boost pressure and overall engine output. As it is A 1D airpath modelling serves as a vital tool for optimizing engine breeding dynamics, where the equations (2.4 to 2.12) help for turbocharger matching, emission control, and transient performance by understanding the gradients in the simulation environment. By simplifying complex fluid flow and preserving key dynamics, one of the models provides valuable insight into engine efficiency, emissions, and real-world performance under various operating conditions.

2.5.2 Engine Cylinder Modelling

a. 0D thermodynamic model of engine cylinder

GT Suite combustion models are typically based on a zero-dimensional (0D) thermodynamic framework, which simplifies the intricate process with an engine cylinder by assuming uniform properties such as pressure and temperature across the entire volume at any given time set-up, this assumption enables the model to efficiently simulate engines cycles without the computational complexity associated with multidimensional models like 1D or 3D computational fluid dynamics CFD. Despite its simplicity, a 0D model captures the key thermodynamic behaviours essential for understanding engine performance.

The 0-D thermodynamic model is primarily governed by the first law of thermodynamics, which for a closed system can be expressed in equation 2.13 (Gamma Technologies, 2024a).

$$\frac{dE}{dt} = \dot{Q} - \dot{W} + \sum \dot{m}i.hi \qquad 2.13$$

In the equation above $\frac{dE}{dt}$ is the rate of change of the internal energy within the cylinder, $\dot{Q}$ is the rate of heat added to the system, $\dot{W}$ is the rate of work done by the system on the piston, and $\sum \dot{m}i.hi$ represents the enthalpy associated with mass entering or leaving the system.

However, during the compression and expansion strokes, the engine cylinder is typically considered a closed system, meaning that there is no mass flow in or out. Thus, the energy conservation equation is simplified by equation 2.14 (Gamma Technologies, 2024a).

$$\frac{dU}{dt} = \dot{Q} - \dot{W} \qquad 2.14$$

In equation 2.14, U is the internal energy of the gas in the cylinder, $\dot{Q}$ represents the heat transfer from the gas due to combustion and heat exchange with the cylinder walls, $\dot{W}$ is the work which has been done by the gas on the piston as it expands or compresses.

The simplified equation reflects the balance between the heat transfer to the system and the work done by the gas which directly impacts the internal energy.

The internal energy of the gas in the cylinder is related to its specific internal energy (u) and the mass (m) of the gas. For an ideal gas specific internal energy is a function of the temperature, and it can be stated as $u = C_v T$. The C_V has a specific heating capacity and constant volume. Therefore, the rate of change of internal energy can be expressed as in equation 2.15 (Gamma Technologies, 2024a).

$$\frac{dU}{dt} = m.Cv.\frac{dT}{dt} \qquad 2.15$$

This equation shows that changes in internal energy are directly related to changes in temperature, assuming the mass of the gas remains constant during compression and expansion strokes. Another crucial factor is work done by the gas on the piston stated before in equation 2.14 during the engine cycle which can be denoted by the following equation (Gamma Technologies, 2024a).

$$\dot{W} = P.\frac{dV}{dT} \qquad 2.16$$

As P is the pressure inside the cylinder. Volume V and its time derivative $\frac{dV}{dT}$ are determined by the crankshaft kinematics, which are predefined based on the engine's design. In GT power these values are pre-calculated by a crank train sub-model and passed to the cylinder model at each time step.

The gas inside the cylinder is treated as ideal gas and its behaviour is governed by the ideal gas law: $PV = mRT$. Where R is the specific gas constant. This equation combined with the energy conservation law allows the model to solve either pressure or temperature based on known variables.

To ensure computational efficiency the 0-D model makes several key assumptions such as uniform pressure and temperature throughout the cylinder treats the gas as following the ideal gas law and considers the specific heat capacity C_v as constant although

advanced key models may account for temperature dependence. Overall, the 0D thermodynamic model in GT power simplifies complex engine processes effectively balancing efficiency and accuracy. By capturing essential phenomena such as combustion, heat transfer, and work generation it serves as a valuable tool for engine design and real-time simulations**.**

b. Combustion modelling

Combustion modelling refers to resolving the term $\dot{Q}_{\text{comb}}$ in the energy balance equation, which represents the rate of heat release during the combustion process. The term is critical for determining the thermal energy added to the system as a result of chemical reactions in fuel and oxidizer. Hence, the solution is typically obtained under equilibrium chemistry constraints where the concentrations of individual species are assumed to reach the equilibrium state. This equilibrium state is determined by assuming that pressure and temperature remain constant for a sufficiently long period allowing the system to reach chemical equilibrium (Nabi et al., 2019)..

In equilibrium combustion, the combustion products such as carbon dioxide and water are considered final at the end of the combustion process. Once chemical equilibrium is achieved the product can no longer undergo further oxidization to release additional heat. This assumption simplifies the combustion simulation process by eliminating the need to modelling intermediate reaction kinetics and treating them as instantaneous and final stage reactions. The general form of energy balance equation for an engine system which accounts for heat release from combustion, is expressed in equation 2.17 (Gamma Technologies, 2024a).

$$\frac{d}{dt}\left(\sum micv, iT\right) = \dot{Q}wall + \dot{Q}comb - p\frac{dV}{dt} + \dot{Q}evap + \sum \dot{m}\, ihi \qquad 2.17$$

Above equation, $\sum micv, iT$ represents the change in internal energy, where mi is the mass of species, $C_{v,i}$ is the Specific heat constant volume, and T the temperature, $\dot{Q}wall$ is heat transferred through the system boundaries, $\dot{Q}comb$ heat release from combustion the term to be modelled, $p\frac{dV}{dt}$ work done by the system as a result of volume change,

$\dot{Q}evap$ energy from evaporation or phase change, and $\sum \dot{m}\, ihi$ Mass flow and enthalpy exchange across system boundaries. The term $\dot{Q}comb$ which represents the heat release during combustion, is the key to understanding the thermal energy dynamics within the engine. In equilibrium chemistry, the term is derived by considering the complete oxidation of fuel to its final products without any additional reaction after equilibrium is reached.

In equilibrium combustion, the heat release is constrained to the point where no further oxidation occurs after products reach their final state. This means that for any given cycle the fuel and oxidizer have fully reacted to form stable products, and no further chemical reactions are possible. The approach simplifies the calculation of heat release by assuming that chemical reactions proceed directly to the completion without intermediate or partial states.

Coming to combustion heat release term the heat released during combustion $\dot{Q}comb$ is determined by the amount of fuel burned and the heat it produces upon combustion. The general form of the heat release equation is given below.

$$\dot{Q}comb(t) = mfuel \times\ LHV \times \dot{X}(t) \qquad 2.18$$

In the equation, $mfuel$ is the mass of the injected fuel, LHV is the lower heating value of the fuel indicating the amount of heat released per unit of fuel burned, $\dot{X}(t)$ is the time-dependent burn rate representing the friction of fuel combustion over time. The cumulative burn fraction X(t) is obtained by integrating the burn rate represented in equation 2.19. The resulting heat release profile directly influences the temperature and pressure in the cylinder affecting engine performance.

$$X(t) = \int_0^t \dot{X}\,(t)dt \qquad 2.19$$

In combustion modelling the fuel is typically a hydrocarbon or hydrogen that reacts with an oxidizer, usually oxygen either pure or in terms of air to produce heat and combustion products. A simple form of combustion reaction is given below:

$$\textit{Fuel} + O_2 \rightarrow CO_2 + H_2O + \textit{Heat}$$

In equilibrium chemistry, the fuel is completely oxidized into carbon dioxide and water with no intermediate species such as carbon monoxide remaining. The oxidizer is typically an air that contains about 21% oxygen and 78% nitrogen. Nitrogen acts as an inert substance not participating in the combustion process but absorbing some of the heat which affects overall thermodynamic behaviour. In the case of HAPC as it is a closed-loop cycle there will be no use of air as the oxidizer, but your oxygen and argon mixture will be used instead of air.

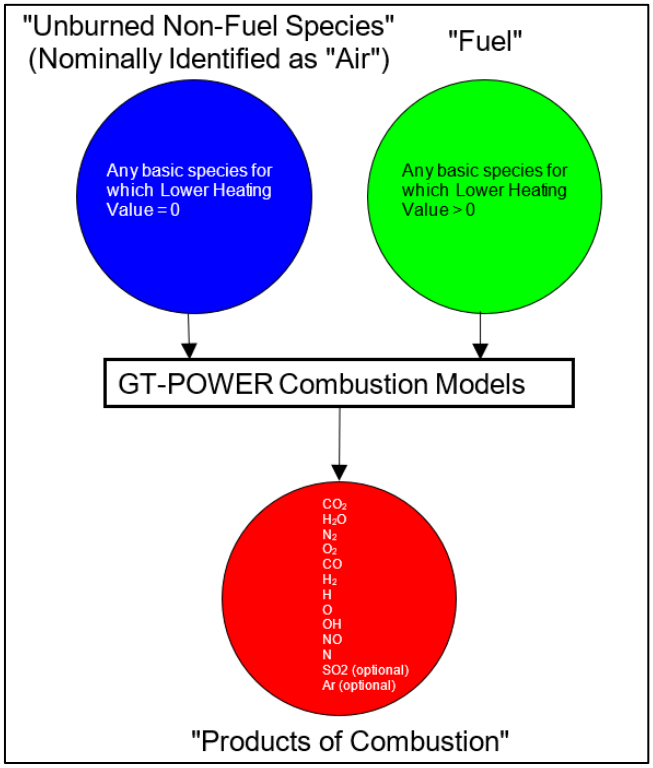

Figure 14 Fluid Properties Applicable to Combustion Systems Overview (Gamma Technologies, 2024a)

The working fluid in internal combustion engines consists of a mixture of combustion products such as CO_2 and H_2O and any residual unburned components. In equilibrium combustion models the working fluid composition is used to determine important properties such as temperature and pressure which drive the system's mechanical work output. A detailed overview of products of combustion in Combustion Modelling (CM) is shown in Figure 14 (Gamma Technologies, 2024a).

Seven types of reference objects can be used in GT Suite modelling to define fluid properties for combustion circuits (a combustion circuit is any flow circuit that contains one or more Engine cylinder, Catalyst brick, or Burner parts): Fluid Gas, Fluid Liquid in compress, Fluid Mixture, Fluid Mixture Burned, Fluid Mixture Combined, Fluid NASA-Liquid Gas, and Fluid Predefined. In GT-Suite from these reference fluid objects total energy added to the system from combustion is the integral of the heat release rate over time which can be determined from equation 2.20 below (Gamma Technologies, 2024a). Where, τ is the combustion duration.

$$Qcomb = \int_0^{\tau} \dot{Q}\, comb\,(t)dt = \int_0^{\tau} mfuel \times\ LHV \times \dot{X}(t)\ dt \qquad 2.20$$

The heat release rate contributes to increasing the temperature and pressure inside the engine cylinder, which directly drives the work output. The energy release profile is vital for modelling the cycle performance of the engine. In engine simulation, the combustion process can be modelled using various approaches, each balancing physical accuracy with computational complexity. GT power, a leading engine simulation tool, provides several combustion models, as summarized in Table 8. These models fall into three main categories: predictive models, non-predictive models, and combustion profile models (Gamma Technologies, 2024a).

Table 8 Combustion Models Overview for SI, Diesel, and HCCI Systems (Gamma Technologies, 2024a)

<table>
<tr><td></td><td colspan="2">Only 2-zone</td><td></td></tr>
<tr><td>Category</td><td>SI</td><td>Diesel</td><td></td></tr>
<tr><td rowspan="3">Predictive</td><td rowspan="2">SITurb</td><td>DIPulse</td><td>(Multi-zone → 2 + n pulses)</td></tr>
<tr><td>DIJet</td><td>(Multi-zone ~10-30)</td></tr>
<tr><td colspan="2">HCCI (Kinetic Combustion Model)</td><td>Only 1-zone; only kinetic solver</td></tr>
<tr><td rowspan="3">Non-Predictive</td><td>SIWiebe</td><td>DIWiebe</td><td rowspan="3">2-zone (default) or single-zone</td></tr>
<tr><td colspan="2">Multi-Wiebe</td></tr>
<tr><td colspan="2">Combustion Profile</td></tr>
</table>

A predictive combustion model is a combustion model where the burn rate is predicted from the appropriate inputs (pressure, temperature, equivalence ratio, residual function, etc), and then applied in the simulation. In predictive models, the rate of mass fraction burned $\dot{X}$(t) is computed based on real-time cylinder conditions and evolves dynamic alley with changes in the engines operating environment. Predictive models aim to capture the detailed physical processes of combustion but require more computational resources. For spark ignition (SI) engines, the burn rate model simulates combustion based on turbulence and Eddie dissipation, offering a high level of accuracy in the real-life engine. The G-equation model, another predictive approach, tracks flame propagation, making it particularly useful for complex flame dynamics. Both models provide detailed insights but take longer simulation times. For diesel engines, the DIJet models use a multi-zone approach typically 10-30 zones to simulate direct fuel injection and combustion offering a comprehensive view of spray and mixing dynamics. Alternatively, the mixing control model focused on air-fuel mixing and combustion requiring fewer computational resources while maintaining solid predictive capability (Gamma Technologies, 2024b).

Non-predictive models, in contrast, prioritize computational speed over physical accuracy. The “SIWiebe” and “DIWiebe” functions used for SI and diesel engines respectively applied simplified mathematical functions to approximate the combustion process. These models are particularly useful for fast simulations such as parametric studies of preliminary design iterations where detailed accuracy is less critical.

The semi-predictive combustion model builds upon the non-predictive approach by allowing the burn rate to vary based on model inputs like pressure from a temperature, and air-fuel mixture. The model is still relying on empirical data to look up tables, offering more flexibility than the non-predictive approach. The burn rate is adjusted according to the changes in engine operating conditions but does not fully simulate the underlying physical processes of combustion. Input parameters are updated through redefined relations, enabling quick adjustment to the burn rate under different conditions without

the need for complex computational models. Moreover, combustion profile models such as the two-zone and single-zone options allow users to define heat release profiles based on experimental or estimated data from real-life engines. The two-zone model divides the combustion chamber into burned and unburnt regions offering a more accurate representation than the single Joan model which assumes uniform combustion. The models are computationally efficient and often applied in early design phases or when experimental data is available for validation.

Selecting the appropriate commercial model in GT power depends on the trade-off between physical accuracy and computational efficiency. Predictive models are the best suited for detailed high-fidelity simulations while non-predictive and combustion profile models provide faster solutions for border preliminary investigation and system-level simulation outcomes.

c. Wiebe Combustion model

A widely used method in a nonpredictive category is the Wiebe function, which describes the mass fraction burned (MFB) during the combustion process. The Wiebe function allows user to define the rate of fuel combustion as a function of time or crank angle through a parameterized function. This model is useful for performance simulation where detailed combustion chemistry is not the primary focus.

Wiebe function, which approximates the typical shape of an SI burn rate. The model provides a convenient means of implementing a reasonable burn rate if measured cylinder pressure is not available. If cylinder pressure has been measured, it is recommended to perform a reverse run calculation and to use the resulting engine cylinder combustion profile to provide a more accurate burn rate. One further benefit of performing the reverse run calculation is that a Wiebe function will be fit to the burn rate, which can be used to set up a semi-predictive combustion model as well. The Wiebe equations (2.21-2.26) are given below by the calculated constants (Gamma Technologies, 2024a):

$$\mathrm{BMC} = \text{-}\ln(1\text{-}\mathrm{BM}) \qquad 2.21$$

$$\mathrm{BSC} = -\ln(1-\mathrm{BS}) \qquad 2.22$$

$$(\mathrm{BEC}) = -\ln(1-\mathrm{BE}) \qquad 2.23$$

$$\mathrm{WC} = \left[\frac{\mathrm{D}}{\mathrm{BEC}^{1/(\mathrm{E}+1)} - \mathrm{BSC}^{1/(\mathrm{E}+1)}}\right]^{-(\mathrm{E}+1)} \qquad 2.24$$

$$\mathrm{SOC} = \mathrm{AA} - \left[\frac{(\mathrm{D})\ (\mathrm{BMC}^{1/(\mathrm{E}+1)})}{\mathrm{BEC}^{1/(\mathrm{E}+1)} - \mathrm{BSC}^{1/(\mathrm{E}+1)}}\right] \qquad 2.25$$

$$\mathrm{Combustion}\ (\theta) = (\mathrm{CE})\left[1 - \mathrm{e}^{-(\mathrm{WC})(\theta-\mathrm{SOC})^{(\mathrm{E}+1)}}\right] \qquad 2.26$$

In equations 2.21-2.26 the following symbols have been used to define the equations.

AA	Anchor Angle (deg)
D	Duration (deg)
E	Wiebe exponent (def=2)
CE	Fraction of fuel burned (also known as combustion efficiency)
BM	Burned fuel percentage at anchor angle (def=50%)
BS	Burn fuel percentage at duration start (def=10%)
BE	Burned fuel percentage at duration end (def=90%)
BMC	Burned midpoint constant
BSC	Burned start constant
BEC	Burned end constant
WC	Wiebe Contant
SOC	Start of Combustion
θ	Instantaneous crank angle

The Cumulative burn rate can be calculated, which is normalized to 1.0. The combustion starts at 0.0(0.0% burned) and progresses to the specified values by the fraction of fuel burned attribute, which is typically 1.0 or 100%.

d. Predictive Flame propagation-based model for SI engines

The study of flame propagation in SI engines is crucial for improving engine performance and efficiency. Various models including laminar flame speed (SL), Level set, G-equation, Lagrangian flame-kernel, and entertainment models have been developed to predict

flame behaviour more accurately. These models, when applied in GT-Suite simulations account for factors such as turbulence, flame speed, and heat transfer, leading to better alignment with experimental data. Fractal models further enhance accuracy by simulating flame wrinkling, while mean value models predict combustion phasing based on engine conditions. These predictive models contribute significantly to optimizing engine performance and design (Gamma Technologies, 2024a).

The Spark-Ignition Turbulent Flame Model in GT Suite is listed as "EngCylCombSITurb" template where the model predicts the bond rate for homogeneous charge, and spark ignition engines and is based on the works references of the model. The prediction considers the geometry of cylinders, spark location and timing, air motion, and fuel properties, unless the pistons have simple Dome and cup geometries. In addition, STL files are required to define the shape of the combustion chamber. There are four attributes in the combustion template that should be used for calibration, which are indicated in the equation below with different sub-sections.

Laminar Flame speed

The laminar flame speed is calculated by the equation except for the hydrogen and methane option which use proprietary equations to quantify the flame speed for that reason Heywood book pages 402-405 need to be referred (Heywood, 1988). The effect of dilution can be modified using the dilution effect multiplier (C_{DE})

$$SL = ((Bm + B\emptyset(\emptyset - \emptyset m)^2)(\frac{Tu}{Tref}^{\propto})(\frac{P}{Pref})^{\beta} f(Dilution) \qquad 2.27$$

$$f(Diluion) = \begin{cases} 1 - 2.06(Dilution)^{0.77 \times C,DE}, & Model\ version \leq v74 \\ 1 - 0.75 \times C, DE(1 - (1 - 0.75 \times C, DE \times Dilution)^7), & model\ version \geq v75 \end{cases} \qquad 2.28$$

The symbols used in the equations are illustrated below:

SL= laminar flame speed

Bm= maximum laminar speed

Ø= equivalence ratio

BØ= laminar speed rolls off value

Tu= Unburn gas temperature

T_{ref}= 298K

P= pressure

P_{ref}= 101325 Pa

Dilution= residual mass fraction in Unburned zone

Øm= equal balance ratio at maximum speed

∝= temperature exponent

β = pressure exponent

Entrainment and burn-up

The unburned fuel-air mixture enters the flame front through the flames own at every rate that is proportional to the combined turbulent and laminar flow flame speeds. The burn rate is proportional to the quantity of unburned mixture behind the flame front (M_e-M_b) and divided by a time constant τ.

$$\frac{dMe}{dT} = \rho u Ae(S\tau + SL) \quad 2.29$$

$$\frac{dMb}{dt} = \frac{(Mb - Me)}{\tau} \quad 2.30$$

$$\tau = \frac{\lambda}{SL} \quad 2.31$$

$$ST = CYTFSu'(1 - \frac{1}{1 + CFKG(\frac{Rf}{Li})^2}) \quad 2.32$$

$$\lambda = \frac{CTLS \times Li}{\sqrt{Ret}} \quad 2.33$$

$$Ret = \frac{\rho u \times u' \times Li}{\mu u} \quad 2.34$$

In the equations above the symbols are denoted as:

Me= entrained mass

Mb= Burned mass

ST= turbulent flame speed

Rf= flame radius

Ae= surface area at the flame point

ρ = Unburned density

t= time

λ= Taylor microscale length

Li= integral length scale

u’ = turbulent intensity

Ret= turbulent Reynolds number

μu= unburned zone dynamic viscosity

This model requires that in-cylinder flow is described by an engine cylinder flow reference object so the turbulent intensity and length scale will be provided. However, the effect of turbulent intensity and length scale can be modelled using the Turbulent Flame Speed Multiplier (CTFS) and Taylor Length Scale Multiplier (CTLS) described in equations (2.29 to 2.34) (Gamma Technologies, 2024a). Additionally, the Flame Kernel Growth Multiplier (CFKG) can be used to adjust the initial growth rate of the flame Kernel.

2.5.3 Heat Transfer Modelling

To estimate heat transmission and wall temperatures in the solid components of a gasoline engine, (Margot et al., 2021) proposed a combustion modelling system that combines a 1D model with 3D discretized parts. To achieve accurate heat loss calculation and effective engine calibration, it incorporates these predictions into 3D Conjugate Heat Transfer (CHT) simulations and validates them against experimental data see Figure 15. The study demonstrates how well it works to speed up design improvements for internal combustion engine heat management.

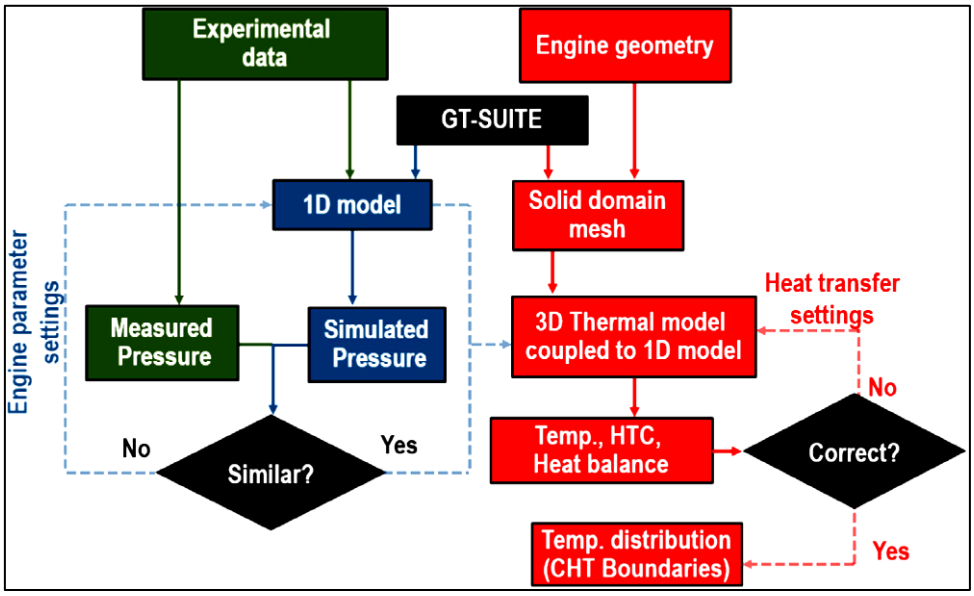

Figure 15 Combustion and heat transfer methodology employed for the calculations (Margot et al., 2021).

Heat transfer in the cylinder $\dot{Q}$ Represent the exchange of thermal energy between the gas and the cylinder walls. This can be modelled using newtons law of cooling which is stated in the following equation (Gamma Technologies, 2024a).

$$\dot{Q} = h.A.(T - T\omega) \qquad 2.35$$

In the equation above, h is the heat transfer coefficient, which is a function of cylinder pressure, temperature, and time, A is the surface area of the cylinder walls exposed to the gas, T is the temperature of the gas, Tw is the temperature of the cylinder walls. In GT-Power, the heat transfer coefficient h is typically computed using empirical correlations, while the wall temperature Tw can either be imposed or modelled dynamically based on the operating conditions.

(Margot et al., 2021) mentioned to simulate engine fluid dynamics, this study used a 1D multi-physics model in GT-Suite software. Based on geometric data, a detailed schematic of the experimental setup built a single-cylinder engine. A thorough examination of the engine's cycle, including the stages of combustion, exhaust, and intake, was made possible by the model, which also offered a thorough simulation of engine operation for performance assessment and optimization.

2.5.4 Argon Power Cycle in 1D-Simulation

a) Ar-H2 Closed Cycle Engine 1D model in GT-Suite

In the latest released GT-SUITE 2022 build-1, Gamma Technologies has come up with a splendid model of the closed-cycle argon-hydrogen engine (see in Figure 16). This state-of-the-art model for the engine is known as the 'Ar-H2_ClosedCycle_Engine', and it comes with such features as the condensation of the burnt products, water ejection within from the cycle, and a semi-predictive condenser (Tingting, 2022). In this system, argon is recirculated while oxygen is supplied to the combustion chamber by an injector object. Hydrogen, which acts as a sole fuel, is inducted into the combustion chamber of the engine cylinder. After combustion, in the condenser, the water vapor is converted into its liquid state most efficiently before it leaves the exhaust system.

In closed-cycle simulations, maintaining equilibrium is essential for the stability of the result. Its balanced amassed flow between the incoming and outgoing inputs is crucial in this context, requiring precise control of both the oxygen injection rate and hydrogen flow to sustain the simulation process (Heitor et. al., 2012). Notably, efficiency and specific heat ratio trends vary, with specific condenser design parameters significantly impacting efficiency. High-efficiency condensers demonstrate a heightened sensitivity to changes in argon concentration (Hamarashid, 2009).

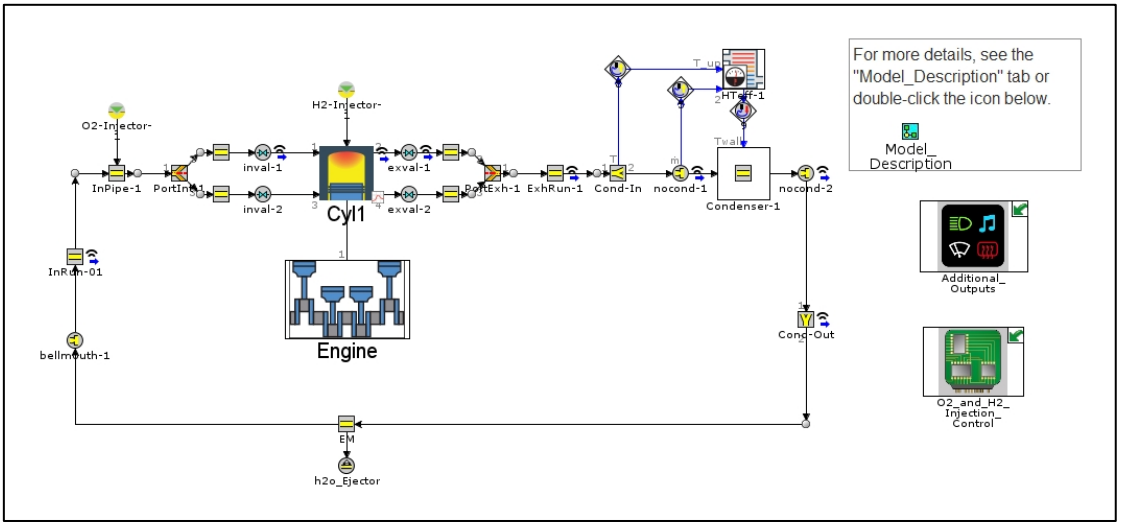

Figure 16 An overview of Ar-H_2 Closed Cycle Engine Model Configuration in GT-suite (Tingting, 2022)

This closed-cycle engine simulation in GT-SUITE utilizes a semi-predictive combustion model; despite this, it provides strong evidence for the use of the hydrogen/noble gas engine simulation. It remains a useful citation providing the foundation to further alter, specifically, the incorporation of predictive combustion models that are the ever-used SI Turbulent Flame Combustion Model commonly used in gasoline engine modelling (Gamma Technologies, 2023).

b) Kinetically Oriented Modelling of APC Combustion by University of California, Berkeley

Researchers at the University of California, Berkeley (Sierra Aznar, 2018a) investigated the APC using a single zone kinetic model and the ARAMCO chemical kinetics mechanism

to simulate combustion under Homogeneous Charged Compression Ignition (HCCI) conditions. This approach effectively predicts ignition timing, species formation, and heat release model in the combustion of hydrogen and oxygen within an argon-rich working fluid. The HCCI model driven primarily by chemical reactions without requiring external ignition is well suited to the kinetically oriented model.

However, while suitable for HCCI, this approach had noticeable limitations when applied to other combustion models such as spark-assisted compression ignition (SACI) or diffusion combustion. These models involved more complex physical processes such as flame propagation, turbulence, and heat transfer, which are not captured by kinetic solvers. This is where more comprehensive multidimensional or multi-zone models are needed to account for the interaction between chemical kinetics and fluid dynamics.

Furthermore, (Sierra Aznar, 2018a)mentioned as an open-loop model this approach is more appropriated for fundamental-level research. It does not account for the recirculation of exhaust gas, which is a key component in a practical APC system that affects real-world efficiency and performance. Referring to the process diagram in Figure 17 which illustrates combustion model types it is clear that kinetic solvers are most effective for each HCCI combustion but are insufficient for broader applications involving more complex combustion models or closed-loop systems.

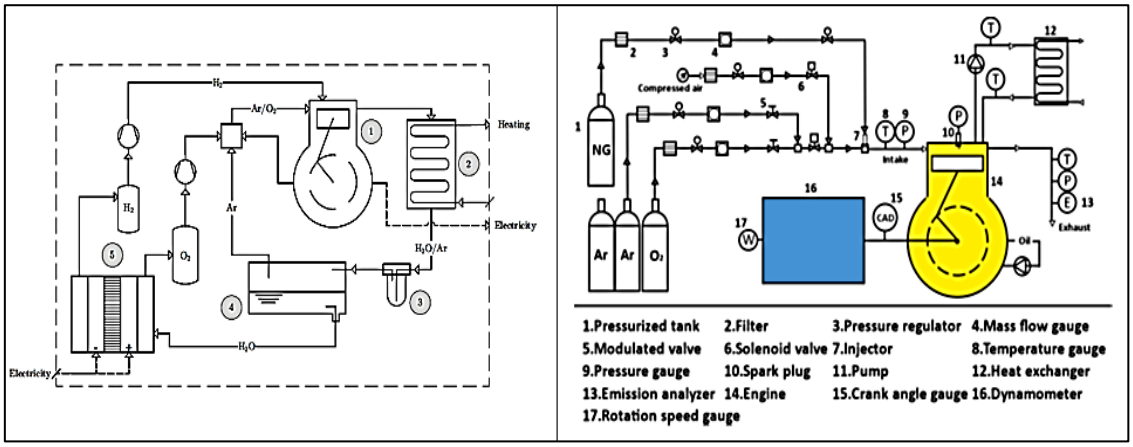

Figure 17 An expanded detailed model diagram of the air separation unit by using Aspen Plus (Sierra Aznar, 2018a)

Therefore, while used for fundamental studies kinetically oriented models have limited applicability in the comprehensive modelling of the APC system. Different software has been used by this research group such as Cantera software used to evaluate the reaction rate of each elementary reaction and compute the net production rate of every species in the mechanism, Aspen Plus software was used to simulate the ASU, and LabVIEW software for data acquisition and engine control systems.

c) APC combustion modelling by Computational Fluid Dynamics in Eindhoven University of Technology

In this stated research project by (Van Den Brink, 2022a) injection strategies for the Argon Power Cycle in converge CFD were explored, which utilized a finite volume method (FVM) for discretizing using CFD equations. The software autonomously generates a mesh using cubic cells, with the option of adaptive mesh refinement (AMR) to refine the coarsen mesh based on criteria, optimizing accuracy and computational efficiency. The Reynold Averaged Navier Stokes (RANS) turbulence model was chosen for suitability in focusing on key engine performance parameters without needing the high detail of a more complex model shown in Figure 18.

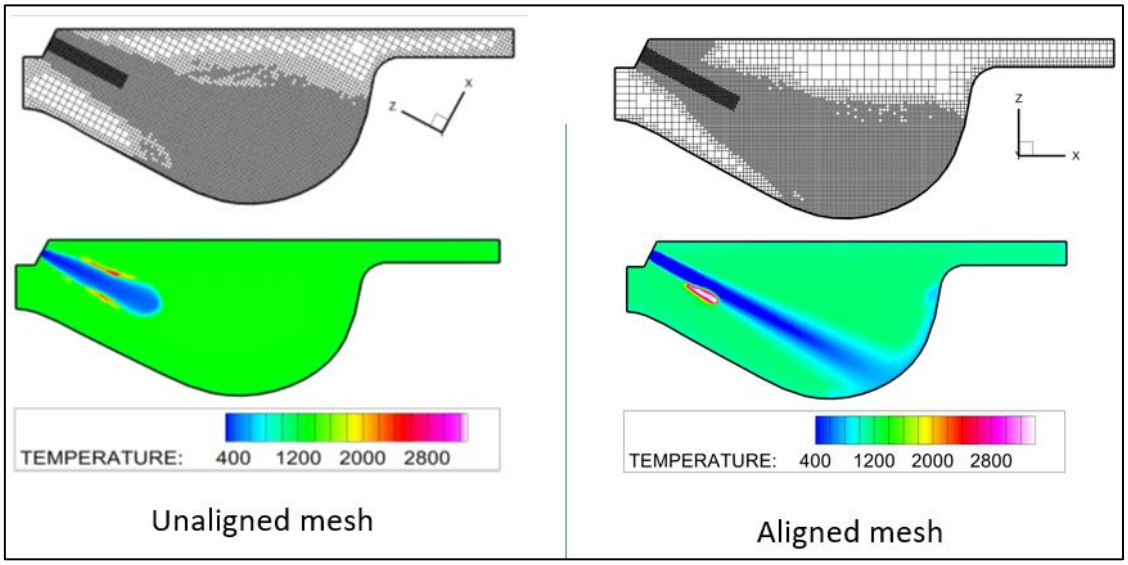

Figure 18 Model overview with Contour plot showing the temperature (Van Den Brink, 2022a).

The result section of this paper demonstrates the significant capabilities of this approach in providing detailed insights into the combustion process within the APC for different

injection strategies. The analysis reveals that the intake charge composition is notably influenced by specific heat ratios, leading to varying theoretical efficiency between direct injection of hydrogen (DI-H_2) and oxygen (DI-O_2). Furthermore, the SuperJet penetration of DI-O_2 enhances mixing, resulting in a higher heat release rate. However, the advantage is counterbalanced by the increased heat loss due to the distinct thermal properties of the gas mixture. This approach effectively elucidates the complex interplay of factors affecting engine performance paving the way for optimizing combustion strategies in future research.

Additionally, CONVERGE's SAGE solver is used for handling detailed chemical kinetics. Despite its advantages, CFD has limitations due to the discrete nature of the calculations, assumptions in physical submodules, and high computational costs.

d) Modelling of the Argon Split Cycle Engine (ASCE) by Tongji University

Research by Tongji University (Dong et al., 2022) presents an Argon Split Cycle Engine (ASCE) focusing on enhanced thermal efficiency. The simulation was conducted using LMS. AMESim Software, which offers extensive capabilities for internal combustion engine modelling. The software allows for preconfiguring gas compositions and physical properties which is particularly useful for simulating the ASCE's unique intake process.

The IFP-Engine library simulates a virtual engine with a timeframe similar to the crankshaft. This IFP engine model within AMESim specifically integrates the effect of argon on the intake gas thermal properties and heat transfer dynamics which are crucial for improving efficiency. These parameters fed into the dual flame combustion model, which predicts fuel heat release using a simplified Arrhenius correlation. This approach considers the thermodynamic state within the cylinder and the composition of the intake mixture. In Figure 19 the architecture of the thermodynamic cycle modelling solution model in the software has been illustrated by the following schematic diagram.

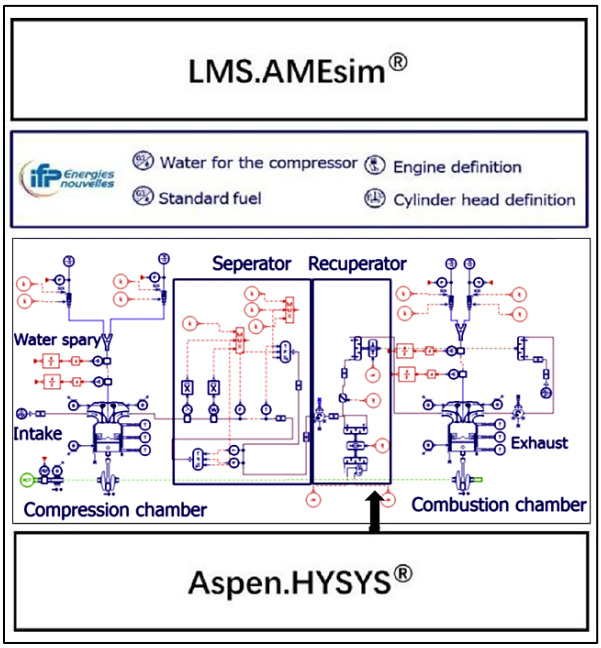

Figure 19 Schematic of the architecture of the Argon-Split-cycle engine model (Dong et al., 2022).

The modelling process begins by configuring intake and combustion parameters for ASCE. The model emphasizes the impact of argon in the split cycle which effectively reduces heat losses and boosts thermal efficiency. Using AMESim simulation capability the model demonstrates how are we going to enhance the overall performance of the engine. However, the limitations of the model include its reliance on simplified assumptions in the Arrhenius correlation may not fully capture the complex combustion dynamics under all operating conditions. Additionally, the model's accuracy is sensitive to the input data such as the precise composition of the intake mixture and insulin are conditions which may limit its applicability to more complex engine varying fuel types. Finally, the model provides a detailed accurate representation of the ASCE allowing for a comprehensive analysis of advanced combustion strategies and their potential to improve thermal efficiency. It has been suggested that future model refinements should focus on addressing their limitations by incorporating more sophisticated combustion dynamics and expanding applicability to multi-cylinder engines and real-world scenarios.

3 Object and Methods

This chapter presents the methodology employed to develop, validate, and analyze simulation models for HAPC after collecting related literature on APC. The process as illustrated in Figure 20, is presented through a flow chart that outlines a systematic and iterative process. The process begins with a comprehensive analysis and experimental validation of the Wärtsilä W6L20-2STC engine, which serves as the reference model for all subsequent simulations during this thesis work. The six-cylinder W6L20 engine model provided by Wärtsilä is thoroughly examined to understand engine performance metrics, geometry, and technical specification to form a foundational basis to convert into the corresponding HAPC simulation model. And this baseline HAPC GT-suite model is adapted during this thesis research work for understanding the HAPC system performance under W20-engine boundary conditions.

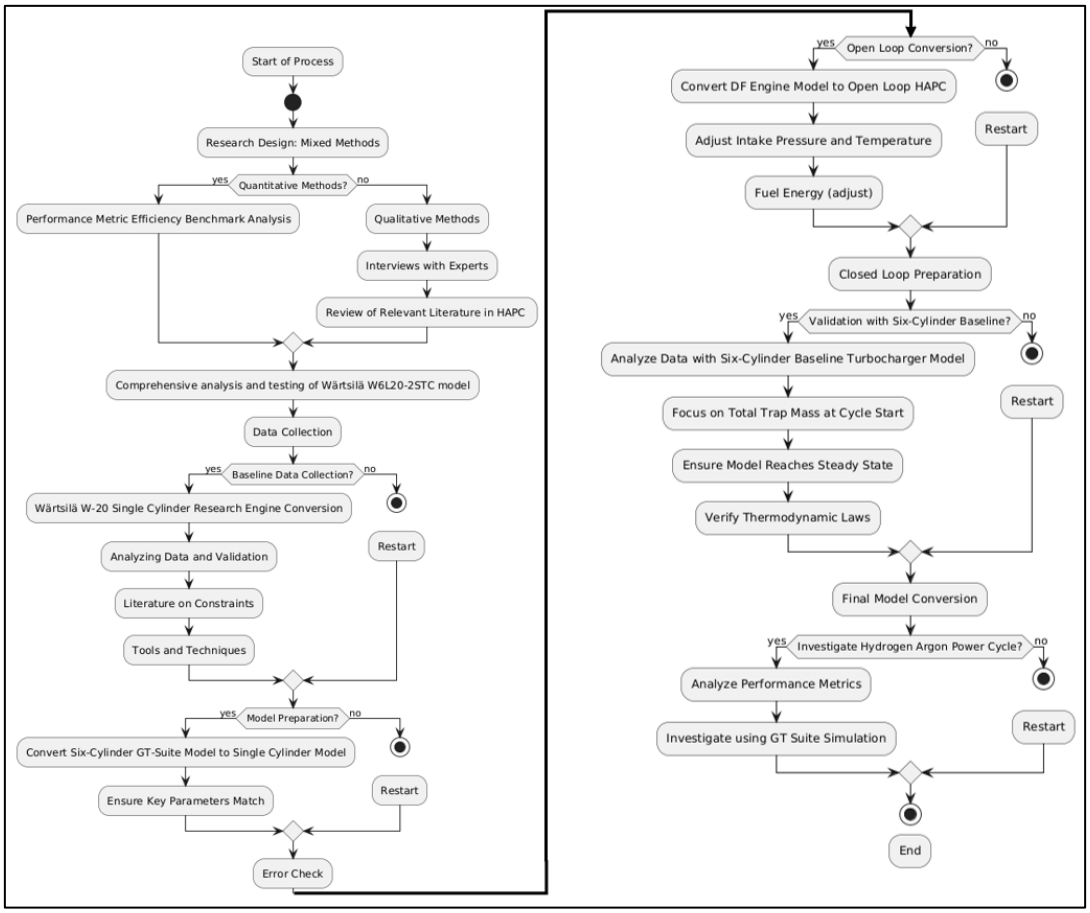

Figure 20 Research design and methodology flow chart.

An important part of the methodology is the creation of sub-models for essential engine functions, including combustion objects, intercooler and condenser units, piping volumes, and controllers. These sub-models are carefully tuned and validated against experimental data to ensure the simulation operates accurately under different load conditions. In addition, post-processing and data analysis techniques were applied to assess the model's performance, ensuring it is optimized across different configurations for accuracy.

Every step of the methodology is designed to build a reliable simulation framework that combines real-world data with theoretical models. This ensures the prediction of engine behaviour is both accurate and dependable. The following sections detail the specific steps taken to the develop the simulation models, the assumptions made for each sub-model, and the validation techniques used to confirm the results.

3.1 Reference Engine and Experimental Data for Model Validation

3.1.1 Technical Specifications of the W6L20-2STC Engine

The reference test engine is a research version of a six-cylinder two-stage turbocharged in-line engine with a 200mm bore. The Wärtsilä 20 (W20) engine, especially the six-cylinder (W6L20-2STC) variant, is renowned for its robust design, efficiency, and versatility. These four-stroke, turbocharged, and intercooled dual-fuel engines are extensively utilized in both marine and power generation applications. Its compact dimension and high-power output render it an ideal choice for vessels and power plants that require reliable and efficient performance. The basic specification for the engine is presented in Table 9. For more detailed description, the readers are directed to the Wärtsilä 20 product guide (Wärtsilä, 2020).

Table 9 Specification of the research engine

Specification	Details
Engine Type	4-stroke, non-reversible, turbocharged, inter-cooled diesel engine with direct fuel injection

Cylinder Bore	200 mm
Stroke	280 mm
Piston Displacement	8.8 liters per cylinder
Number of Valves	2 inlet valves and 2 exhaust valves per cylinder
Cylinder Configuration	In-line, 6 cylinders
Direction of Rotation	Clockwise (counterclockwise available on request)
Speed	900, 1000, 1200 RPM
Mean Piston Speed	8.4 m/s (900 RPM), 9.3 m/s (1000 RPM), 11.2 m/s (1200 RPM)
Power Output (Diesel Electric Propulsion)	1110 kW (900 RPM), 1200 kW (1000 RPM), 1320 kW (1200 RPM)
Environmental Compliance	Supports SCR systems, compliant with IMO Tier II standards

For the purpose of this thesis, it is sufficient to outline the original engine model in terms of engine load at 50.20%, 75.25%, and 101.20% operating conditions. Similarly, the process of redesigning the engine model has been extensively conducted in accordance with the documentation and requirements provided by Wärtsilä. However, some modifications have been applied to all components except the crankshaft and connecting rod.

3.1.2 Modelling Assumptions for W6L20-2STC in GT-Power

a) Experimental Data and Reference Conditions

The provided W6L20-2STC Gt-Suite model simulates three different conditions, 50.20%, 75.25%, and 101.20%. The W20-DF engine utilizes a common rail fuel injection system for liquid fuels, enabling precise control of fuel pressure and timing. For gaseous fuels, it employs a dedicated gas injection system which may use either pre-chamber or direct injection technology. This dual-fuel configuration allows for efficient engine operation across several types and conditions. Throughout the testing campaign, the combustion process involved marine diesel oil (MDO) and Methane, with Methane injected as port fuel injection (PFI) and MDO as direct injection (DI) technology.

The methane is maintained at a temperature of 15°C with a vaporized fluid fraction of one. Methane gas was injected at 10 bar pressure with injection timing set at -360° crank angle, with variation in gas injection timing across different load levels. For direct injection of fuel (MDO), the injection timing was set at -65 °, -65 °, and -36 ° for 50%, 75.25%, and 101.20% loads, respectively. The fuel was injected at a temperature of 67 °C, with additional adjustments made to timing and pressure depending on the load.

The intake and exhaust pressure were kept constant at 1.01 bar absolute pressure, while intake air temperature varied between 28 °C and 32.4 °C. The air composition was set as nitrogen at 76.24%, oxygen at 23.16%, and water vapor at 0.6%. The boost pressure was maintained at 3.46 bar, 4.82 bar, and 5.95 bar for 50.20%, 75.25%, and 101.2% loads respectively. Pressure drops between the end boundaries were minimal, which can be neglected easily, and the error percentage was below 5%.

b) Integration Methodology of HAPC

In this study, integrating the HAPC into the W6L20 engine GT-Suite model is a critical step requiring careful calibration and validation. The process involves multiple stages, beginning with the model integration and validation. Figure 21 provides a summarised overview of the integrated methodology.

Initially, it is important to examine the factors that will limit the load and efficiency of the two-stage turbocharged W6L20-DF engine. Then, the subsequent step involves constructing a single-cylinder research engine (SCRE) mimicking the configuration of W20 DF from a six-cylinder version, ensuring the use of identical fuel, loads, combustion modelling, and conditions. At this stage, the turbocharger will be removed, and the model will be validated by comparing cylinder pressure, trapping mass, and total energy output with the result from the six-cylinder engine's test run data. The output should align exactly with the six-cylinder engine result which has been obtained from the experimental result provided by Wärtsilä.

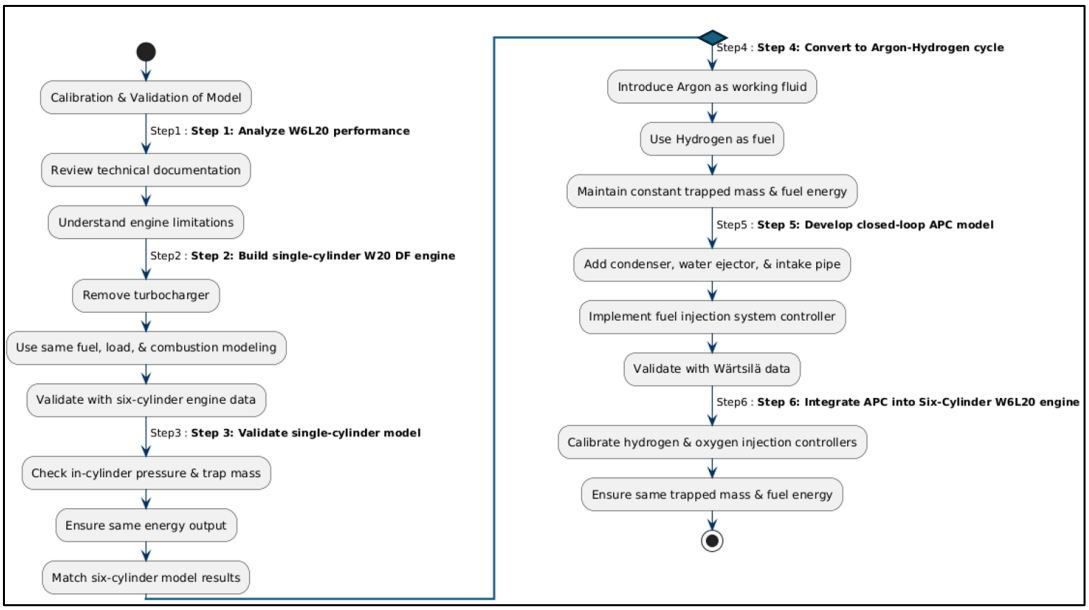

Figure 21 Methodology Flow chart of Integration.

Following this step, the W20-DF SCRE GT-Suite model will be adapted into an open-loop APC model by introducing argon as a working fluid and hydrogen as the fuel. Throughout this stage, the trapped mass and fuel energy will be held constant to observe their effects on the engine output. Once this phase is completed, the model will be ready for the development of a single-cylinder closed-loop HAPC model in GT-Suite. This will involve scaling up the default argon power cycle model from the GT-Suite template (refer to section 2.5.4) to a closed-loop W20 SCRE model.

The SCRE closed-loop model will incorporate new components such as a controller for the fuel injection system, a condenser, a water ejector, and an Intake pipe of argon circulation within the system. Finally, the single-cylinder closed-loop HAPC model will be integrated into the six-cylinder W20 engine model. At this final stage, the hydrogen and oxygen injection systems, as well as the output controller, will need to be recalibrated due to the additional introduction of five cylinders into the system to ensure that the fuel energy entering the cylinder remains consistent with injected oxygen.

3.2 W20-SCRE Model Validation Methodology

Once the single-cylinder research engine (SCRE) has been developed, it requires to validate for accuracy and reliability. The validation process involves comparing the experimental and simulation results from the developed W20-SCRE GT Suite model with experimental data provided by the Wärtsilä Engine R&D team for the W6L20-2STC engine. The experimental data obtained under medium speed conditions at varying engine loads (medium-low to high), includes cylinder pressure, trapped mass, and fuel energy entering the cylinder.

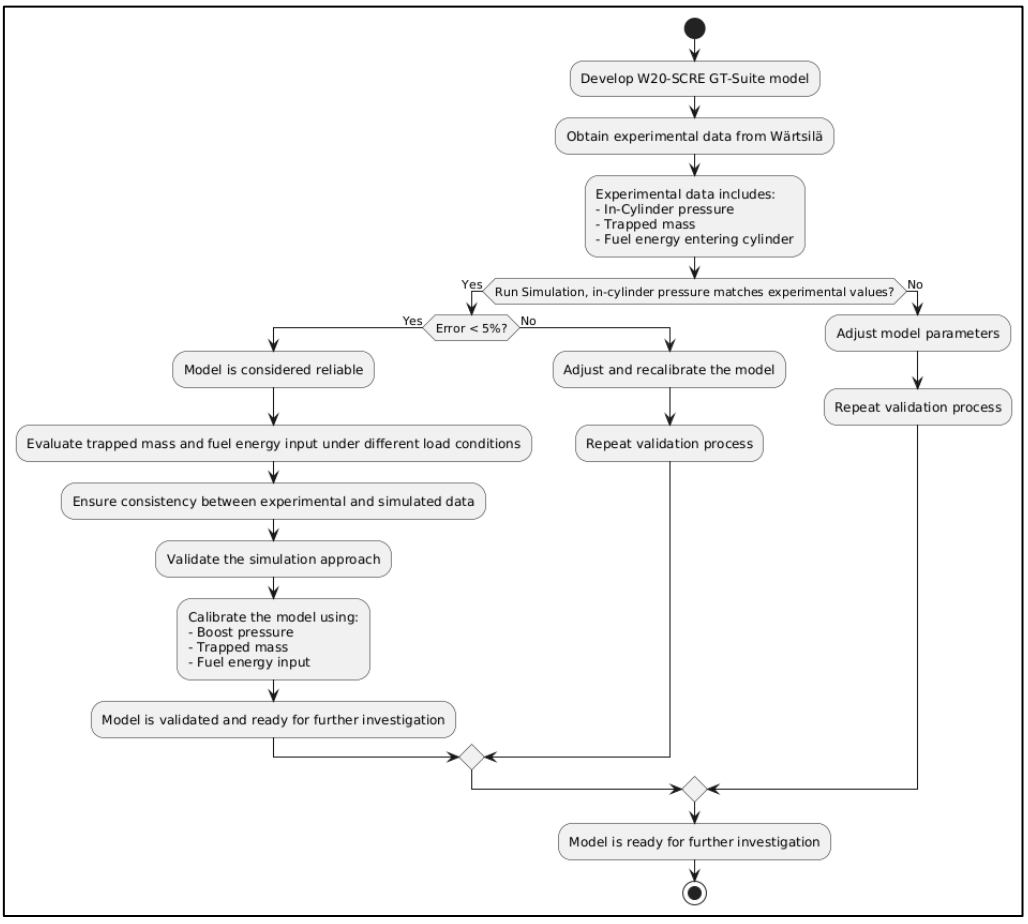

Figure 22 Model Validation Flow chart.

In Figure 22 The validation process of the study is Illustrated clearly for a better understanding of where the model's accuracy is accessed by comparing the simulated in-cylinder pressure data with the experimental values. If the error between the simulation results and the experimental data remains below 5%, the model is considered reliable. At this stage, the model's trapped mass and fuel energy input for different load

conditions were further evaluated to ensure consistency. By demonstrating the closest agreement between experimental and simulated data, the validation of the simulation approach was established. Once the model is calibrated based on cylinder pressure, trapped mass, and fuel energy, it is considerably validated and ready for further investigation. The validation process establishes the model's accuracy and stability for simulating engine performance under the specified operating conditions.

3.3 Simulation Models

3.3.1 W6L20-2STC Engine: Detailed Model Configuration Description

The W6L20-2STC engine provided by Wärtsilä Finland, is built by defining individual flow elements for each bend, orifice, contraction, intercooler unit, and flow split in the system. The combustion process in the model was managed using a simplified zero-dimensional method, while the turbocharger was modelled using map-based sub-models.

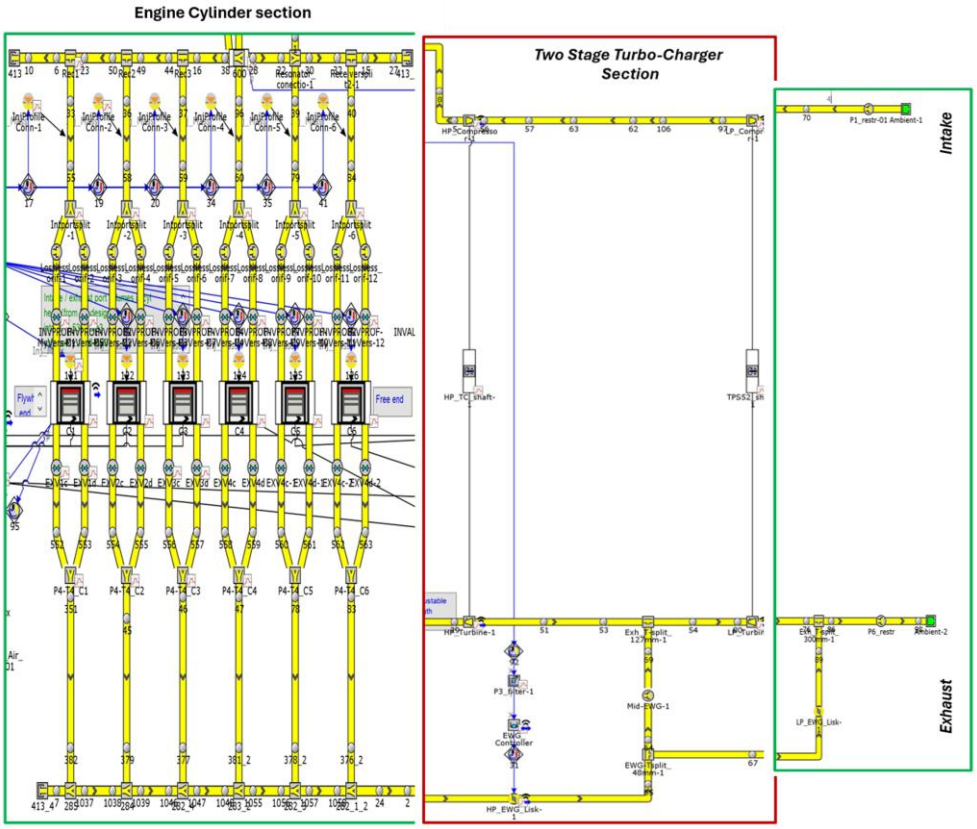

Figure 23 Overview of the 1-D model representing the Wärtsilä 6L20-2STC research engine.

Figure 23 provides an overview of the flow components, showing a total of 662 elements. The model performed efficiently, completing a steady-state simulation in one minute and three seconds. The figure also illustrates key components including the engine cylinder, turbocharger, intake, and exhaust systems, along with the piping layout for better understanding. The flow within the engine and associate systems such as intake, exhaust, and fuel based on the assumption that intake manifold pressure and temperature vary predictively with engine speed and load for this modelling purpose, ambient pressure and temperature have been used as reference conditions specifically for 50.20%, 75.25% and 101.2% load.

The engine features a two-stage turbocharging system which includes low- and high-pressure compressors and turbines. The setup enhances the efficiency of air intake and exhaust improving engine performance. Engine cylinders are modelled using a non-predictive combustion approach, where the burn rate profile is imposed based on the three-pressure analysis (TPA) method. Additionally, heat transfer is modelled using the WoschniGT model, which estimates convective heat transfer within the cylinder contributing to the calculation of engine efficiency. The fuel injection system combines port fuel injection for methane vapor and direct injection for marine diesel oil (MDO) by using the "Injection Profile Connection" template. The governor injector controller facilitates seamless switching between fuel modes optimizing combustion based on the user-imposed model in both dual fuel and diesel models. The valve timing is controlled by the RLT variable creator, ensuring precise synchronization of intake and exhaust valve events for optimal engine performance. The model has been optimized at a compression ratio of 12.3. The model was calibrated and validated using experimental data to better reflect the characteristics of the research engine.

3.3.2 W20-SRCE-Based Geometry Template for Model Development

In Figure 24, the reference GT Suite model of the W6L20 engine has been converted into an open-loop single-cylinder DF model, where the turbocharger has been removed. However, the fuel injection system and fuel composition were kept constant as the six-

cylinder engine. Then the model was validated (detailed process has interpolated in section 4.1) and ensured the error percentage was below 5%.

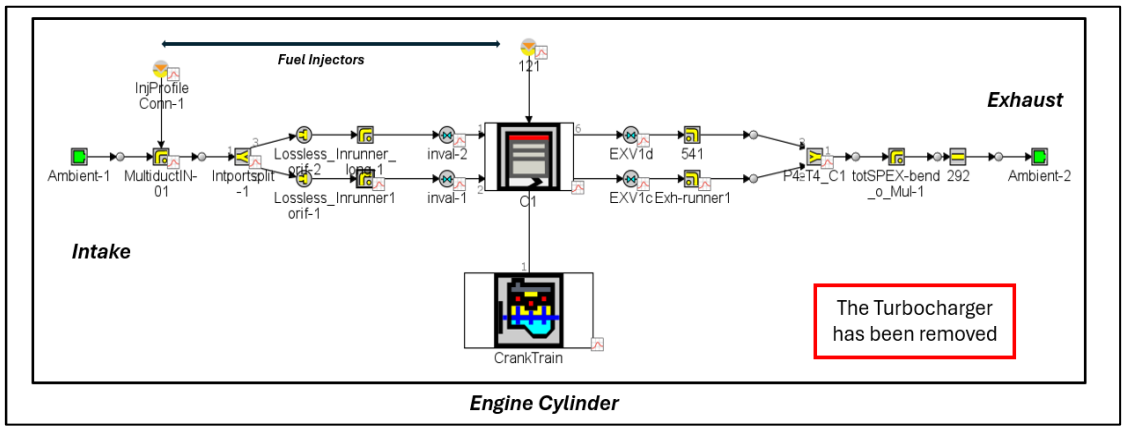

Figure 24 Overview of W20-DF SCRE model geometry.

After this stage, the model was converted to an open-loop APC utilizing hydrogen as fuel and introducing argon in the intake pipe as detailed in the methodology section. The geometry of the open-loop APC remained consistent with the W20 DF SCRE model, but significant modifications were made to the fuel injection system and the intake and exhaust ports of the model. Argon was replaced by air in both intake and exhaust systems with composition, oxygen was injected into the port in place of methane, and hydrogen was directly injected into the cylinder, replacing MDO. Finally, the model was calibrated and validated using test data to ensure accuracy.

3.4 HAPC Engine Model Development

3.4.1 W20-SCRE Model Adapted for Closed-Loop HAPC Implementation

In Figure 25, the W20-SCRE engine layout has been converted into a closed-loop, single-cylinder hydrogen argon power cycle model. This modification includes the introduction of a new injection system for both oxygen and hydrogen. Argon has supplied the engine cylinder via the flow pipe (Inrun-01), serving as a crucial component in this cycle.

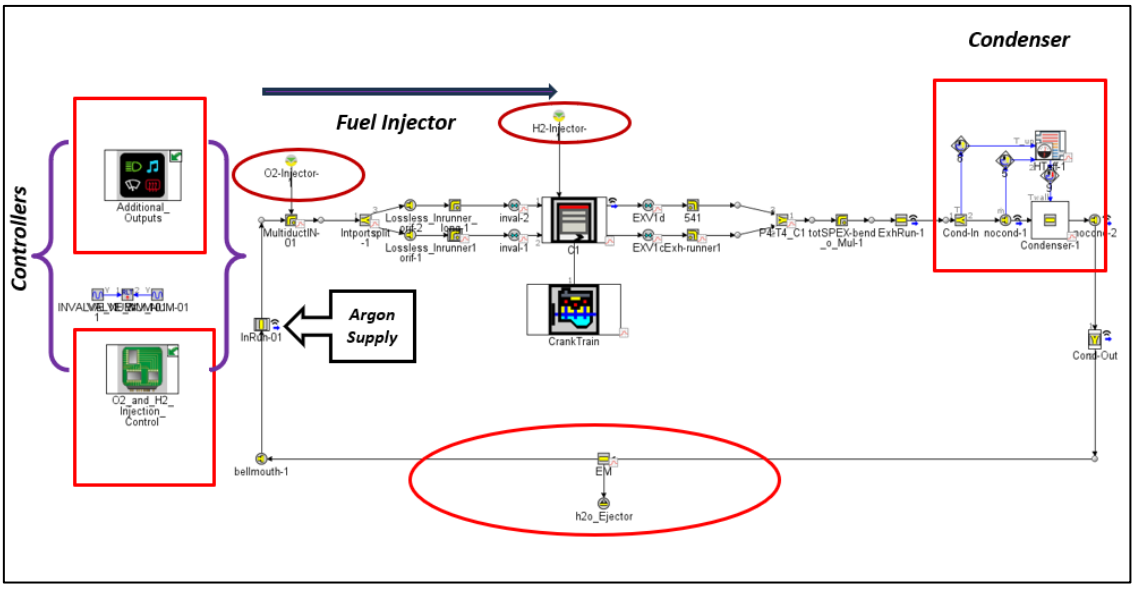

Figure 25 A 1D closed loop GTP Model of W20-SCRE layout for HAPC.

To manage the byproduct of combustion, a water ejector and condenser have been incorporated, enabling efficient removal of water. Controllers have also been implemented to regulate the injection rates of oxygen and hydrogen, ensuring the mass balance remains at a steady state and the system operates efficiently. The current version of the model has been used to validate and implement the closed loop HAPC in the Wärtsilä 20 engine and this will provide a basis for creating the final multi-cylinder model to conduct further investigation.

3.4.2 Key Sub-models Utilized in HAPC Simulation

a. Combustion Modelling Approach for HAPC

The combustion model employed in this study for the HAPC is based on a non-predictive approach, implemented through GT-Suite software. The combustion profiles used in this thesis are based on the reference model provided by Wärtsilä. An example of the combustion profile is illustrated in Figure 26 for three different loads. The user-imposed combustion profile was derived using the three-pressure analysis (TPA) method, which utilize measured pressures from the intake, cylinder, and exhaust. Unlike the first-law analysis-based approach (heat release rate), TPA does not require pre-estimation of residual fraction or trapping ratio. The simulation runs over multiple cycles until convergence, after

which the trapping ratio, residual fraction, and other trapped quantities are calculated automatically, eliminating the need for these inputs at the outset.

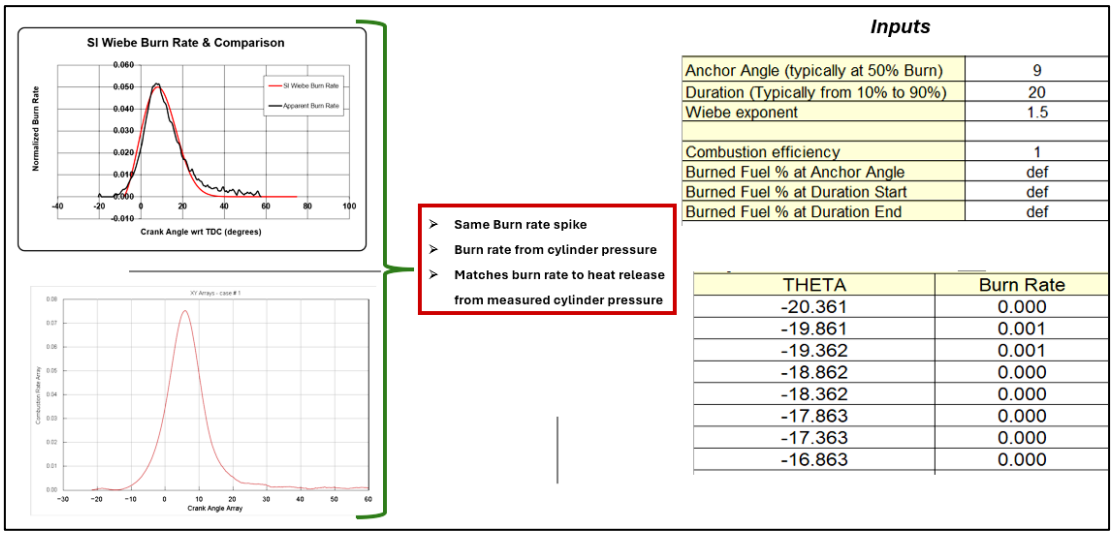

Figure 26 Conceptualization view of the combustion object.

Although the Wiebe SI approach is recognized as a suitable method for the HAPC combustion modelling object, for this performance level simulation the combustion model based on an imposed burn rate will be employed, as the provided GT-Suite model by Wärtsilä. The Wiebe SI Function approach specifies same specific parameters such as anchor angle (Crank angle of 50% mass burnt denoted as CA50), Duration of combustion (from CA 10 to CA 90), and the Wiebe Exponent, instead of relying solely on user-imposed burn rates has been illustrated in Figure 27 for three different load points.

The inclusion of this additional combustion object which is imposed burn rate using the TPA analysis has a minimal impact on the non-predictive burn rate. However, the apparent heat release rate and in-cylinder energy balance are not computed after the exhaust valve opens (EVO), meaning any fuel burned beyond this point is not accounted for the combustion. Despite this, defining a combustion object is essential, particularly for managing the startup cycle when using an external cylinder model, ensuring a seamless integration during the initial combustion phases.

The start of combustion (SOC) is optimized for this model at -21.57° for 50.20% load, -20.40° for 75.25% load, and -15.76 for 101.2% load (see in Figure 27), with corresponding

CA50 anchor angles set at 6.18 °, 6.92 °and 9.15 ° respectively. The WoshniGT model is employed for heat transfer calculations, which accounts for cylinder heat transfer without swirl, critical in accurately simulating the thermal properties of argon as the working fluid.

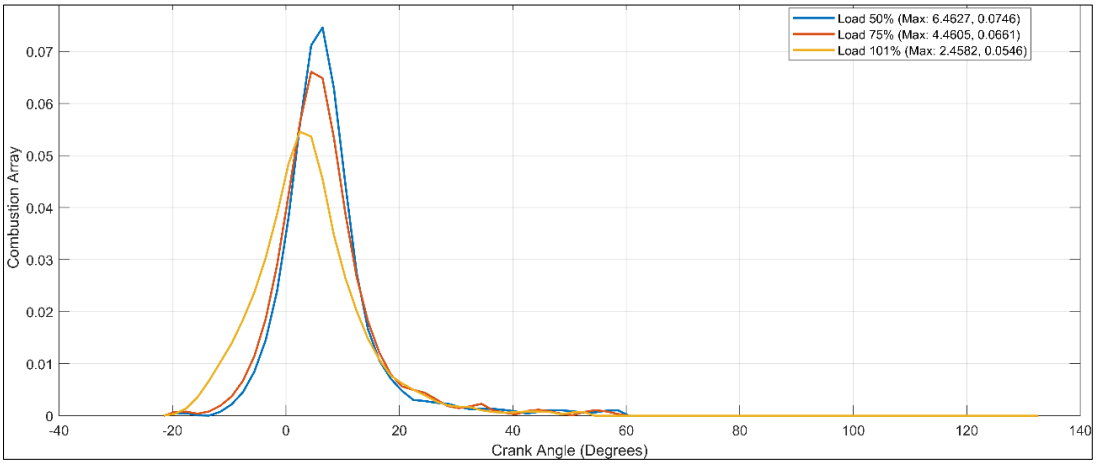

Figure 27 An overview of imposed burn rate combustion profiles derived from TPA method at 50.20%, 75.25%, and 101.2% load conditions.

The combustion models build upon combination of non-predictive methods and real-world performance data provides an accurate simulation of the integrated HAPC system combustion characteristics. The model can be used to assess the engine performance while changing, airpath geometry, mixture composition, charge pressure, or fuelling, assuming combustion is always kept at its reference point via combustion control means. The employed non-predictive model however cannot reproduce the effect of argon ratio, or fuel/charge stratification on combustion duration at the given ignition setpoint. This is an acknowledged limitation in this study.

b. Configuration of Condenser and Intercooler Efficiency Template

The water vapor condenser is located downstream of the exhaust runners and modelled using a pipe object, following the method used for intercoolers in GT-Suite software. This semi-predictive heat exchanger model relies on the intercooler efficiency template to guide the condensation of water vapor, a key combustion byproduct for HAPC. The model configuration and connection to the airport is shown in Figure 28. The condenser

consists of 33 identical pipes, each 17.4 mm in diameter and 1205 mm in length, providing a significant surface area for heat transfer which has been calculated from the intercooler unit dimensions of the reference engine model. The “condense or evaporate” attribute in the condenser object enables the phase to change the system to capture and condense water vapor generated during combustion. The condensed water is removed from the system via a separate Ejector template, described later in this section.

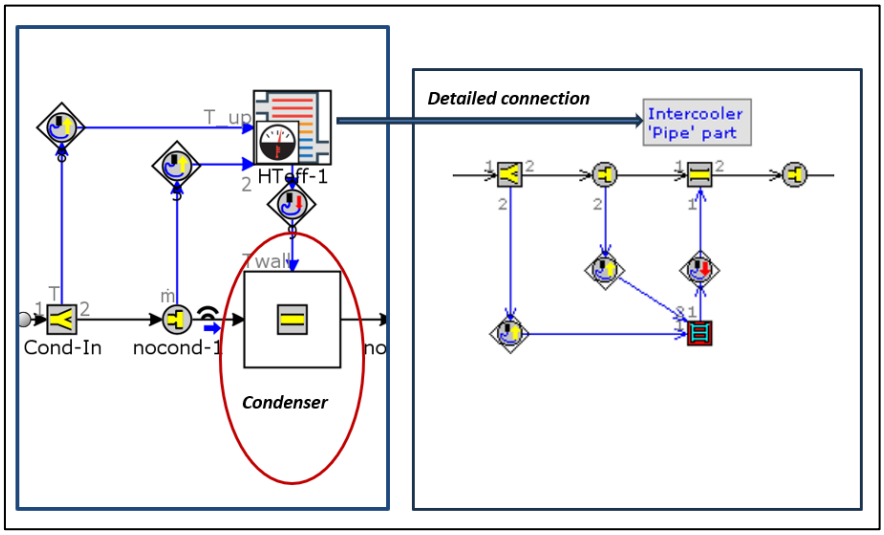

Figure 28 Condenser configuration and Intercooler Efficiency sub-model connection.

A control system regulates the desired condenser outlet temperature by adjusting the world temperature of the pipes. The heat transfer multiplier is set high to ensure the outlet matches the wall temperature. The target temperature is calculated using the Temperature Effectiveness (T_{eff}) part from the effectiveness table of the condenser. Though the geometry used for this model is illustrative, it offers valuable insights into the thermal performance of a closed-loop hydrogen argon power cycle engine under various load conditions.

The steam water separation characteristics subassembly analyses the efficiency of phase separation. Outputs from this section are crucial for evaluating the condensation process and downstream flow behaviour. A critical output of these subassemblies is the steam water separation rate (SepRate) is calculated using equation 3.1.

$$SepRate = \frac{(h2oLiq_{Dnste_{mass}} - \ h2oLiq_{Upstr_{mass}})}{max\ (h2oVap_{\_Upstr\_mass}, 1 \times 10^{-5})} \qquad 3.1$$

In the above equation, $\mathrm{h2oLiq_{Dnste_{mass}}}$ and $\mathrm{h2oLiq_{Upstr_{mass}}}$ are downstream and upstream liquid water masses, while $h2oVap_{\_Upstr\_mass}$, represents upstream water vapor mass. The coefficient 1×10^{-5} simply prevents division by zero as a stability criterion for numerical simulation.

The condensation process significantly influences downstream flow properties. As water vapor condenses latent heat is released lowering the flow's temperature and pressure. The heat of condensation is calculated by tracking the enthalpy change across the condenser. GT-Suite recognizes phase separation in real-time by differentiating liquid and vapor flows, providing vital feedback for system optimization. Effective condensation as indicated by a high separation rate results in a cooler more stable downstream flow. In contrast, inefficient condensation leads to higher vapor content altering the exhaust conditions and potentially compromising engine performance.

The intercooler efficiency template is used to regulate the intercooler outlet gas temperature. Note that in this case, this template will connect to the intercooler pipe part to actuate the intercooler pipe wall temperature. To effectively actuate the intercooler pipe outlet temperature, the intercooler pipe part attribute "Heat Transfer Multiplier" should be set to a high value (e.g. 50) which denotes efficiency. This will allow sufficient heat transfer between the gas and intercooler pipes so that the intercooler gas outlet temperature achieves the same value as the pipe wall temperature. After running a simulation, comparing the intercooler outlet gas temperature with intercooler pipe wall temperature in GT post is recommended to confirm the gas has cooled to the desired conditions.

Each intercooler efficiency controller has three signals: two input signals and one output signal. The first input signal must connect to a sensor connector part that senses the upstream temperature of a pipe or flow split component. The second input signal should

connect to another sensor connector part that has measured the upstream flow rate from an orifice connection. The flow rate must be in the same units (e.g. Mass flow rate in kg/s or velocity in m/s) as the X data in the effectiveness table. The output port must be connected to an actuator connector object to regulate the intercooler pipe wall temperature. The temperature of the intercooler outlet fluid temperature is calculated by using the following equation:

$$T_{out} = T_{in} - (\text{Intercooler Effectiveness}) \times (T_{in}\text{-}T_{coolant}) \qquad 3.2$$

In equation 3.2, T_{in} interpolates the Temperature of the intercooler inlet gas, while T_{out} is the temperature of the intercooler outlet gas, and $T_{coolant}$ is the temperature of the intercooler coolant. The relationship between mass flow rate and intercooler effectiveness is typically defined using an XY table object, while X data represents the flow rate or fluid velocity, and the Y data indicates the effectiveness fraction.

To prevent significant reductions in volumetric efficiency while recirculating the working fluid (Ar) back to the system, adjustments were made to both condenser efficiency and coolant temperature. An effectiveness function table was employed to define condenser efficiency where the relationship between mass flow rate and intercooler effectiveness was employed. Typically, the effectiveness of the condenser is represented using a XY table, with the x-axis corresponding to the flow rate or fluid velocity and the Y-axis representing the effectiveness function as outlined in equations 3.6 and 3.7. The setup template for this configuration is provided in GT-Suite software.

$$\text{XGT} = (\text{X DataARRAY} * \text{X Multiplier}) + \text{X Shift} \qquad 3.3$$

$$\text{YGT} = (\text{Y DataARRAY} * \text{Y Multiplier}) + \text{Y Shift} \qquad 3.4$$

Following these, four different test runs were conducted across the model using 75%, 85%, 90%, and 95% efficiency by intercooler effectiveness tables, as illustrated in Figure 29. Note that once the mass flow rate exceeds the defined limit in the intercooler effectiveness table, the intercooler effectiveness automatically reaches its maximum value. Moreover, the effectiveness of the system was calculated based on the wall temperature

and intake requirements. A detailed analysis of condenser efficiency in conjunction with coolant temperature was conducted followed by critical adjustments.

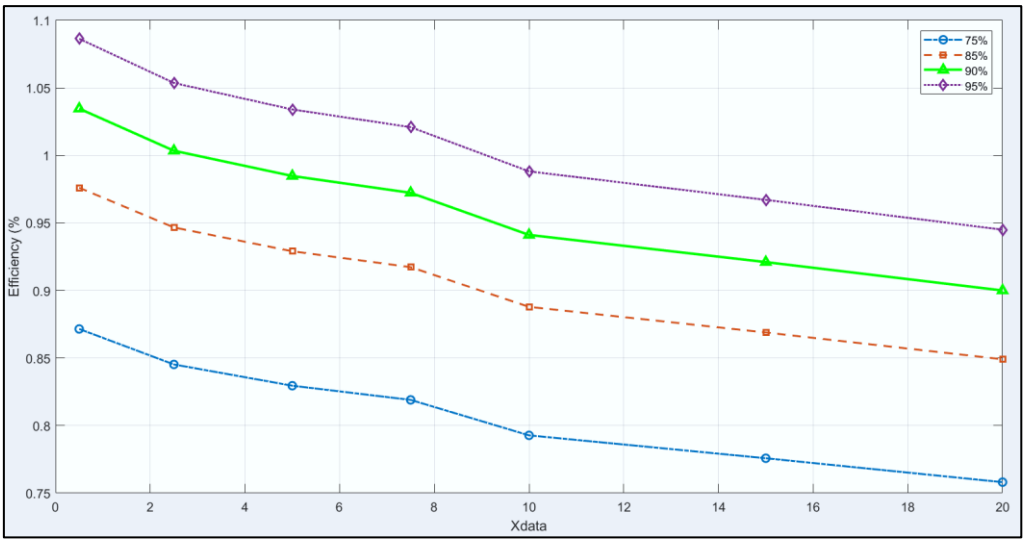

Figure 29 An overview of condenser effectiveness visualization.

It was observed from the sweep that at 90% effectiveness and a coolant temperature of 345 K, the volumetric efficiency closely matched with the reference engine. The effective Lambda at the intake valve closing and the exhaust temperature showed no significant effect on volumetric efficiency if the condenser effectiveness was set to 90% (green data line) by the equations above.

c. Water Ejector

In the baseline HAPC model, the water ejector sub-model is essential for maintaining stability in the close-loop HAPC. During combustion oxygen and hydrogen continuously entered the system resulting in water as a byproduct. The accumulation of the water can lead to pressure imbalances that jeopardize operational integrity therefore its effective removal is critically important. Conversely, the ejector functions as a selective removal mechanism targeting excess water. This is the opposite of the injector connections. This connection is attached directly to the down pipe which is located after the condenser unit in the system. Ejection occurs at the normalized location along the pipe, with values

ranging from 0.0 at the inlet to 1.0 at the ejection outlet. Figure 30 shows an overview of the sub-model.

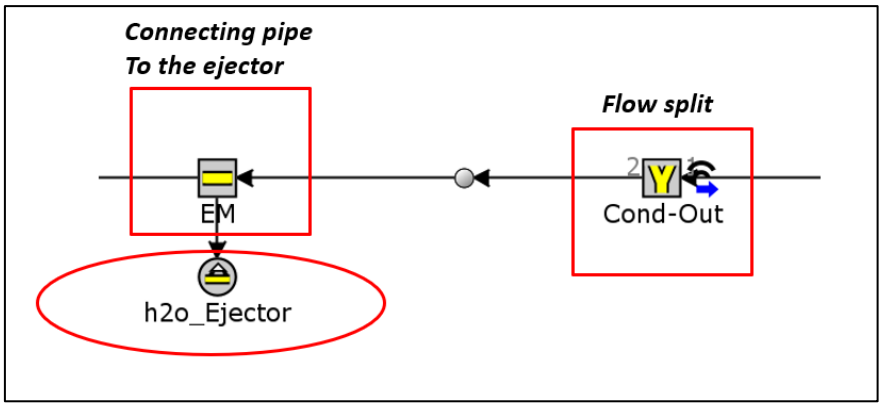

Figure 30 An overview of water ejector sub-model.

The ejector provides two operational modes, complete ejection of the water from the flow steam or controlled removal at a precise mass flow rate. This flexibility enables the system to regulate water levels efficiently, preventing disruptions to performance. Additionally, the ejector must be connected to the component such as pipes, flow splits, or cylinders in a manner that ensures the flow direction aligns from the component to the ejector connection.

In addition to the automatic convergence check, additional convergence criteria need to be added, which is the net mass of the system during each cycle, namely the mass into the system should be nearly the same as the mass out of the system which is outlined in equation 3.5. In reality, if net mass is not in Balance the system pressure will likely oscillate and prevent the system from steady operation. For this reason, the newly added criteria parameter will be calculated in the System Mass Balance Steady State Check (SMBSSC) section during control objects which will be located under the sub-assembly of 'Additional outputs'.

$$SMBSSC = \frac{mass\_in - mass\_out}{mass\_cyl\_ss} \qquad 3.5$$

Importantly, the design and operation of the ejector adhere to the principle of mass, energy, and momentum conservation. This adherence ensures the system functions optimally, maintaining balance and preventing potential failure.

c) O2 and H2 Injection and Injection control sub-models

The 'O_2 and H_2 Injection Control' subassembly includes a control circuit that is used to determine the amount of injected hydrogen based on the requirement of maintaining the closed-system mass balance. These two sub-assembly models are designed to regulate the precise quantities of oxygen and hydrogen introduced in the system, ensuring the proper stoichiometric balance essential for optimal combustion in the integrated HAPC. This sub-model is a control circuit responsible for determining the necessary amount of hydrogen injections. The baseline six-cylinder model incorporates six oxygen injectors and six hydrogen injectors, which are governed by a single injection control system. In the oxygen and hydrogen injection controller, several components are used including the receiver of the virtual signal value by mass fraction of each fluid, sense and monitor RLT variables, and mathematical signal equations.

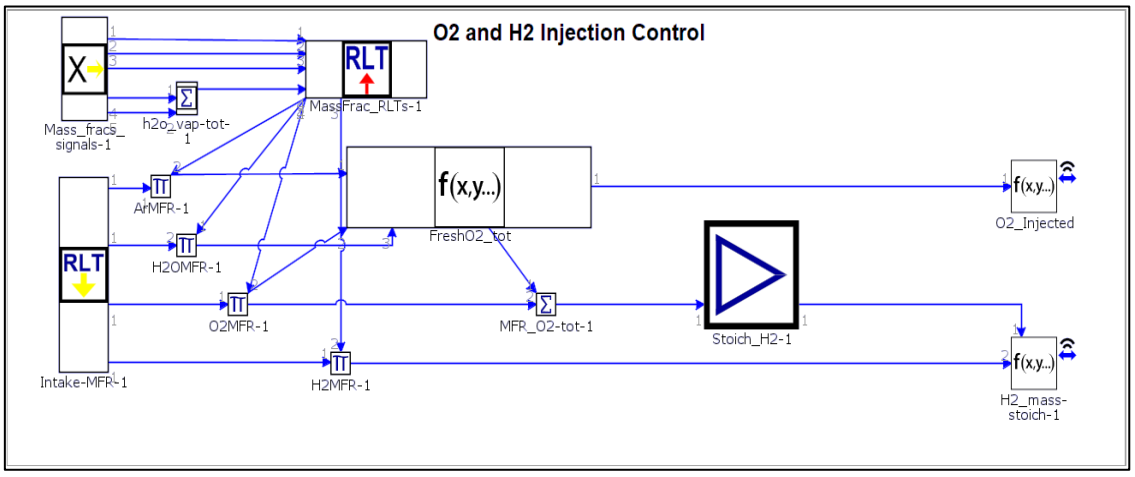

Figure 31 An overview of O2 and H2 Injection Control subassembly.

For this purpose, a “Sequential Injector” with “Imposed Pulse Width” has been used in detail in Figure 31. To achieve this, each six injectors is defined in the control input and linked through a specific port number to enable precise control over the injection of oxygen and hydrogen. The mass fraction of each controller is then calculated based on the input of the system, ensuring mass balance throughout the process.

For optimal combustion, hydrogen is injected to maintain a stoichiometric oxygen-fuel mixture, while the controller's gain system adjusts the oxygen injection accordingly to minimize the fluctuation in the stoichiometric balance. This relationship is governed by mathematical equations derived from the GT Suite template, which are communicated through wireless signals at “Oxygen injected” and “Hydrogen mass Stoich-1” objects. Figure 31 above provides an overview of the oxygen and hydrogen injection control system assembly. The total mass of injected oxygen (O2_injected) is computed using the equation 3.6.

$$O2_{injected} = \frac{1000000 \times (O2\ Fresh) \times 2}{60 \times 6 \times Engine\ Speed\ (RPM)} \times Load\ \% \qquad 3.6$$

In equation 3.4, the fresh oxygen must flow rate is scaled by a factor of 1000000 and adjusted by a factor of 2, reflecting the stoichiometric needs of the combustion process. It is then divided by the product of 60 and the engine is sped in rpm to yield a mass flow rate consistent with the operational requirements, ensuring a controlled and precise injection of oxygen into the system. The equation will be multiplied by load percentage as the engine will run into three different loads according to IMEP. Similarly, the hydrogen injection is managed by the following equation 3.7.

$$H2mass - stoich = \frac{1000000 \times (H2 - Req - H2\_Current) \times 2}{60 \times 6 \times Engine\ Speed\ (RPM)} \times Load\ \% \qquad 3.7$$

Here the difference between the required hydrogen (H2_Req) and the current hydrogen (H2_Curr) is scaled and adjusted similarly ensuring the correct hydrogen-to-oxygen ratio is maintained for optimal combustion efficiency which will differ according to the load as well. So, it could be stated that oxygen and hydrogen injectors correlated linearly and proportional to combustion efficiency as it is predefined in a gain signal. The control circuit continuously monitors and adjusts the hydrogen flow to balance the system's mass balance requirements, ensuring stable, efficient combustion processes in the closed loop cycle.

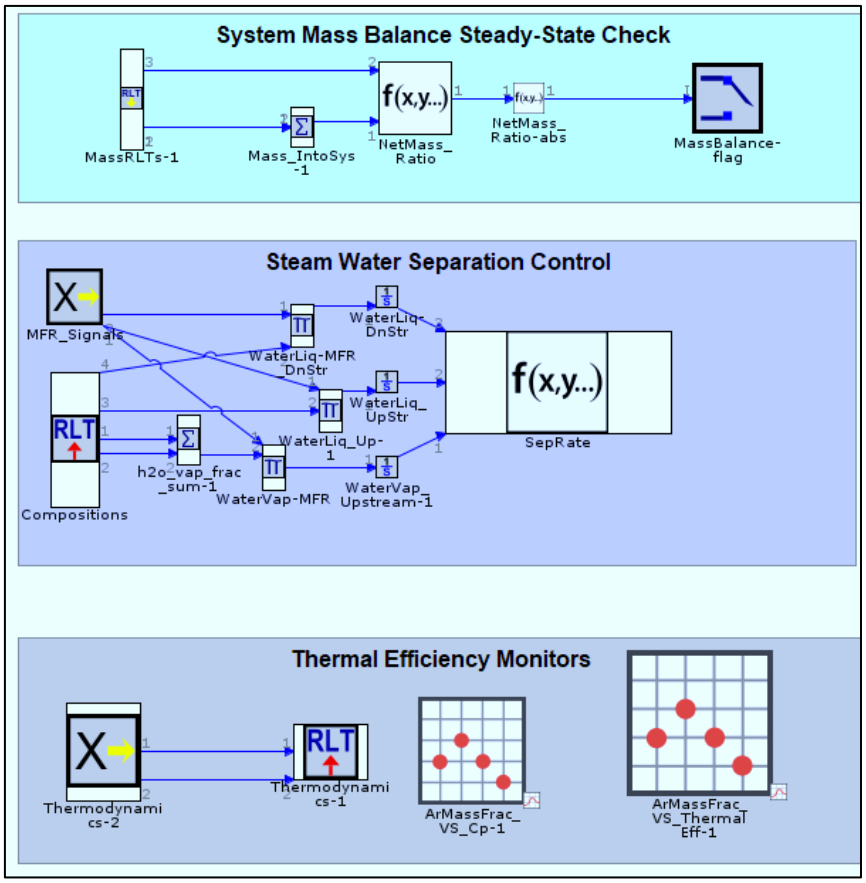

Figure 32 An overview of Additional controller units of sub-models.

The sub-models shown in Figure 32 is critical in maintaining the operational integrity of the closed-loop system preventing disruptions caused by the imbalance in fuel-oxidizer ratio, and ensuring the system operates within its designed performance parameters.

3.4.3 W6L20 Multicylinder Model for iHAPC Analysis

After successfully developing and validating the single-cylinder closed-loop HAPC model, and establishing relevant sub-models the comprehensive closed-loop six-cylinder hydrogen argon power cycle model has been established in Figure 33. The next critical phase involved optimizing the controller mechanism for hydrogen and oxygen injections to ensure precise regulation of these inputs. It was necessary to adjust the boost pressure to achieve the required trapped mass in the cylinder while maintaining stable energy levels. The same valve timing from the six-cylinder reference model was employed at this stage.

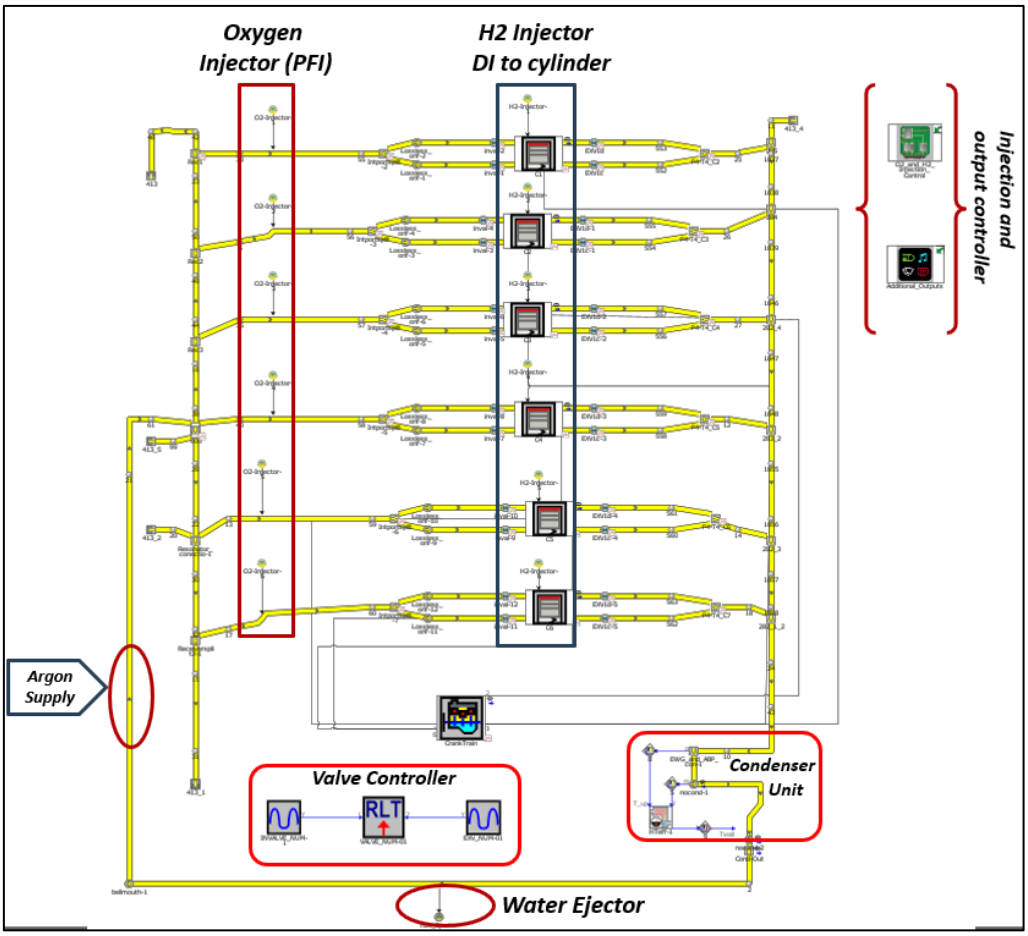

Figure 33 A 1D closed loop multi-cylinder HAPC GT-Suite Model of Wärtsilä 20 layout.

After the calibration is completed, the modified GT-Suite model will represent the intended operating conditions accurately. The next step involves validating the model to confirm that all sub-models and controllers operate according to the specified set up conditions. This process includes through error checking and ensuring consistency across all components. Once validation is completed, the multi cylinder closed-loop HAPC model will be ready for detailed analysis. Note that, the port fuel injection system is used for oxygen injection, whereas hydrogen is directly injected into the cylinder. This model will be used to explore the specific research questions outlined in this thesis, providing insight into the performance, efficiency, and viability of modified power cycles under various operating conditions.

3.5 Post-Processing and Data Analysis Methods

The methodologies for analysing simulation outputs and experimental Data, a systematic approach to post-processing and data analysis is presented, utilizing both experimental and simulation data to deepen their understanding of the Argon Power Cycles Performance. This methodology involves several key steps: comparing simulated data with real test data, evaluating various performance measures, and conducting statistical analysis to validate the results. Furthermore, understanding all the parameters of internal combustion engines which are affected by various equations as well as the limitations and delimitations of the study, for the essential aspects of this thesis. These elements are considered integral to the post-processing phases of the project where detailed mathematical explanations for calculating efficiencies and combustion parameters, such as CA50, Gross indicated efficiency, Net indicated efficiency, brake thermal efficiency, and other parameters will be provided. This calculation is crucial for analyzing the hydrogen argon power cycle performance and interpreting the results which have been illustrated in equations (3.8-3.22) (Gamma Technologies, 2024a; Heywood, 1988).

Net indicated efficiency considers the network output, considering losses such as pumping and frictional losses within the engine relationship defined in equation 3.8.

$$\eta_{ig,\,net} = \frac{Wig,net}{\dot{m}fuel \times LHV} \qquad 3.8$$

In equation 3.8, $\eta_{ig,\,net}$ denotes net indicated efficiency, $W_{ig,\,net}$ reflects net indicated work per cycle (Joules), LHV highlights the lower heating value of the fuel (J/ Kg) and $\dot{m}fuel$ indicated mass flow rate of fuel (kg/s).

Net indicated work is calculated over the entire engine cycle, including intake, compression, power, and exhaust strokes shown in equation 3.9.

$$Wig,net = Wig,gross - Wpumping \qquad 3.9$$

In equation 3.9, $W_{pumping}$ is the present work done to move the intake and exhaust gases in and out of the cylinder.

Gross indicated efficiency represents the efficiency with which the engine converts the chemical energy to the fuel into indicated work, before accounting for losses such as friction. The formula for gross indicated efficiency is illustrated in equation 3.10.

$$\eta ig, gross = \frac{Wig, gross}{\dot{m}fuel \times LHV} \quad 3.10$$

Here in equation 3.10, $\eta_{ig,\,gross}$ reflects gross indicated efficiency, and $W_{ig,\,gross}$ reflects gross indicated work per cycle (Joules). The gross indicated work $W_{ig,\,gross}$ can be calculated by integrating the pressure-volume (P-V) diagram over the compression and power strokes, accounting only for the work done by the combustion gases in equation 3.11.

$$Wig, gross = \int_{Vmin}^{Vmax} P\, dV \quad 3.11$$

In equation 3.11, P denotes instantaneous cylinder pressure (Pa) where V reflects cylinder volume (m^3). Fuel energy entering the cylinder is calculated based on the mass of the fuel-injected power cycle and the lower heating value of the fuel by equation 3.12.

$$Efuel = \dot{m}fuel \times LHV \quad 3.12$$

In equation 3.12, E_{fuel} suggests Fuel energy entering the cylinder.

Brake thermal Efficiency is a measure of how effectively the engine converts the chemical energy to the fuel into useful mechanical power at the crankshaft, after accounting for all internal losses can be found in equation 3.13.

$$\eta b = \frac{Pb}{\dot{m}fuel \times LHV} \quad 3.13$$

$$Pb = T \times \omega \quad 3.14$$

In the above equation, η_b highlights Brake thermal efficiency, where P_b denotes brake power (Watts). Brake power Pb is the actual power output of the engine available at the crankshaft and can be calculated in equation 3.14.

In equation 3.14, T suggests torque produced by the engine (Nm), ω depicts Angular velocity of the engine (rad/s), with $\omega = \frac{2\pi N}{60}$ and N suggests Engine speed in RPM.

Indicated mean effective pressure (IMEP) is a fundamental measure of an engine's efficiency and performance, representing the average pressure in the cylinder during the power stroke that would produce the same work output while it was constant. Net IMEP (IMEP720) Considers the entire engine cycle which can be derived in equation 3.15, including intake, compression, power, and exhaust strokes, and incorporates pumping losses.

$$IMEP720 = \frac{Wig,net}{Vs} \qquad 3.15$$

In equation 3.15, Vs is displacement volume (m^3). Gross IMEP (IMEP360) in equation 3.16, considers only the power-producing part of the cycle (compression and power strokes).

$$IMEP360 = \frac{Wgross}{Vs} \qquad 3.16$$

In the above equation, $IMEP_{360}$ is the gross indicated mean effective pressure (bar). Mechanical efficiency assesses how efficiently the work done by the gases is transferred to the crankshaft after accounting for the mechanical losses. Mechanical efficiency (η mech) is shown in equation 3.17. P_{ig} is indicated power (Watts), calculated from the pressure inside the cylinder.

$$\eta\, mech = \frac{Pb}{Pig} \qquad 3.17$$

Gas exchange efficiency (η_{GE}) can be expressed in equation 3.18.

$$\eta\, GE = \frac{Wig,net}{Wig,gross} \qquad 3.18$$

Therefore, to describe the relationships between various efficiencies of ICE, Equation was proposed by (Wang, Jin, et al., 2023a):

$$\eta Brake = \eta Combustion \times \eta Thermodynamic \times \eta GasExchange \times \eta Mechanical \quad 3.19$$

This equation provides a comprehensive understanding of how different processes and losses within the engine impact the overall conversion of fuel energy into useful mechanical work. Each term represents a specific stage in the energy conversion process from combustion to mechanical power output which will be crucial for the hydrogen argon power cycle.

CA50 (Crank Angle et 50% Mass Fraction Burned) is a critical parameter for understanding the combustion characteristics within the engine cylinder. It represents the crank angle at which 50% of the fuel mass has been burned. The calculation on CA50 involves analysing the cylinder pressure data obtained during the combustion process. The detailed step-by-step equations are given below: The heat release rate ($\dot{Q}_{comb}$) can be calculated by equation 3.20.

$$\dot{Q}_{comb} = \gamma . \rho . \frac{dV}{dt} + \frac{1}{1-\gamma} . V . \frac{dP}{dt} \quad 3.20$$

In the above equation, γ *is the* Ratio of specific heat (typically about 1.67 for Argon), ρ highlights Instantaneous Cylinder pressure (bar), $\frac{dV}{dt}$ suggests *the* rate of change of volume with time, *V* denotes instantaneous cylinder volume (m^3), and $\frac{dP}{dt}$ is *the* Rate of change of pressure with time.

The cumulative mass fraction burned (MFB) is a measure of how much fuel has been burned up to a particular crank angle. It is calculated by integrating the heat release rate over time or crank angle in equation 3.21.

$$MFB\ (\theta) = \frac{\int_{\theta\ start}^{\theta} \dot{Q}\ comb\ d\theta}{\int_{\theta\ start}^{\theta\ end} \dot{Q}\ comb\ d\theta} \quad 3.21$$

In equation 3.21, θ is the crank angle (degrees), where θ_{start} denotes the crank angle at the start of combustion (degrees) and θ_{end} reflects the crank angle of the end of combustion (degrees).

CA50 is defined as the crank angle at which the MFB reaches 50%. Once the MFB is calculated as a function of crank angle, CA50 can be identified by finding the crank angle at which the MFB is equal to 0.5 or 50%. So mathematically by equation 3.22.

$$CA50 = \theta when\ MFB\ (\theta) = 0.5 \qquad 3.22$$

This can be determined either graphically, first by plotting MFB against crank angle, or numerically, by solving the MFB equation for crank angle that gives 0.5. CA50 is a vital parameter for optimizing combustion timing, improving fuel efficiency, and reducing emissions. Properly understanding and calculating CA50 allows fine-tuning engine settings for optimal performance and compliance with the emissions regulations in HAPC.

Detailed post-processing and data analysis methods require optimizing the iHAPC by enhancing combustion efficiency, reducing mechanical losses, and improving gas exchange. Understanding parameters such as CA50, Net and Gross indicated efficiencies and mechanical efficiencies allows for precise control of the combustion process, maximizing energy conversion. These insights lead to higher thermal efficiency and lower emissions, meeting stringent environmental standards. By utilizing comprehensive equations that incorporate various efficiencies, the overall performance of the hydrogen argon power cycle can be fine-tuned. This approach ensures that the engine operates effectively, providing a sustainable solution for future energy needs in ICEs.

3.6 Targeted engine design constraints

The design constraints and requirements for achieving the proposed step-change in efficiency through innovative HAPC solutions centred on addressing key knowledge gaps and overcoming system-level challenges. Currently, state-of-the-art lean burn large bore engines if the engine is adiabatic, would be an ideal cycle with efficiencies up to 65%. However, by utilizing an argon-based oxy-fuel mixture notable increase in real-world efficiency estimated at 15% to 20% becomes feasible. To bridge the gap between theoretical prediction and practical applications specific design requirements have been

established in the model interpolated in Table 10, these requirements guide the development and testing of a modelled Wärtsilä 20 HAPC engine.

Table 10 An overview of Targeted engine design constraints

Parameters	Design Requirement
Net Efficiency (%)	60
Maximum In-Cylinder Pressure (bar)	230
Maximum In-Cylinder Temperature (K)	3000
Power Output (kW)	1200
Maximum Exhaust Gas Temperature (EGT) (K)	950-1000

The investigation aims to evaluate the influence of the current engine configuration on these requirements and determine the performance outcome of implementing the hydrogen argon power cycle in this context. Moreover, this investigation will provide a comprehensive comparison of design constraints, targeted outcomes, and system-level impacts ensuring alignment with the project's goal of achieving a maximum percentage of efficiency improvements and economic feasibility in hydrogen-based power systems. Through rigorous evaluation the research aims to advance the practical realization of HAPC, establishing a foundation for future innovation in sustainable energy systems.

4 Result and discussion

4.1 Simulation Results of the Reference Model

The reference W6L20-2STC Dual Fuel engine model has been simulated for 175 cycles until it reaches a steady state and collected data across three distinct load levels of 50%, 75.25%, and 101.20%. The engine performance metrics for the specific load have been illustrated in Figure 34.

At a 50% load level, the engine operates at a boost pressure of 3.50 bar, with a fuel-injected mass per cycle of 310.85 mg. The IMEP reaches 15.77 bar while BMEP is recorded at 13.70 bar, indicating a moderate level of net effective pressure contributing to cylinder power. The load condition provides an indicated efficiency of 47.89% and brake efficiency of 41.95%, signifying effective fuel utilization in combustion, and generates a maximum pressure and temperature of 160.98 bar and 1693.73 K, respectively. At this stage, the maximum exhaust gas temperature has reached 814 K. The Lambda values which represented the air-to-fuel ratio at key points in the cycle, are 4.26 at cycle start or intake valve closing (IVC), and 2.56 at exhaust valve opening (EVO). This results in a brake power output of 602.58 kilowatts.

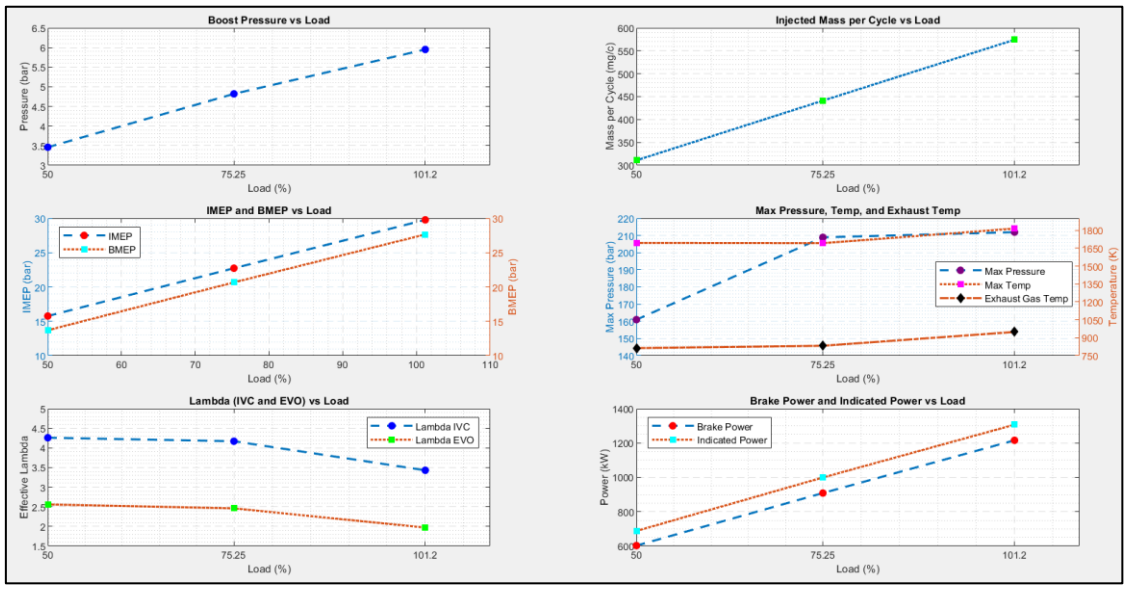

Figure 34 Reference GTP simulated data of engine performance metrics of W6L20-2STC model.

As the load increased to 75.25%, the boost pressure rose to 4.82 bar, and the injected fuel mass power cycle increased substantially to 441.17 mg, in line with the higher power demand. The IMEP and BMEP increased to 22.73 bar and 20.67 bar respectively, enhancing the pressure extended on the Pistons. The indicated and brake efficiency also slightly improves to 48.98% and 44.60% respectively, indicating a more efficient combustion process at this load level. In-cylinder pressure and temperature reach 208.91 bar and 1691.89 K, respectively reflecting the elevated thermal and mechanical stress at this operating point. The effective Lambda value adjusted to 4.17 at IVC and 2.46 at EVO which indicates a leaner mixture, with a brake power output of 908.59 kilowatt and a maximum exhaust temperature increased to 833 K.

At full load (101.20%), the engine attains a higher boost pressure of 6.00 bar, with an injected fuel mass per cycle of 574.14 mg. The IMEP and BMEP reach 29.77 bar and 27.65 bar, demonstrating the engine's maximum capability to generate power through in-cylinder pressure. Indicated and brake efficiency reaches 49.21% and 45.82% showing optimized combustion efficiency at high load. The maximum in-cylinder pressure increases to 211.93 bar, while the maximum temperature peaks at 1813.91 K. But effective Lambda values dropped to 3.43 at IVC end 1.97 at EVO, reflecting the turbocharger is probably limiting achieving higher lambdas during power operation. Consequently, the brake power output achieves a maximum of 1215.75 kilowatts (kW), and the exhaust temperature peaks at 948.50 bar.

Before running the final simulation sweeps, the W6L20-HAPC GT-Suite model was calibrated, with IMEP, power output according to the load condition, and total fuel energy entering the cylinder held constant. The baseline operating point was selected based on maximum combustion efficiency observed under normal operating conditions with the addition of noble gas in the cycle with premixing techniques. The baseline serves as a reference for analysing the effects of noble gases, injection strategies, and other combustion dynamics detailed in Table 11.

Table 11 Baseline operating points and initial values for simulation.

Description	Parameters
Speed (rpm)	1000
Injected Fuel mass (mg)	ref.
Test Fuel	Hydrogen (H_2)
Test Working fluid	Argon (Ar), Helium (He), Ar+ He
Simulation Type	Closed-loop, Steady-state
Combustion Model	Imposed burn rate (TPA) modelled for W6L20-2STC
Main Parameters	Fuel output, IMEP, Total Mass Trapped at Cyl. Cycle-Start or IVC, Mixture composition, CR, Time, and Power outputs.

The baseline operating point is primarily user-defined. The study employs a performance-based simulation analysis with a fixed combustion burn rate and constant valve timing as used in the W6L20-2STC GT-Suite model to assess the impact of the closed-loop hydrogen argon power cycles on the specific engine. For further analysis, a 75.25% load condition with a mixture composition of 90% argon and 10% oxygen, is recommended. This composition maximizes the thermal efficiency theoretically, the combustion process while maintaining manageable peak temperatures and pressures. The high argon content, which has a high specific heat ratio (γ), increased compression pressure, and temperature, does improve energy conversion efficiency without reaching excessive thermal stress that could affect engine durability.

4.2 Model Validation at Motoring Condition

4.2.1 Baseline Model Validation

The validation process in this study involved comparing simulated results from the Wärtsilä GT-Suite model with experimental in-cylinder pressure data obtained under 50.20% load conditions. Model validation is essential before conducting a comprehensive simulation sweep, as it verifies that the model accurately reflects real-world performance.

To facilitate this validation, Wärtsilä provided both the W6L20-2STC GT-Suite model and experimental in-cylinder pressure data. The six-cylinder engine model was converted to a single-cylinder research engine (SCRE) model by calibrating the in-cylinder pressure data to align with reference engine's experimental results. For the SCRE dual fuel engine model, alignment was achieved by adjusting the intake pressure to the required level. Key parameters, such as IMEP, trapped mass, and fuel entering the cylinder were held constant to simulate realistic engine operating load conditions. This validation confirms that the adapted SCRE model is now ready to be applied to the final six-cylinder closed-loop HAPC model, facilitating further investigation of the research questions outlined in this thesis.

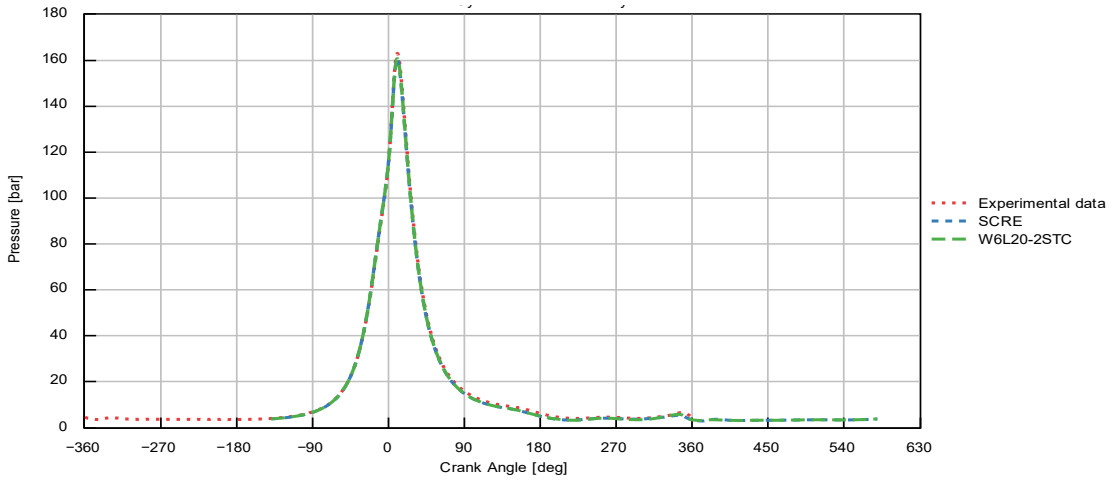

Figure 35 In-cylinder pressure comparison for validation (Experimental data vs W6L20-2STC model vs SCRE)

In Figure 35, a detailed comparison is presented among experimental data, the reference W6L20-2STC model, and SCRE data. The result demonstrated a high degree of consistency between the simulated and experimental data, which simulated pressure curves closely following the experimental curve. This similarity highlights the accuracy of the simulation models in capturing combustion characteristics. The pressure was normalized relative to the experimental maximum pressure and total fuel energy, with peak pressure predictions showing an absolute deviation of 1.93 bar and 1.89 bar. Table 12 compares to maximum in-cylinder pressure for the three data sets at a crank angle of around 11°.

Table 12 Comparison of experimental and simulated data for validation

Data set	Crank Angle Degree (CAD°)	Pmax (bar)	$\frac{\mathbf{Pmax_{sim}}}{\mathbf{Pmax\_exp}} \times \mathbf{100\%}$
Experimental	11	162.94	-
W6L20-2STC	11	161.01	98.81%
SCRE	11	161.05	98.84%

Both Figure 35 and Table 12 illustrated that in-cylinder peak pressure (P_{max}) differences within the specified crank angle are less than 5%, underscoring the model's precision in predicting other critical engine performance parameters.

4.2.2 Motoring Pressure and Temperature Comparison

The graphs in figures 36 and 37 illustrate an analysis of the pressure and temperature profiles in a W20 engine using two different gas mixtures: one consists of argon and oxygen (78% Ar+ 22% O_2), and the other of air (78% N_2 + 22% O_2). Both mixtures were tested under identical conditions, with an in-cylinder flow rate of 214.25 g/s during motoring condition. Notably, no fuel injections occurred within the cylinder during the experiment, and the same motoring condition was replicated in the simulation.

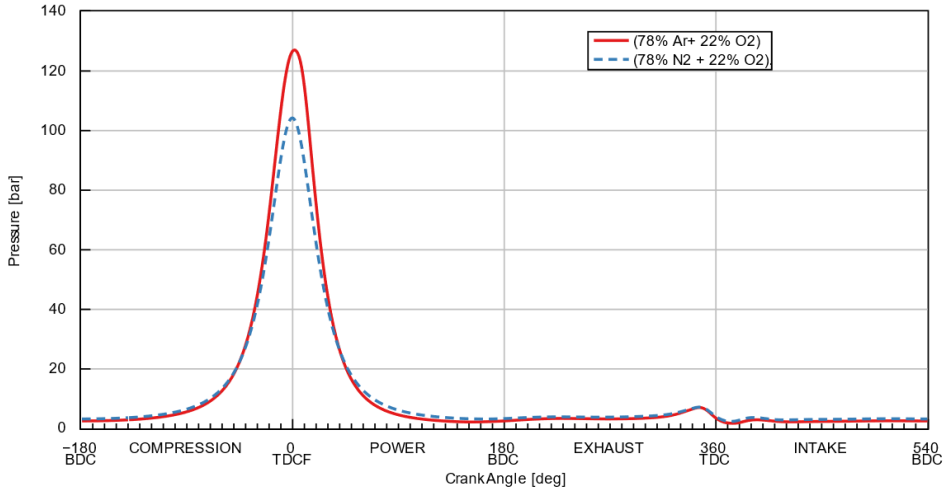

Figure 36 Motored Pressure vs Crank Angle plot for Argon-Oxygen Mixture vs. Air.

Figure 36 presents the motored pressure, measured in bar, plotted against the crank angle, ranging from -180° to 600°. Both mixtures exhibit a pronounced peak pressure near

the top dead centre (0°crank angle), indicative of the compression phase. The argon-oxygen mixture generates a peak pressure of approximately 127.06 bar, compared to the air mixture recorded at 104 bar. This indicates that the argon-oxygen mixture offers enhanced pressure generation during combustion. Beyond the peak, both pressure curves decline rapidly, followed by minor fluctuations corresponding to the subsequent exhaust and intake strokes. The overall trend highlights the comparative efficiency and behaviour of two mixtures during the internal combustion process, with the argon-oxygen Mixture demonstrating a 122.2% increase in peak pressure than nitrogen and oxygen mixture.

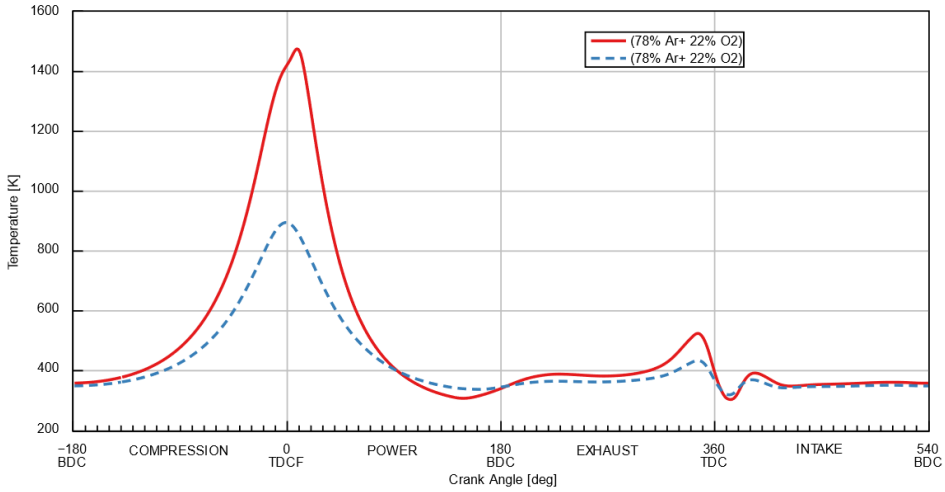

Figure 37 Motored Temperature vs Crank Angle plot for Argon-Oxygen Mixture vs. Air.

Figure 37 compares the corresponding in-cylinder temperature profiles of the two gas mixtures discussed. The argon-oxygen mixture reaches a peak temperature of approximately 1477 K, significantly higher than the 895 K observed for the air mixture, indicating more intense combustion. Both profiles then decline rapidly, with the argon-oxygen mixture consistently maintaining a slightly higher temperature during the exhaust and intake phases as it represents the imposed burn rate for the model.

It can be concluded that the use of argon as a working fluid increases the temperature due to its high specific ratio (γ), which is a key factor in thermodynamics that affects the power cycle of internal combustion engines. A higher γ results in increased pressure and temperature during the adiabatic compression and expansion phases, following the

relationships $P \propto V^{-\gamma}$ and $T \propto V^{1-\gamma}$. This leads to more efficient energy conversation from the fuel producing higher peak pressures and temperatures compared to air, which contains nitrogen with lower γ. Furthermore, argon's inert nature minimizes heat loss through the chemical reactions and combustion process, thereby retaining more energy within the system.

In the literature, it was reported hydrogen as a fuel in an argon-oxygen mixture that offers advantages, but it also presents several critical challenges. Hydrogen's low molecular weight and high diffusivity increase the risk of leakage, requiring advanced sealing technologies during combustion. Additionally, its wide flammability range (4 to 75%) and low ignition energy demand precise control over the oxygen-full mixture to avoid combustion instability and backfiring. Pre-ignition is a concern due to hydrogen's low auto-ignition temperature of 585°C (858 K) (Sánchez & Williams, 2014). This makes hydrogen prone to self-ignition, especially in high-compression engines, where premature combustion can cause knocking, reduced efficiency, and damaged engine components. Managing compression ratio, ignition timing, and cooling system is crucial to avoid these issues. Moreover, thermal loading, particularly in lean burn conditions, exacerbates engine stress. Hydrogen's high energy content and leaner mixture lead to higher combustion temperatures, creating hotspots that increase the risk of material fatigue and engine failure. Incomplete combustion from insufficient fuel supply exacerbates thermal stress, requiring an advanced cooling system, high-temperature resistant materials, and real-time temperature monitoring. Despite these challenges, the use of an argon-oxygen mixture offers valuable benefits in hydrogen combustion as discussed in the literature section which will be investigated according to the simulated result in the section below.

4.3 Effect of Argon-to-Oxygen Ratio

4.3.1 Design of Experiments (DOE)

The optimal argon-to-oxygen-to-fuel ratio for achieving maximum combustion efficiency will be examined at sweeps of three engine loads such as 50.20%, 75.25%, and 101.20%.

The argon-to-oxygen ratio is adjusted by progressively increasing the argon pressure within the closed-loop system. Several parameters are systematically adjusted to ensure consistent power output across the different argon-to-oxygen ratios, including the hydrogen fuel amount and oxygen-to-argon ratio in the located pipe by adjusting mass by fraction in the system. This is achieved by providing the necessary boost pressure and fine-tuning the fuel injection control unit. The experimental design is detailed in Table 13, which outlines the constant combustion parameters corresponding to various loads.

Table 13 Constant combustion Parameters for different loads.

Combustion Parameters	**Loads**		
	50.20%	**75.25%**	**101.2%**
Combustion Start [CA00] (°)	-21.57	-20.37	-15.76
Combustion Delay [CA02-CA00] (°)	15.28	13.43	8.36
CA02 (°)	-6.29	-6.93	-7.40
CA50 (°)	6.18	6.92	9.16
Burn Duration [CA90-CA10] (°)	16.39	18.43	22.61
Burn Duration [CA90-CA00] (°)	36.93	37.75	37.07
Condenser Efficiency (%)	95		
Coolant Temperature (K)	345		
Compression Ratio (CR)	12.3		
Ar-to-O_2 Ratio (Swept parameters)	▪ 90% Ar +10% O2 ▪ 88% Ar + 12% O2 ▪ 85% Ar + 15% O2 ▪ 80% Ar + 20% O2		
Fuel (H_2)-to-O_2 Ratio	Stoichiometric (1:8)		
H_2 fuel Value (g/cycle)	Varies with load and Ar-to-O_2 ratio		

The table summarizes the constant combustion parameters used for the simulation sweeps for different loads, including combustion timing, burn duration, fuel consumption, and range of Ar-to-O_2 ratios with constant condenser efficiency, coolant temperature, and compression ratio. It is important to note that the combustion burn rate is constant for all the cases for different loads where the CA10, CA50, and burn duration

do not change for all these cases and are kept constant, as shown in Table 13 but constant for three different loads.

4.3.2 Mid-Load Point (50.20% Load)

Performance Results

The simulated results illustrated in Figure 38 explore the impact of varying argon concentration on the performance and efficiency of the HAPC W20 engine model for 50.20% load of the reference engine. The simulation results depict that the required boost pressure reduced from 2.65 to 1.87 bar with the reduction of argon percentage from 90% to 80%. At an argon concentration of 90%, the engine achieves a net indicated mean effective pressure (IMEP) of 15.90 bar and BMEP of 13.70 bar with a net indicated efficiency of 55.59% and brake efficiency of 47.90%. As the Argon concentration decreases to 88%, 85%, and 80% there is a slight drop in IMEP with values of 15.89 bar, 15.77 bar, 15.78 bar, and 13.64 bar, 13.70 bar, 13.70 bar for brake mean effective pressure (BMEP) respectively though it is maintaining the 50.20% load conditions. Simultaneously, the efficiency matrix shows a slight declining Trend at 80% argon the net indicated efficiency reduces to 50.70% and brake efficiency to 43.98%.

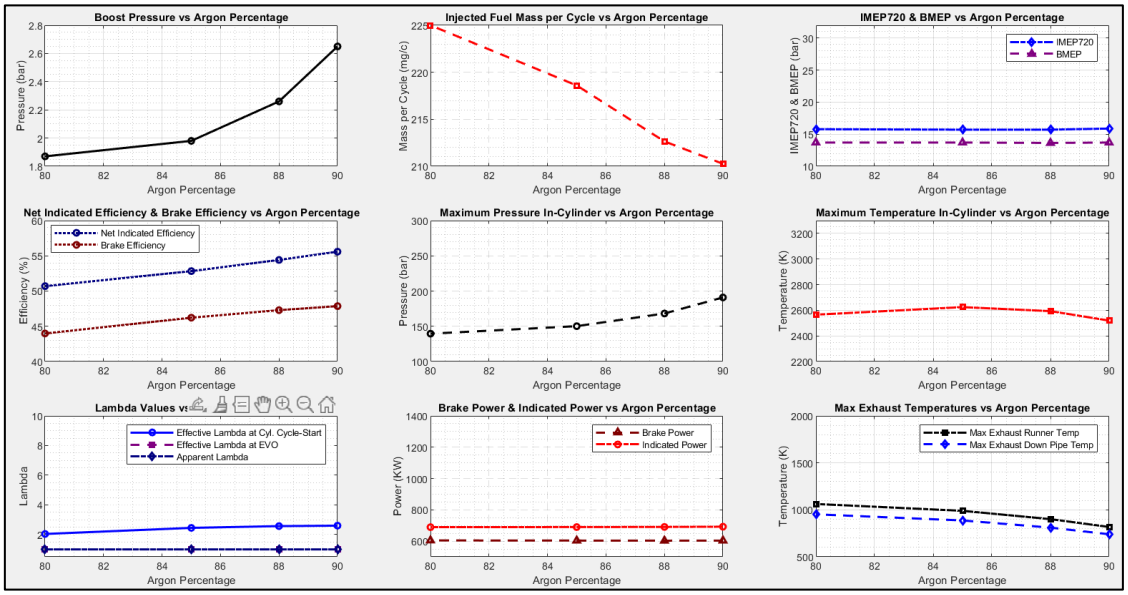

Figure 38 Performance Metrics Analysis of Closed-Loop HAPC at 50% Load for Different Diluted Mixture Compositions.

The maximum in-cylinder pressure reaches 190.94 bar, and the peak in-cylinder temperature is 2519.50 K at a 90% argon concentration. As argon concentration decreases, both cylinder pressure and temperature also affected, with lower argon concentration at 88% argon the pressure is reduced to 168.17 bar the temperature increases slightly to 2593.32 K while at 85% argon, these values are 150.19 bar and 2624.65k respectively. At lowest argon concentration 80% yields a pressure of 139.52 bar but a slightly elevated temperature of 2565.70 K. The oxygen-fuel ratio represented by effective Lambda and apparent Lambda during combustion remained constant at 1.00 throughout the range of argon concentration signifying stable stoichiometric combustion but varying slightly which is very low.

However, the exhaust temperature shows notable increases at lower argon levels. The maximum exhaust gas temperature rises from 817.88 K at 90% Argon to 1062.40 K at 80% Argon. Similarly, the exhaust gas running through downpipe temperature increases from 740.13K to 952.09 k, suggesting higher thermal losses and increased heat stress on exhaust gas as the argon level decreases which was working as a thermal buffer. In terms of power output, the indicated power remains stable at approximately 690 Kw across different argon percentages, where the brake power shows constantly approximately 604KW according to the maintained load power output.

In Cylinder Pressure and Temperature Analysis

Figures 39 and 40 serve as visual representations of the in-cylinder pressure and temperature variation as a function of crank angle for the six-cylinder models under steady-state conditions at 50.20% load. The composition of the working fluid varies with differing percentages of argon and oxygen. The injection (INJ), ignition (IGN), exhaust valve opening (EVO), and intake valve opening (IVO) point a line consistently for all cases highlighting the control and predictability of the closed-loop cycle.

The key observation from the plot explores that the compression phase shows a consistent rise in pressure across all cases, culminating near the top dead centre (TDC) as

the piston compresses the mixture. The high argon content as a noble gas with a high specific heat ratio in the working fluid significantly influences the pressure rise during compression. It is also observed that ignition occurs shortly before TDC marked up by a sharp pressure spike indicating rapid combustion of the hydrogen-oxygen mixture.

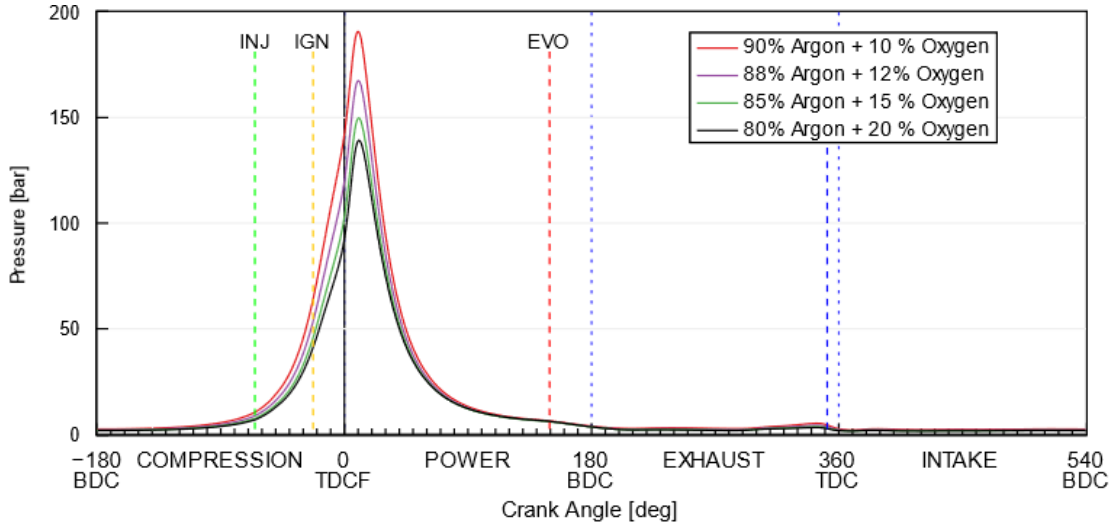

Figure 39 In Cylinder Pressure Analysis of 50% Load for different mixture compositions.

Note that 90% argon content is noticed as the maximum in-cylinder pressure, while 80% argon concentration illustrates the lowest maximum pressure in the cylinder. The peak in-cylinder pressure decreases as oxygen content increases and argon content decreases as it should increase. However, due to the decreasing boost pressure for the intake to maintain the same load but different mixture composition, the in-cylinder pressure reduces. The pressure decreases gradually after the peak as the piston moves toward the bottom dead centre (BDC) during the expansion or power stroke.

The graph in Figure 40 illustrates the in-cylinder temperature profiling across a complete engine cycle at 50.20% load, comparing various argon-to-oxygen mixture compositions. During compression stroke, the temperature rises steadily due to the adiabatic compression of the gas mixture. The trend for all four different mixtures is closely aligned in this phase. A sharp temperature increase is observed immediately after TDCF Considering the ignition of the hydrogen-oxygen mixture. This phase exhibits a distinct

temperature peak for each composition. The 90% argon, with a 10% oxygen mixture achieves the lowest peak temperature reflecting argon's superior thermal insulation properties due to the high specific heat ratio.

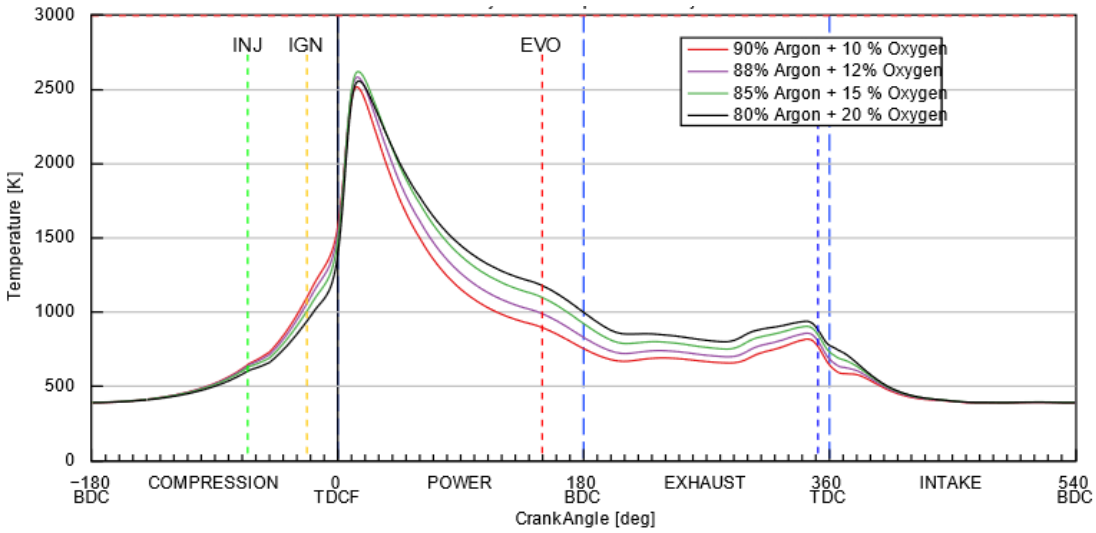

Figure 40 In Cylinder Temperature Analysis of 50% Load for different mixture compositions.

Mixtures with lower argon content, such as 85% argon, show the highest peak temperature of 2625 k. This is mainly due to the higher oxygen fraction, which improves heat transfer and speed of energy dissipation. Although the mixture of 80% argon and 20% oxygen is expected to produce a higher peak temperature, it results in a slightly lower temperature of 2566 K. This difference can be explained by the engine's 50.20% load limit, which may limit combustion efficiency and reduce the temperature rise. The lower in-cylinder temperature with 80% argon might primarily be caused by the higher oxygen content, which increases heat capacity, speeds up combustion, enhances heat absorption, and lowers peak pressure- together limiting the temperature rise despite the lower argon content. As the exhaust valve opens, a significant drop in temperature occurs as the hot combustion products exit the cylinder. Mixtures with lower argon concentration with oxygen exhibit marginally higher exhaust gas temperatures due to their comparability to higher thermal conductivity than other mixtures. During the intake phase the in-cylinder temperature stabilized at a minimal level all mixtures exhibit a similar trend during this phase with negligible differences.

4.3.3 75.25% Load Point

Performance Results

Figure 41 depicts the performance characteristics of 75.25% load condition. As argon percentage decreases from 90% to 80% there are notable changes in engine performance. The boost pressure shows a downward trend from 3.12 bar at 90% argon to 2.00 bar at 80% argon indicating a reduction in the pressure within the combustion chamber as Argon content decreases.

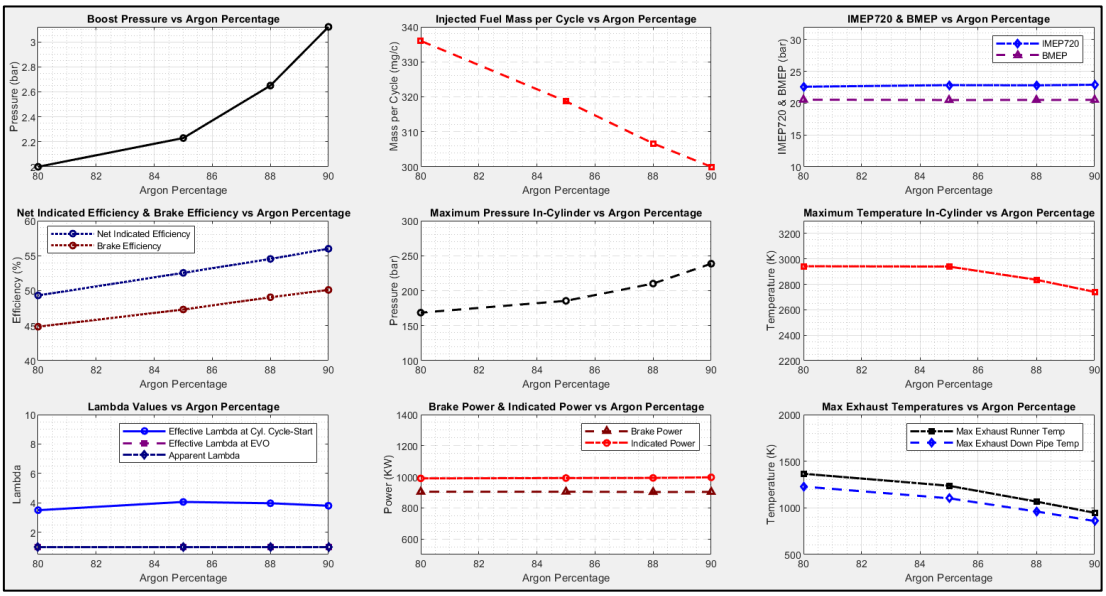

Figure 41 Performance Metrics Analysis of Closed-Loop HAPC at 75.20% Load for Different Diluted Mixture Compositions.

The injected fuel mass increased from 300 mg/c at 90% Argon to 336 mg/c at 80% argon, reflecting a higher fuel demand as argon content decreases facilitating more oxygen which requires a higher amount of fuel to burn. The net efficiency follows a decreasing pattern from 56% at 90% Argon to 49.32% at 80% Argon. Similarly, brake efficiency shows a similar decline from 50.11% at 90% argon to 44.85% at 80% argon. At 90% argon, the maximum in-cylinder pressure reaches 238.59 bar, and the maximum in-cylinder temperature peaks at 2740.36 k. As the Argon percentage decreases the maximum pressure

declines due to the reduction of boost pressure but the temperature increases, reaching 168.60 bar and 2942.03 K at 80% argon respectively.

However, effective Lambda values at EVO remain constant across the argon percentage variation with both maintaining a stoichiometric value of 1.00. In contrast the maximum exhaust gas temperature and maximum exhaust downpipe temperature both increase as the Argon percentage decreases. At 90%, the exhaust temperature is 947.28 K and 858.63 K respectively. By the time the argon content drops to 80%, the temperature rises to 1365.80 K and 1228.16 K. This temperature increase could be indicative of energy release in the exhaust gas as the engine operates with a lower argon content. Both brake power and indicated power remain constant as it is following the same load power output but, demonstrate a slight fluctuation with decreasing argon concentration. At 90% Argon, the brake power is 902.70 kW, and the indicated power is 996.49 Kw while at 80% Argon, these values change to 903.54 KW and 989.71 Kw respectively.

In Cylinder Pressure and Temperature Analysis:

The graph in Figure 42 illustrates that in-cylinder pressure analysis of the combustion process for different mixture compositions of argon and oxygen has a constant load of 75.25%. The in-cylinder pressure follows similar trends as explained for 50.20% load.

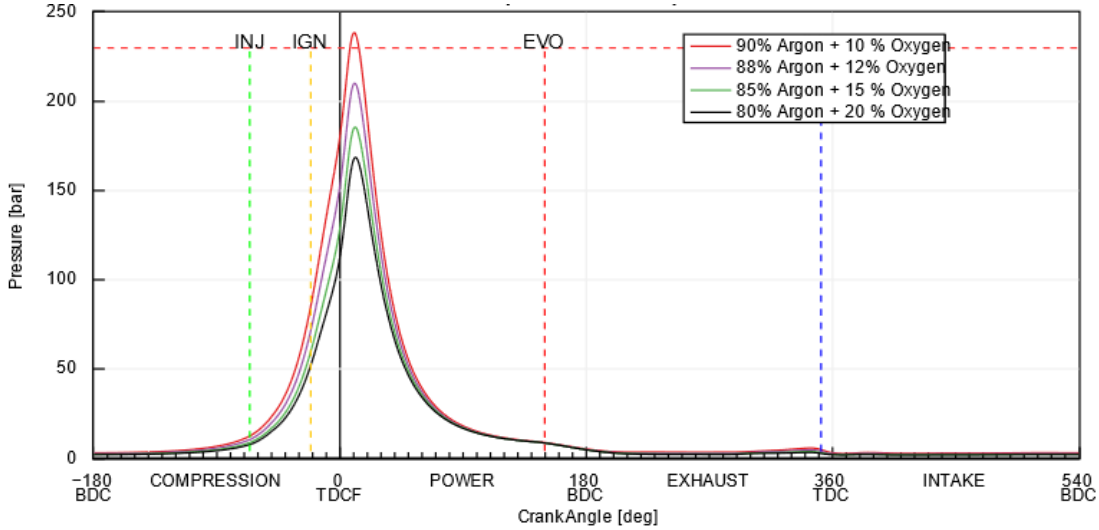

Figure 42 In Cylinder Pressure Analysis of 75.25% Load for different mixture compositions.

The peak pressure is the highest for the mixture containing 90% argon with 10% oxygen and decreases as the oxygen content increases. All mixture exhibits similar trends during the compression and power strokes. However, the slight variation in pressure rise is noticeable after ignition, especially at TDC and during the power stroke. The symmetry of the pressure curve after EVO indicates an efficient exhaust and intake process as there is no significant residual pressure after the combustion cycle.

Figure 43 examines the effect of different argon percentages in mixture compositions at in-cylinder temperature during a complete engine cycle at 75.25% load for four different mixtures. From the graph, as the oxygen content increases the specific heat capacity of the mixture is altered slightly, raising the compression temperature. A mixture of 20% oxygen with 80% argon produces the highest peak temperature as greater oxygen availability enhances the rate of hydrogen combustion.

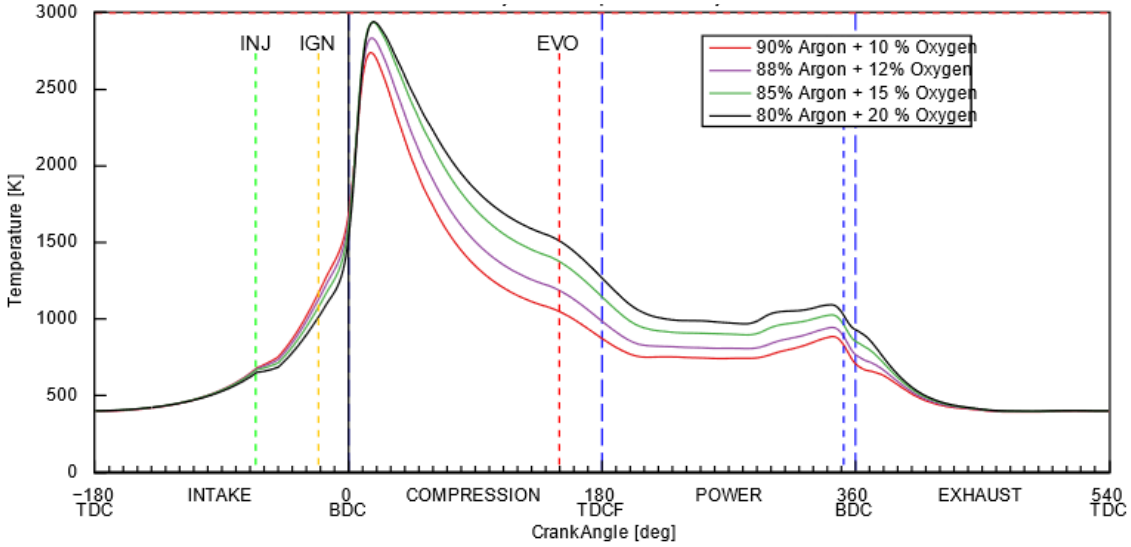

Figure 43 In Cylinder Temperature Analysis of 75.25% Load for different mixture compositions.

Conversely, the mixture of 90% argon with 10% oxygen results in a lower peak due to the presence of higher argon levels contributes to better thermal insulation enhancing combustion efficiency. As the argon concentration decreased, the exhaust gas temperature increased, as indicated by the higher temperatures observed during the exhaust stroke near the BDC.

4.3.4 Full-Load Point (101.20%)

Performance Results

In Figure 44 the simulated result presented for 101.2% load for four different mixtures as investigated for 75.25% and 50.20% load. As the argon concentration decreases from 90% to 80% similar trends in engine performance and efficiency are observed.

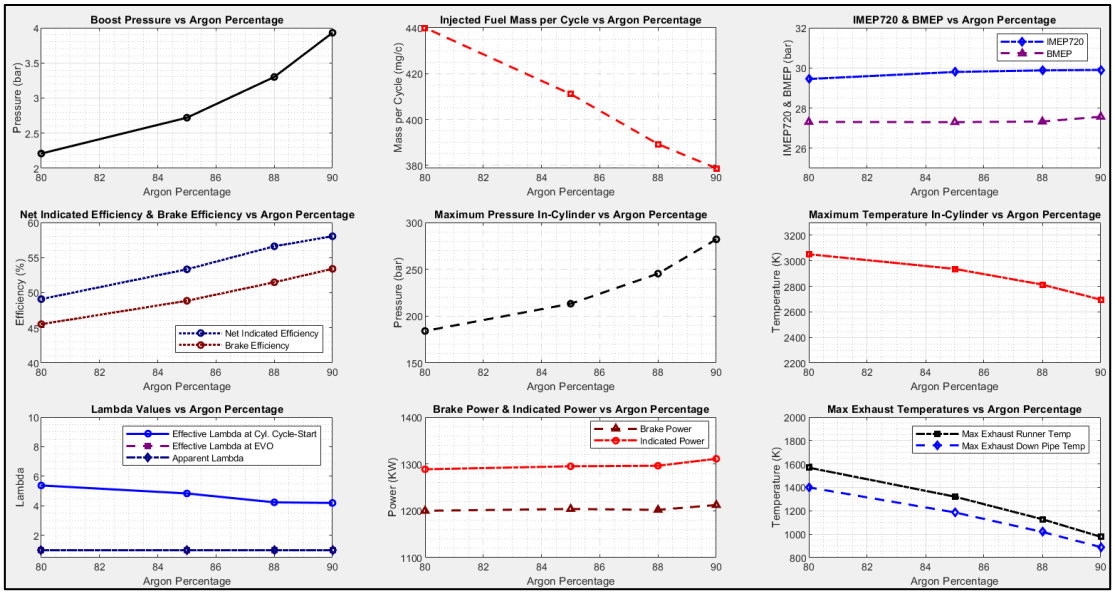

Figure 44 Performance Metrics Analysis of Closed-Loop HAPC at 101.1% Load for Different Diluted Mixture Compositions.

The boost pressure starts at 3.93 bar at 90% argon dropping to 2.21 bar at 80% argon. Additionally, the injected fuel mass per cycle increases from 378.71 mg at 90% argon to 440.00 mg at 80% argon as noticed for 75.25% load case. Indicated efficiency shows a decreasing trend as the argon concentration decreases. Starting at 58.04% at 90% argon, it decreases to 49.09% at 80% argon. Brake efficiency follows a similar pattern starting at 53.40% and decreasing to 45.52%.

The maximum in-cylinder pressure decreases but the temperature increases as observed previous sweep. At 90% argon, the maximum pressure reaches 282.01 bar while the temperature in the cylinder peaks at 2695.52 K. As argon concentration decreases the maximum in-cylinder pressure decreases to 184.15 bar at 80% argon and the maximum

temperature rises to 3051.36 K. Another key observation is that as argon concentration decreased from 90% to 80%, the exhaust gas temperature increased significantly at full load, raising from 977.98 K to 1568.78 K. Although both brake power and indicated power showed a slight decrease but remained within acceptable limits for the constant power output.

In Cylinder Pressure and Temperature Analysis

In Figures 45 and 46 the visual representation of in-cylinder pressure and temperature variation as a function of crank angle for a six-cylinder model under steady state condition at 101.20% load is shown.

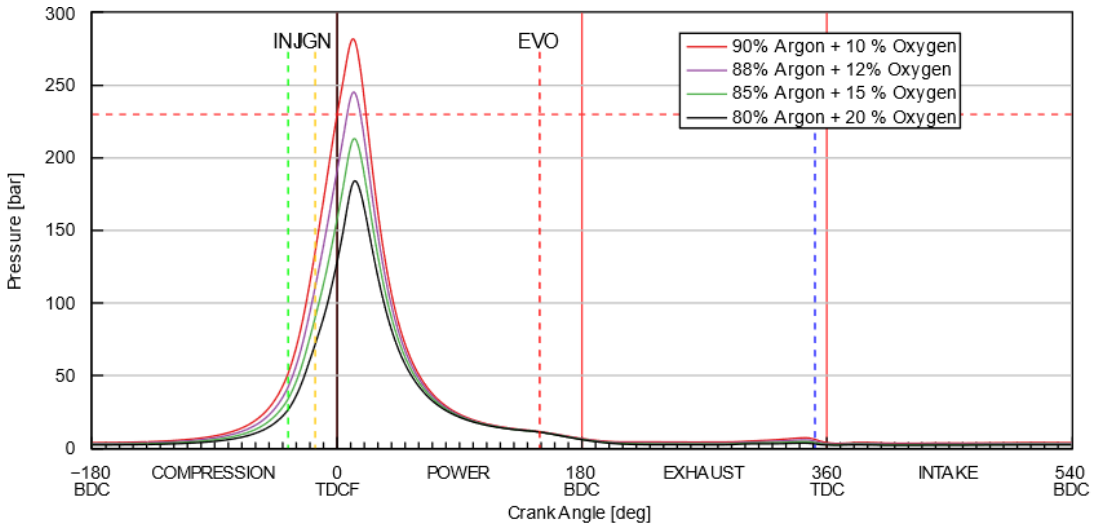

Figure 45 In-Cylinder Pressure Analysis of 101.20% Load for different mixture compositions.

The in-cylinder pressure graph in Figure 45 shows a consistent trend across the full load for different mixture compositions, as discussed for 50.25% and 75.25% load conditions. However, no significant changes were observed during the simulation, suggesting that the in-cylinder pressure exhibits a similar trend across all load conditions for different mixtures. As anticipated, the mixture of 90% argon with 10% oxygen illustrated the maximum in-cylinder pressure, whereas 80% argon concentration showed the lowest pressure.

Similarly, the temperature curves in Figure 46 demonstrated that during compression stroke the temperature increases progressively for all mixtures. Mixtures with higher oxygen content such as 80% argon with 20% oxygen exhibit a slightly higher temperature compared to mixtures with lower oxygen like 90% argon with 10% oxygen as observed for 75.25% load.

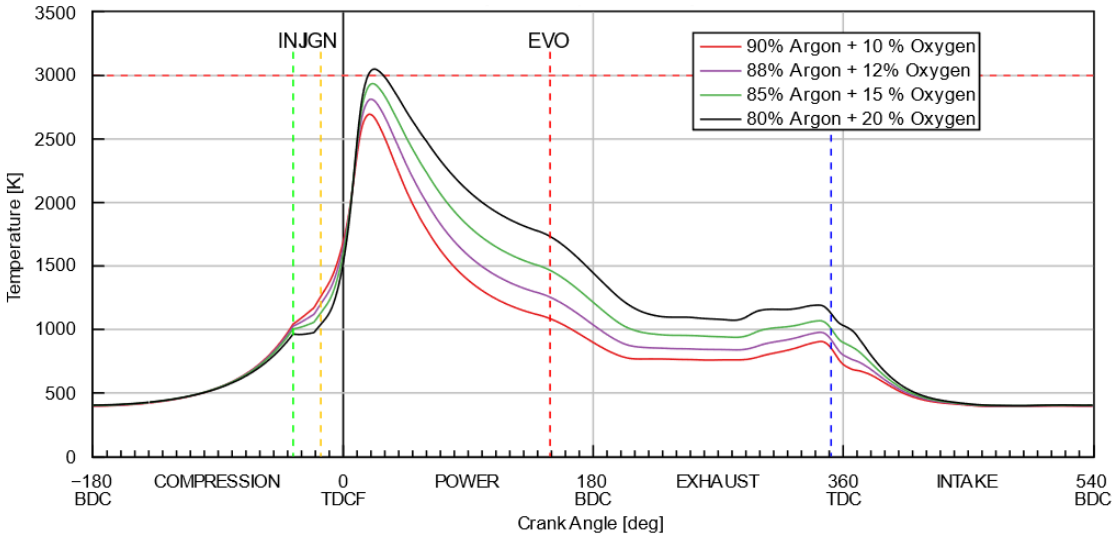

Figure 46 In Cylinder Temperature Analysis of 101.20% Load for different mixture compositions.

The mixture containing 90% argon and 10% oxygen achieves a peak temperature of approximately 2700 K, accompanied by a low-temperature exhaust profile, indicative of enhanced energy extraction and reduced thermal stress. Conversely, the 80% argon and 20% oxygen mixture exhibit a peak temperature of around 3051 K which is the highest in-cylinder temperature recorded during the simulation, sustaining elevated temperatures throughout the expansion and exhaust phases, thereby increasing thermal stress and diminishing overall efficiency.

4.3.5 Discussion

At full load conditions, the boost pressure observed in the cycle is influenced by mixture content, which directly affects the volumetric efficiency and compression ratio. A highly reactive mixture enables faster combustion with reduced heat retention, decreasing the required boost pressure. For loads of 50.2%, 75.7%, and 101.2% with a 90% Ar and 10%

O_2 mixture, higher argon concentration provides a greater heatsink effect, stabilizing the combustion and requiring a higher boost pressure as it absorbs heat during compression. Conversely, at higher oxygen concentrations of 15% and 20% the reaction kinetics accelerate, and the fuel burns more quickly requiring lower boost pressures needed respectively. This is supported by the general thermodynamic principle that compression work is inversely proportional to the reactive fuel mixture, less compression is needed when combustion is more efficient.

This observed trend suggests a shift in combustion dynamics, where the reduction of argon results in elevated combustion temperature and reduced pressure. This effect can be attributed to the increased fuel quantity and higher oxygen concentration, alongside a decrease in the argon content (both in terms of percentage and absolute quality, due to the lower boost pressure). Furthermore, the lower specific heat ratio of the mixture at intake valve closure (IVC), resulting from the diminished argon presence, contributes to the higher combustion temperatures, as argon typically functions as the effective heat sink in the combustion process.

IMEP and BMEP are crucial for understanding the engine's effective utilization of the input fuel energy. As the oxygen content increases, both BMEP and IMEP drop slightly (90%-Ar) to a certain level (80%-Ar), which aligns with the reduction of boost pressure and associated decrease in compression work but is covered by extra fuel amount. From the thermodynamic standpoint, increasing oxygen content results in a more reactive combustion process which allows for faster combustion and less peak pressure buildup, thereby reducing the IMEP. This is corroborated by the observed decreased Indicated efficiency which declines for (90% Ar) slightly to (80%-Ar). Efficiency losses arise due to the reduction of thermal retention capacity, which diminishes by engine's ability to retain heat within the system for work production.

It is important to highlight that, as indicated by the in-cylinder temperature curves in Figures 38, 41, and 44, increasing oxygen content within the thermodynamic cycle

reduces the argon's buffering effect, leading to a greater release of heat during the expansion and exhaust strokes. This results in lower thermal efficiency, which can be analysed through the Carnot efficiency equation $\eta = \mathbf{1} - \frac{\boldsymbol{Tcold}}{\boldsymbol{Thot}}$, where the loss of thermal retention reduces the temperature differential between the hot combustion gases and the cold exhaust gases, thereby reducing the overall thermal efficiency of the system. The boost pressure enhanced power by increasing the air-fuel mixture in the combustion chamber while lowering boost reduces mixture mass and in-cylinder pressure. A reduction in argon concentration raises combustion temperatures, as it no longer moderates heat buildup, but also decreases the mixture volume, resulting in lower peak pressures. While reduction in argon concentration in the mixture raises in-cylinder temperature but increases the risk of knocking unless boost pressure is adjusted. In the absence of argon thermal stabilization, higher combustion temperatures occurred due to less effective heat dissipation.

Targeted engine design constraints

The approach to determining the optimal mixture composition for the targeted engine design necessitates the careful consideration of several key factors. The maximum in-cylinder pressure and temperature should not exceed 230 bar and 3000 K, with an indicated efficiency of 60%, with an indicated power of 1200KW. Additionally, the exhaust temperature must be maintained within the range of 950 K to 1000 K. Following the mixture composition sweep conducted in GT-Suite, a power output and efficiency matrix graph has been reported in Figure 47 to identify the optimal mixture composition, considering the targeted engine design constraints. It is crucial to emphasize that, as depicted in Figure 47, the mixture composition of 90% argon with 10% oxygen and 88% argon with 12% oxygen predominantly satisfied the targeted engine design constraints along the three different load conditions. For instance, at full load, the indicated efficiency for the 90% argon and 10% oxygen mixture is recorded at 58.04%, approaching 60%, with the highest brake efficiency of 54%. For the 88% argon and 12% oxygen mixture, the efficiency slightly drops to 57%, yet it remains closer to 60% compared to other argon-to-oxygen concentration variations.

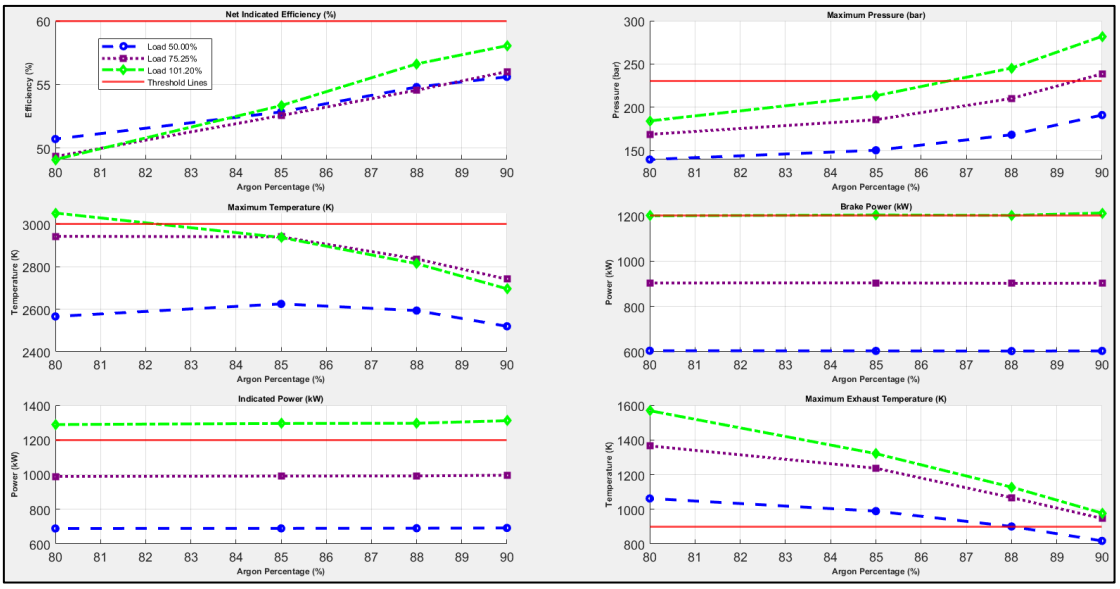

Figure 47 Comparison of Mixture Composition for Targeted Engine Design Constraint.

In contrast, the mixture of 80% argon with 20% oxygen is not technically feasible, as it achieves an efficiency of 49.90%, which falls significantly below the 60% threshold, and exceeds both the exhaust gas and in-cylinder temperature limits, potentially damaging the exhaust runner pipe and the closed-loop system. The mixture results in a maximum temperature of 3052 K, posing a risk of damaging the cylinder wall. Although this composition may offer low-cost advantages for the W20 engine, it would require heat insulation to prevent damage to the cylinder wall and the cylinder head. Additionally, the exhaust gas temperature exceeds the design limit, requiring the installation of a new exhaust pipe capable of withstanding temperatures above 1200 K. Therefore, it is recommended to use a mixture with 90% to 88% argon concentration of working fluid across the three different load conditions.

4.4 Impact of Alternative Monatomic Gases on HAPC Performance

4.4.1 Design of Experiments (DOE)

In this analysis, the performance of the six-cylinder closed-loop HAPC W20 engine is examined through 1D GT-Suite simulation results under three different inert gas configurations as a working fluid: pure argon, pure helium, and a 50%-50% argon-helium gas

mixture. Table 14 shows all the inputs and initial values of DOE that have been used for this configuration where it shows that 75.25% reference load has been used with a 90% dilution and 10% oxygen mixture to investigate the impact of those monatomic gases on HAPC performance.

Table 14 Inputs and Initial values of DOE.

Reference load	75.25%
Reference mixture composition	90% Dilution +10% Oxygen
Test working fluid	○ Argon (100%) ○ Helium (100%) ○ Argon + Helium (50%-50% Blend)
Injected fuel mass (mg/c)	300
Combustion Parameters	As in table 13 (75.25% Load)

Performance Results

Figure 48 depicts engine performance using three different inert gas mixtures as mentioned above while maintaining a constant injected fuel mass of 300 mg/c. The result revealed significant variations in initial pressure, referred to as injection pressure, which increased substantially from 1.05 bar for Argon to 23 bar for the Argon-helium blend and peaked at 37.5 bar for helium. The initial pressure was adjusted for the simulation, as applying the same initial pressure as argon's initial pressure to helium- Argon and pure helium resulted in failure. Especially, the error included negative cylinder temperatures and insufficient working fluid due to the low density of helium, which restricted combustion. To resolve this issue, the initial pressure was calibrated to 23 bar for the helium-argon mixture and 37.5 bar for pure helium, while maintaining the temperature consistently at 300 K. Boost pressure increased substantially from 3.12 bar for argon, 3.17 bar for argon and helium blend, and peaks at 3.2 bar for helium.

Despite these differences, the net indicated mean effective pressure (IMEP720) and BMEP remained consistent at approximately 22.90 bar and 20.50 bar respectively across

all cases reflecting similar work output power cycle and a load of 75.2% which was considered as reference load. Efficiency metrics show marginal differences where net efficiency is approximately 56% or above for across all mixtures while brake efficiency is slightly higher for the argon-helium blend which is 50.11% and for helium 50.28% compared to argon 50.11%.

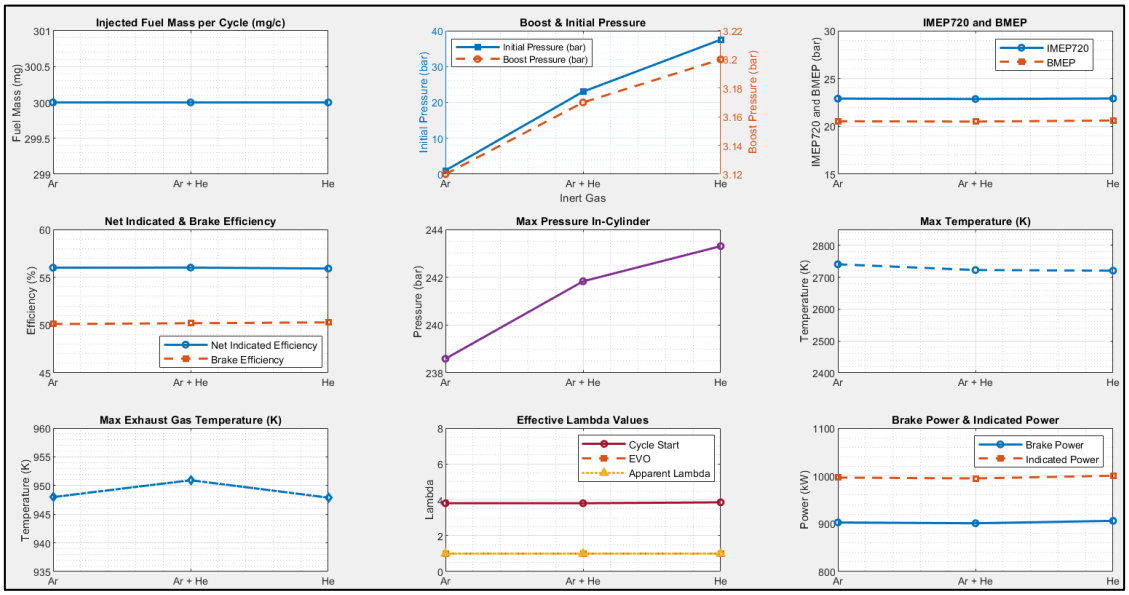

Figure 48 Performance analysis of inert gases configurations in a six-cylinder W20 engine.

The maximum in-cylinder pressure varies significantly with the highest value observed for helium at 243.30 bar, followed by argon-helium blend at 241.83 bar and argon at 238.59 bar which illustrates slight differences among the gases. In-cylinder temperature shows minimal variation with the maximum values ranging from 2720.63 K for helium to 2740.63 K for argon. The maximum exhaust gas temperature is highest for argon and helium blend at 950 K followed by argon at 947.98 K and helium at 947.8 K. Similarly, the maximum exhaust gas down pipe temperature is highest for argon at 858.63 k while the argon-helium blend and helium show slightly lower values of 845.58 K and 848 K respectively. In terms of power output brake power remains consistent across all the mixtures ranging from 902.70 kW for argon to 906 kW for helium while indicated power is very slightly from 996.49 kW for argon to 1000 kW for helium.

In Cylinder Pressure and Temperature Analysis

In Figure 49 the in-cylinder pressure graph has been illustrated throughout the engine cycle to see the difference among them. From the figure, it is observed that helium and its mixture with argon exhibit a slightly steeper pressure increase near TDCF, while peak in-cylinder pressures occur just after ignition during the power stroke. This behaviour suggests that helium and its mixture with argon accelerate compression due to their lower specific heat capacities and thermal conductivity, influencing pressure development and combustion dynamics.

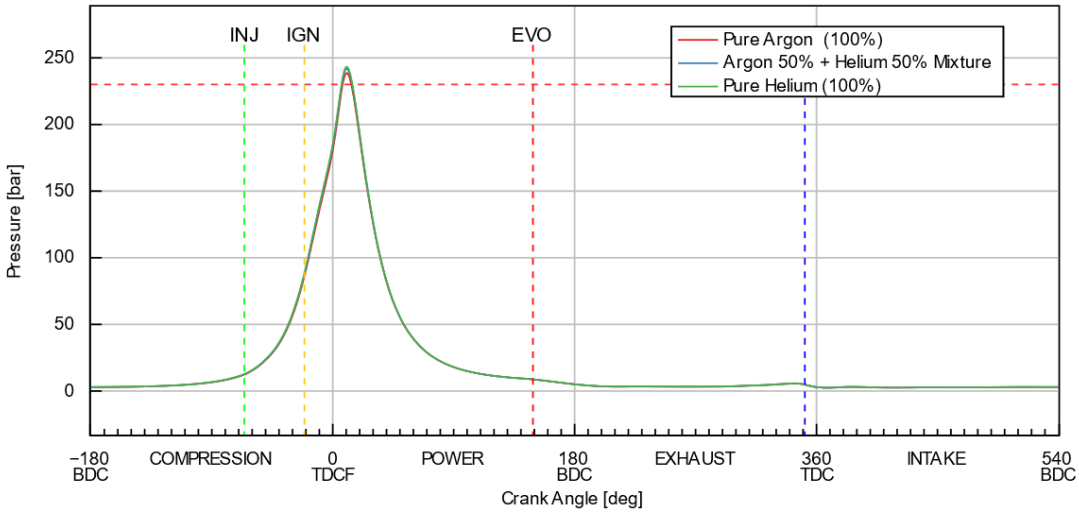

Figure 49 Comparison of In-Cylinder Pressure for Different Inert Gas Configurations.

The second-highest peak pressure is recorded for the argon-helium mixture at 241.83 bar, while 100% helium exhibits the highest peak pressure at 243.30 bar, and 100% argon demonstrates a slightly lower peak pressure of 238.59 bar.

Figure 50 depicts the in-cylinder temperature profiles for the gas mixtures examined across the engine cycle highlighting key phases. During the compression phase, the temperature rise is nearly identical across all te mixtures due to the stoichiometric combustion conditions and consistent heat transfer within the cylinder. However minor differences become apparent near TDCF where helium and its mixture with argon show slightly lower peak temperatures compared to pure argon. The maximum temperature

in the cylinder occurs shortly after ignition during the power stroke with 100% argon reaching the highest value, followed by an argon-helium mixture and 100% helium.

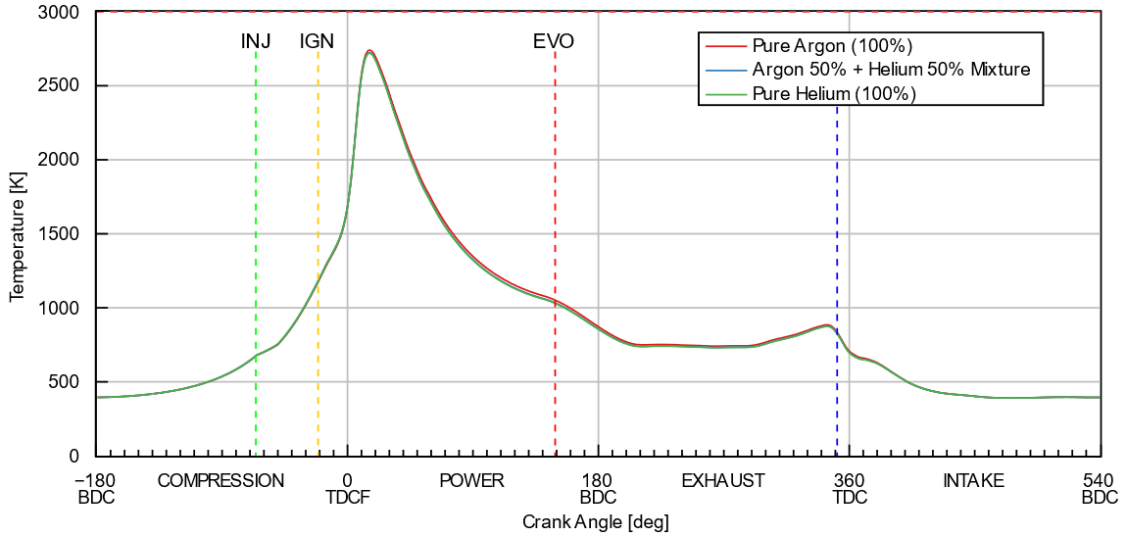

Figure 50 Comparison of In-Cylinder Temperature for Different Inert Gas Configurations.

During the exhaust and intake phases, the temperature drops uniformly for all gas mixtures as the burnt gas exits the cylinder and fresh intake gases are drawn into the cylinder. The consistent trend across all these phases indicated that temperature difference during combustion is primarily governed by the inert gas properties such as thermal conductivity and specific heat capacity rather than the flow or timing of the gases. It can be observed that, although the temperature profiles of all mixtures are similar, argon results in higher peak combustion temperatures, whereas helium and its mixture demonstrated slightly lower peak temperatures.

4.4.2 Discussion

In principle, any combination of monatomic gases can enhance the efficiency of HAPC. However, they are distinct physiochemical properties that influence practical constraints such as cost, thermodynamic efficiency, combustion stability, and heat transfer. In W20 engines utilizing hydrogen as fuel, the selection of inert gas plays a critical role in stabilizing combustion and preventing excessive flame speed.

In the case of pure argon as a dilutant, the system exhibits the lowest recorded boost and initial pressure, primarily due to argon's high density. Argon is 1.4 times denser than nitrogen, allowing for lower boost pressure and increased mass flow, which improves volumetric efficiency. As previously noted, argon acts as a thermal buffer, enhancing flame propagation and energy efficiency by maintaining higher in-cylinder temperatures and reducing cooling losses. This stabilizes combustion under moderate pressures, increasing cylinder pressures and temperatures, which in turn enhances energy conversion and optimizes brake and indicated power output.

In the mixture of argon and helium, higher initial and boost pressures are necessary to compensate for helium's low density, resulting in a mixture density between that of pure argon and helium. This configuration achieved similar IMEP and a slightly increased efficiency, reflecting the combined properties of both gases. While helium's lower intake charge density necessitates higher boost pressures, which improve intake flow, these pressures also increase mechanical load and back pressure, reducing net power output due to higher pumping losses. Although helium shares argon's high specific heat ratio, its higher thermal conductivity leads to faster heat dissipation from the combustion chamber, which reduces effective combustion temperatures. Thus, helium's higher thermal conductivity reduces the thermal insulation provided by argon, resulting in a slight decrease in both brake and indicated power output.

In the pure helium case, an extremely high initial and boost pressure was employed to achieve sufficient intake density and load level. However, this configuration yields almost a similar IMEP and BMEP but results in a reduced net indicated efficiency. The extremely low density of helium requires high initial pressure (37.5 bar) to achieve a comparable intake mass flow to denser gases like argon. This in turn, leads to high pumping work and back pressure, which increases the engine's frictional losses and reduces net efficiency. Furthermore, helium's high thermal conductivity increases heat losses, lowering combustion temperatures. Additionally, the absence of a dense inert gas like argon

diminishes flame propagation control, potentially leading to combustion instability. The rapid flame speed associated with hydrogen could also localize high exhaust temperatures and potential knocking, further exacerbated by the lack of inert buffers like argon.

While noble gases like neon and xenon have theoretical advantages due to their high specific heat ratio like argon and helium their practical application in ICEs is limited by challenges in combustion stability and need for external heating and the requirement for significant engine modifications. Due to these challenges, the investigation of neon and xenon was not conducted within the GT suite simulation. Neon requires elevated intake temperatures and high intake pressures for stable combustion, similar to helium, as its low density (0.90 kg/m3) and molecular weight lead to heat loss and reduced efficiency (Mat Taib et al., 2020). The reliance on external heating complicates engine design and lowers overall thermal efficiency

Xenon Faces significant challenges when paired with hydrogen due to its poor diffusivity, which hinders hydrogen mixing and leads to unstable combustion. Its lower specific heat causes high peak temperatures and increased OH radical concentrations, risking engine knocking and damage. While xenon not does not require external heating, Its heavy molecular structure and sub-optimal mixing demand high initial pressure (20 bar) and temperature (1000 k), with hydrogen injection at 500 K (Shahsavan et al., 2018c). These factors make xenon impractical for hydrogen-fuelled engines due to inefficiencies and operational difficulties.

From this analysis, argon is identified as the optimal working fluid for the W20 engine in HAPC applications, as it meets all critical design specifications, including maximum in-cylinder pressure and temperature, as well as efficiency and power output thresholds. When compared to other inert gases, argon demonstrates superior flexibility in terms of intake pressure and temperature, as well as enhanced mixing rates, which are essential for non-premixed combustion. This combination of characteristics makes argon a highly effective and cost-efficient choice for both emission reduction experiments and standard

ICE setups. Ultimately, this analysis confirms that argon's physical properties position it as the most suitable inert gas for maximizing engine performance and efficiency within HAPC applications, thereby ensuring both practicality and effectiveness.

4.5 Effect of changing Oxygen-to-Fuel ratio (λ)

4.5.1 Design of Experiments (DOE)

This analysis investigates the performance of the HAPC in the W20 engine using simulation to assess the influence of the oxygen-to-fuel ratio on combustion efficiency and exhaust gas temperatures. In this context, the effective Lambda at cycle start (IVC) denotes the available oxygen at the point of inlet valve closing, while the effective Lambda at exhaust valve opening (EVO) indicates the excess oxygen remaining in the exhaust gas. Furthermore, the oxygen-to-fuel ratio (λ) represents the ratio of injected oxygen to fuel during the combustion process. Table 15 provides a comprehensive summary of the input parameters and initial conditions utilized in the design of experiments for this study.

Table 15 Reference inputs for the initial conditions of the simulation.

Reference load	**75.25%**
Reference mixture composition	90% Argon + 10% Oxygen
Injected fuel mass	Varies with λ
Fuel	Hydrogen (H2)
Combustion parameters	As in table 13 (75.25% Load)
Test conditions	λ=0.85,1.00,1.20, and 1.40

The simulation was conducted at a constant load of 75.25% with the working fluid composed of 90% inert argon and 10% oxygen. To evaluate the impact of oxygen-to-fuel ratio variations on engine performance, the injected hydrogen fuel mass changes dynamically with each test case to keep the same reference load output and mixture composition for all the sweeps. Combustion parameters including ignition timing and chamber geometry

are fixed for all sweeps at 75.25% load to isolate the effects of fuel amount variation and oxygen fuel mixture properties.

Performance results

Figure 51 depicts a detailed evaluation of how variation in oxygen-to-fuel ratio while maintaining a constant load and mixture composition affects engine performance. It is observed from simulated results that when λ =0.85 indicating a rich mixture requires high fuel consumption of 346.11 mg due to lower oxygen availability. Moderate efficiency (51.19%) and high in-cylinder pressure (289.83 bar) were observed while the maximum temperature reached 2649 K, leading to high exhaust temperatures of 842.74 K. It produced more H_2 indicative of incomplete combustion.

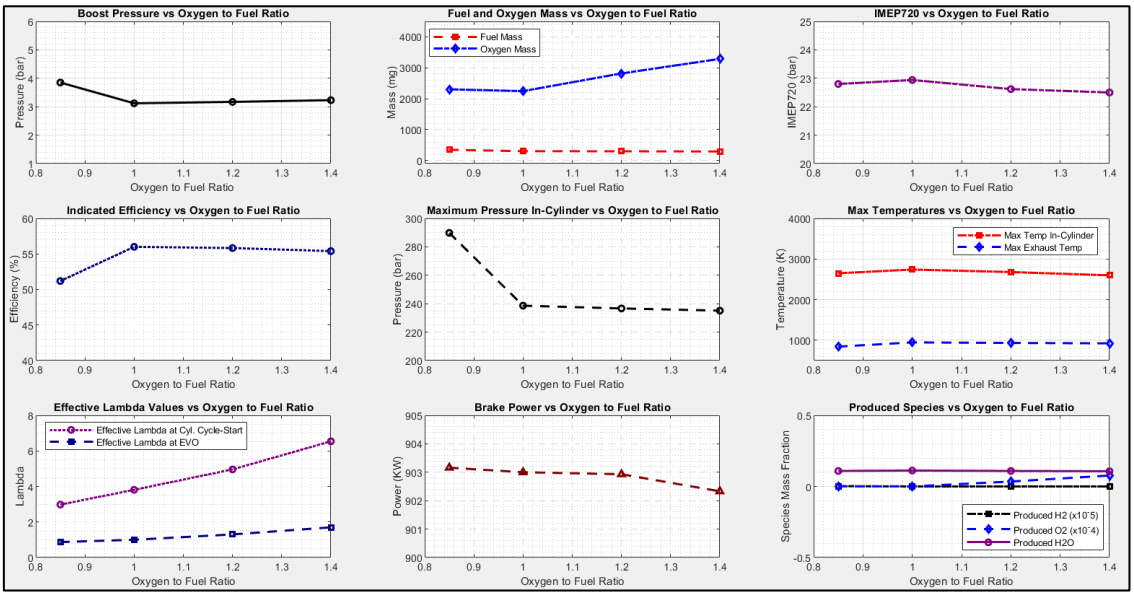

Figure 51 Influence of oxygen to fuel ratio on combustion dynamics and exhaust gas accumulation.

The result also shows lower water production compared to lean mixtures. When the λ = 1.0 reflects a stoichiometric mixture, a reduced fuel mass of 300 mg was observed while achieving a high efficiency of 56.00%. In the cylinder peak pressure reached 238.59 bar and the temperature of 2740 K was slightly higher. Improved combustion completeness,

as seen in reduced H_2 and O_2 by-products noticed. Water vapor production mass fraction increased to 0.112, signalling effective hydrogen-oxygen recombination.

Additionally, when λ = 1. indicates a lean mixture with lower fuel consumption (292.22 mg) and high oxygen availability, reflects moderate indicated efficiency (55.83%). Meanwhile, the peak pressure of 236.67 bar was achieved and the temperature declined slightly to 2682 K. Exhaust temperatures stabilized near 933.41 K. Combustion by-products H_2 reduced further but excess oxygen increased slightly, showing good burn quality. In the leanest mixture in the investigation, λ = 1.4 where the lowest fuel usage of 290.65 mg and the highest oxygen presence, efficiency decreased to 55.40%. A lower in-cylinder peak pressure of 235.10 bar was observed and the temperature jumped to 2598.66 K, with reduced thermal stress. Produced unburnt mass fraction of H_2 (7.71) and O_2 (771), suggesting less complete combustion. Exhaust temperature dropped to 922.91 K. Moreover, the produced water mass fraction (0.107) dips down, possibly due to less efficient hydrogen-oxygen reactions.

4.5.2 Discussion

In this analysis, the net IMEP remained constant across all conditions, indicating stable power output despite changes in the oxygen-to-fuel ratios. This consistent power output was maintained throughout the analysis, which was ensured by adjusting the injected fuel amount. However, the indicated efficiency decreases from 51.19% at λ= 0.85 to a peak of 56.00% at λ=1.0, demonstrating the higher thermal efficiency of the stoichiometric mixture. Maximum in-cylinder pressure and temperature show a decreasing trend as Lambda increases with the highest pressure of 289.83 bar, and the temperature fluctuates significantly. These values are indicative of intense combustion associated with a rich mixture but also result in higher thermal stresses.

Exhaust gas temperature, however, reflects the combustion dynamics with the highest value observed for the stoichiometric mixture (λ= 1.00) entering to gradual decline as the mixture becomes leaner. A noticeable increase in this byproduct in excess oxygen at the leanest condition (λ=1.40) could indicate incomplete combustion due to insufficient

flame propagation and excess oxygen availability in the combustion by-product. The mass fraction of water produced during combustion peaks at λ=1, representing stoichiometric conditions where hydrogen and oxygen recombine most efficiently.

Comparing different oxygen-to-fuel ratios, as indicated by varying Lambda (λ) values, underscores the trade-offs between combustion efficiency, combustion intensity, and the accumulation of byproducts within the design constraints of the W20 engine. A richer mixture, associated with a lower λ value, results in higher cylinder pressure (up to 289 bar, exceeding the engine targeted design limits) and elevated temperatures, there be increasing thermal stress and reduced byproduct formation, yet may compromise combustion efficiency, particularly at very high oxygen to fuel ratios where excess oxygen hinders the completeness of the combustion process. A stoichiometric mixture suggests complete combustion with the controlled environment which maintains all the targeted and required engine design specifications apart from its parameters. So, a stoichiometric mixture which indicates the value of λ= 1.00 is suggested based on the specific engine load conditions for the W20 engine as it is in limit of design output and threshold as it indicates exhaust temperature and pressure and controlled accumulation. Moreover, a slightly lean mixture could be an option as it reduces efficiency slightly but reduces the exhaust gas temperature. These findings provide critical insight into optimizing the operation of HAPC in W20 engines to achieve a balance between performance and fuel efficiency.

4.6 Effects of Compression Ratio and Exhaust Back Pressure

4.6.1 Design of Experiments and Performance Results

In this section, the investigation is divided into two parts. The first section evaluates different compression ratios, ranging from 6 to 12.3, while the second phase examines the exhaust back pressure, defined as pressure before the condenser, which varies between 3.23 and 4.25 bar. Table 16 reflects the parameters used for the design of the experiment.

Table 16 The parameters defined for the design of the experiment.

Reference load	**75.25%**
Reference mixture composition	90% Argon + 10% Oxygen
Injected fuel mass (mg/c)	300
Fuel	Hydrogen (H2)
Combustion parameters	As in table 13 (75.25% Load)
Test conditions	*a) Compression ratio (6 to 12.3)* *b) Exhaust gas Pressure before Condenser (3.23, 3.30, 4.00, and 4.25 bar)*

Throughout the investigation, a similar reference load of 75.25% and a consistent fuel injection of 300 mg per cycle were maintained. The simulated results and discussion presented below to examine the impact of compression ratio on combustion dynamics and efficiency along with the impact of exhaust back pressure influencing these parameters.

4.6.2 Compression Ratio

To understand the insightful overview of how compression ratio (CR) influences engine performance metrics and combustion dynamics, the simulation has been run for different compression ratios. In Figure 52, the data set examines that the effect of increasing compression ratio (CR) requires a slightly consistent higher boost pressure range of 3.12 to 3.10 bar. As the compression ratio increases from 6 to 12.3 noticeable trends emerge such as IMEP and BMEP rising progressively from 20.3 bar 17.93 bar at CR 6 to 22.94 bar and 20.53 bar at CR 12.3. When the engine is operating at CR 11.90 the IMEP remains almost constant, which is 22.90 bar and 20.50 bar of BMEP.

In parallel the indicated efficiency improved from 49.62% to 56.00% while the brake efficiency climbed from 43.73% to 50.11%, highlighting better energy utilization from fuel when the compression ratio increases. The maximum cylinder pressure experienced a substantial increase starting at 107.87 bar at CR 6 and reaching 238.58 bar at CR 12.3. Similarly, the in-cylinder temperature rises from 2578.21K to 2740.60K, demonstrating

the more intense combustion dynamics associated with higher compression. It is noticeable that at CR 11.90 the maximum in-cylinder pressure and temperature recorded 230.18 bar and 2732.70 k with a Net indicated and brake efficiency of 55.84% and 49.95% which is similar to the observed CR 12.3 but negligible reduced.

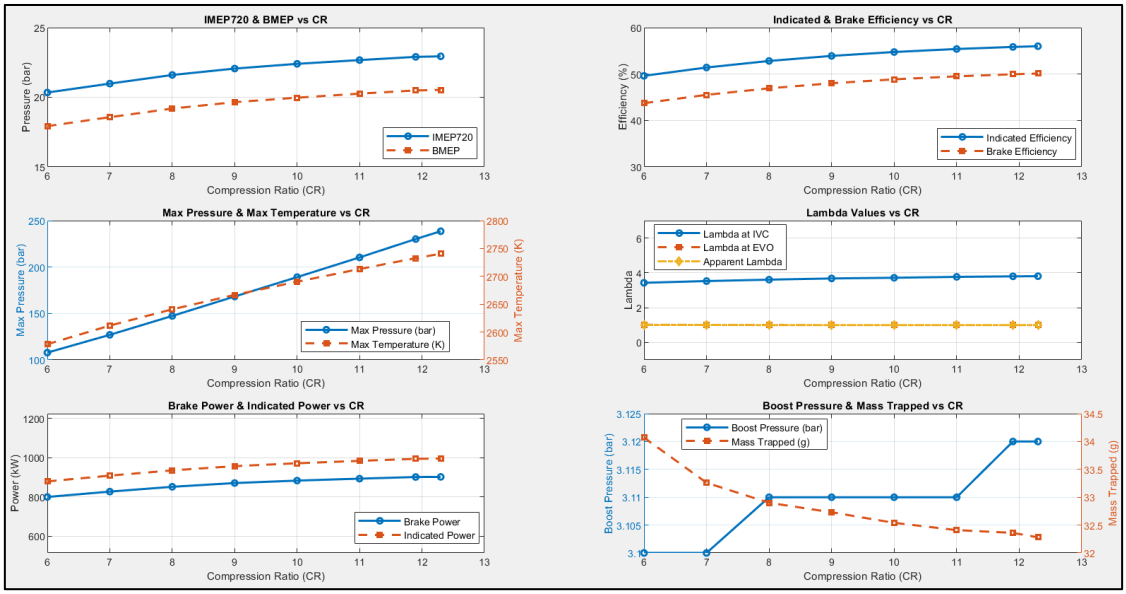

Figure 52 Effects of Compression Ratio Variation for Engine Performance Metrics in GTP Simulation.

These changes reflect the thermodynamic advantages of increased compression such as improved heat release and energy transfer. The Lambda value at IVC rises slightly from 3.43 at CR 6 to 3.81 at CR 12.3. The effective Lambda and apparent Lambda kept constant 1.00 which is stoichiometric. In terms of power output, the brake power increases from 800.27 kW at CR 6 to 902.67 kW at CR 12.3 but it is noticeable that at CR 11.90 the power output remains the same, which is 902.00 kW. Interestingly, the total trapped mass at IVC decreases slightly while increasing CR from 34.07g at CR 6 to 32.28g at CR 12.3. The decline is due to the reduced clearance volume within the cylinder at a higher compression ratio which reduced the total volume available for the trapped charge. Finally, it could be stated that the data demonstrates the increasing compression ratio leads to significant improvements in engine performance metrics such as efficiency power output and combustion intensity. Though the engine was optimized at CR 12.30 while at CR

11.90 the power output remained the same with a slight reduction in cylinder pressure and efficiency.

4.6.3 Exhaust Back Pressure Analysis

In this sweep the exhaust back pressure analysis and the effect on engine performance metrics and combustion dynamics has been analysed. It is important to note that the simulation sweep has been conducted for four different exhaust pressures before entering the condenser of 3.23 bar, 3.32 bar, 4.02 bar, and 4.26 bar where the mixture composition has been used with the reference of 90% argon with 10% oxygen with a fixed combustion parameters for 75.25% load.

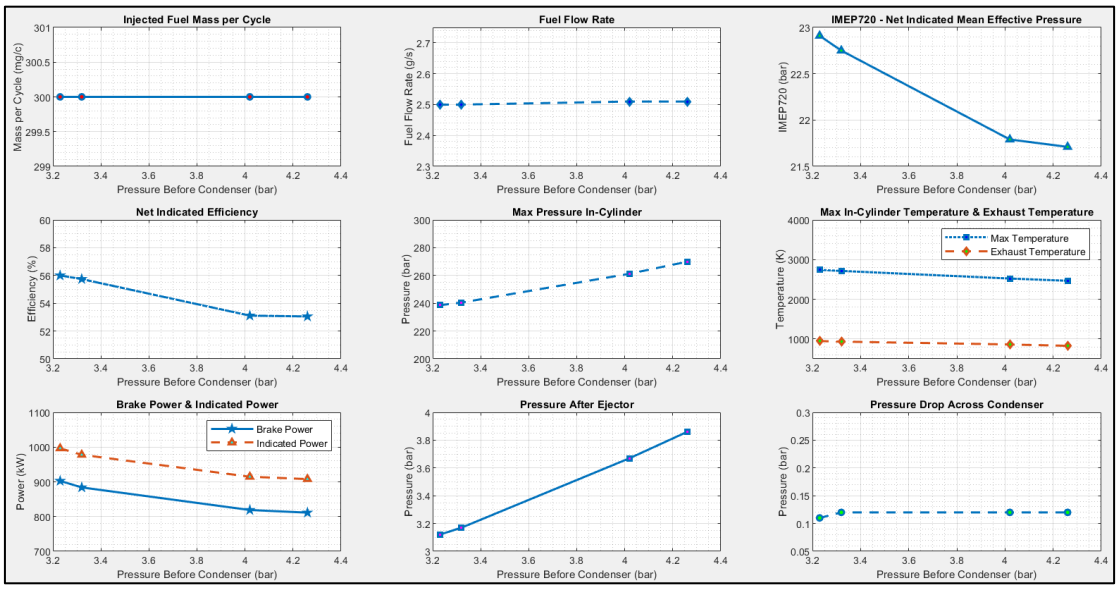

Figure 53 Exhaust Back Pressure Analysis on Combustion Dynamics and Efficiency.

Figure 53 presents the simulated result under varying exhaust conditions with a consistent fuel mass injection of 300 mg/c. It is observed that at pressure before the condenser of 3.23 bar and the pressure after the ejector of 3.12 bar the engine achieves a net IMEP of 22.90 bar and indicated efficiency of 56.00%. The maximum in-cylinder temperature and pressure reach 2740.63K and 238.59 bar respectively producing an indicated power output of 996.49KW. The exhaust temperature is 947.28K, while the maximum downpipe temperature is recorded at 858.63 K with a condenser pressure drop of

0.11 bar. As the pressure before the condenser increased to 3.32 bar and the pressure after the ejector increased to 3.17 bar as well, the IMEP decreased slightly to 22.75 bar with indicated efficiency reducing to 55.74%.

The in-cylinder temperature dropped to 2714.86 K while the pressure marginally rises to 240.50 bar as the pressure before the condenser increased. The indicated power decreased to 977.91 KW accompanied by lower exhaust gas and down pipe temperatures of 933.37K and 844.76 K respectively. Note that pressure drops across the condenser and rises slightly to 0.12 bar. At higher exhaust back pressure before the condenser of 4.02 bar it has observed 3.70 bar pressure after the ejector maintains the same amount of fuel, the IMEP further declines to 21.79 bar with efficiency dropping to 53.11% (net indicated). The maximum in-cylinder temperature reduced to 2522.73K showed a marginal drop, although the pressure increased to 261.24 bar due to the high intake pressure generated after the ejector.

The indicated power output dropped as well to 914.66 KW, and exhaust and downpipe temperature decreased to 861.24K and 756.15 K respectively. There is a huge pressure drop of 0.12 bar before the exhaust gas enters the condenser. Finally, adding the highest exhaust and pressure after the ejector of 4.26 bar and 3.9 bar, the IMEP reaches its lowest value of 21.71 bar with corresponding indicated efficiencies of 53.05%. The in-cylinder pressure drops to 2466.24K when the pressure peaks at 269.94 bar. The engine indicated that power was further reduced to 907.92KW and exhaust and downpipe temperature fell to 827 k and 733.97 K respectively. The exhaust gas before entering the condenser dropped to 0.125 or 0.13 bar. These results highlight the complex interplay between pressure before the condenser and after the ejector influencing key performance and thermodynamic parameters.

In Cylinder Temperature and pressure

In Figure 54 the graph depicts in-cylinder pressure variation as a function of crank angle, covering key phases of the engine cycle compression, power, exhaust, and intake under

wearing operating exhaust back pressures before condenser of 3.23 bar, 3.32 bar, 4.02 bar, and 4.26 bar.

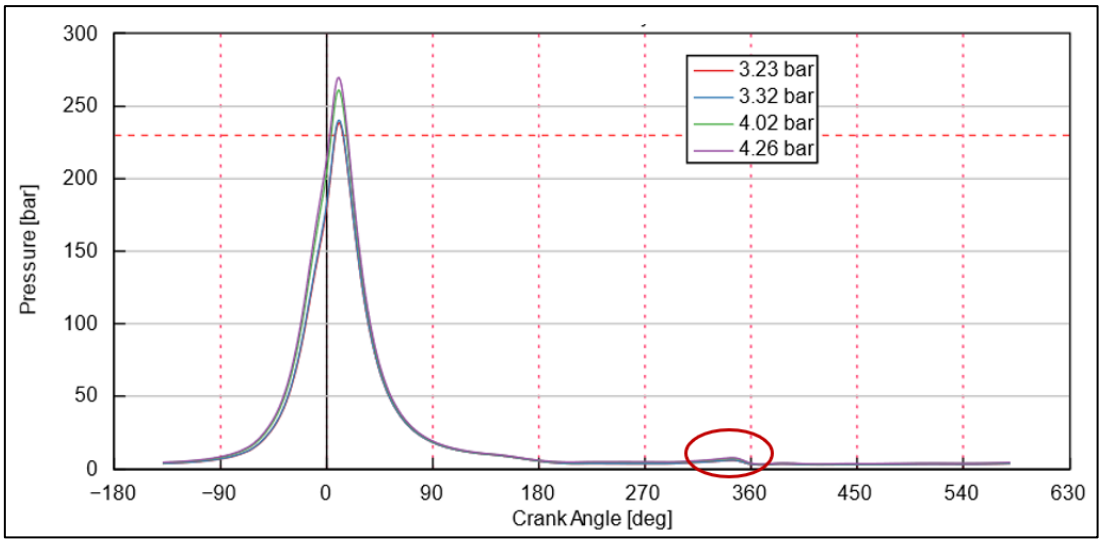

Figure 54 In-cylinder pressure curves for different exhaust back pressure simulations.

A prominent peak at 0° TDC during the power stroke reflects the combustion process, aligning with the expected high-pressure generation for efficient energy conversion. However, subtle but significant abnormal phenomena circled in red near 360° TDC during the exhaust stroke indicate a secondary pressure rise. The bump is likely associated with exhaust back pressure before the condenser. It demands closer examination where it has been noticed that the higher exhaust back pressure reflects the higher bump in the in-cylinder pressure curve. Its potential causes include valves overlap where residual exhaust gases re-entered the cylinder due to inadequate scavenging or flow restrictions within the exhaust system such as narrow passages.

Similarly, the in-cylinder temperature has been illustrated in Figure 55 where the graph illustrates the variation in in-cylinder temperature across the compression, power, exhaust, and intake stages for various exhaust pressures. The temperature peaks during the compression stroke at 0° TDC reflecting the combustion process with maximum values recorded at 2740.63 k, 2714.86 K, 2522.73 K, and 2466.24 K for the pressure before condenser of 3.23 bar, 3.23 bar, 4.02 bar, and 4.26 bar respectively.

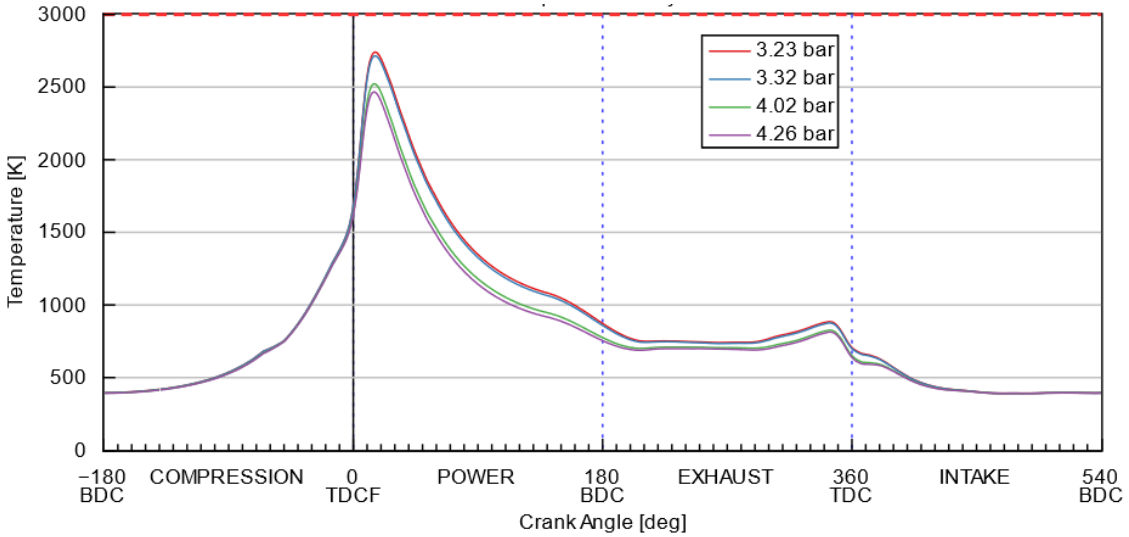

Figure 55 In-cylinder Temperature curves for different exhaust back pressure simulations.

Following the peak during the power stroke, the temperature gradually decreases, and the gases expand and transfer energy to the piston. In the exhaust stroke, the temperature remained elevated but declined further as exhaust gases exited the cylinder. There's a slight fluctuation near 360° TDC suggesting residual heat retention or potential impact from the exhaust backflow or valve overlap. Finally, during the intake stroke, the temperature drops significantly as a cooler working fluid-fuel mixture enters the cylinder stabilizing at its lowest point.

4.6.4 Discussion

Compression Raito

The investigation in the first sweep explores the performance characteristics of a W20 engine converted to a closed-loop HAPC which has been optimized at CR 12.3. The simulated data reveals that as the compression ratio decreases there is a corresponding decline in key performance parameters including boost pressure, indicated efficiency, maximum pressure, maximum temperature, and brake power.

The reduction of boost pressure with decreasing compression ratio can be attributed to changes in the volume at the top dead centre (TDC). The compression ratio is expressed

as, $\boldsymbol{CR} = \frac{\boldsymbol{V,BDC}}{\boldsymbol{V,TDC}}$, while the compression ratio decreases the volume at TDC increases. At higher CR, the volume at TDC decreases, requiring greater boost pressure to ensure sufficient mass is inducted for effective combustion. Conversely, at lower CR, the larger TDC volume accommodates the intake charge which reduces boost pressure. This lower boost requirement is further justified by the decrease in compression temperature and pressures, which lessens the demand for elevated boost pressure. Excessive boost at low CR increases pumping losses without significantly enhancing efficiency, as the inherently lower thermal efficiency at reduced CR limits the potential benefit of additional boost pressure.

The thermal efficiency equation stated in 2.1, shows that when the compression ratio increases the thermal efficiency improves because the engine converts more heat into work. At lower CR a larger fraction of heat energy is lost to the cylinder walls and less converted into useful work. The relationship between pressure volume and temperature during compression and combustion follows the ideal gas law which has been mentioned in the methodology section $\boldsymbol{PV} = \boldsymbol{nRT}$ and the adiabatic process law, $\boldsymbol{P2} = \boldsymbol{P1}(\frac{\boldsymbol{V1}}{\boldsymbol{V2}})^{\gamma}$, with lower compression ratio the volume ratio $\frac{\boldsymbol{V1}}{\boldsymbol{V2}}$ is reduced, leading to lower peak pressures and temperatures during combustion. In a lower compression ratio, the initial pressure and temperature at the start of the combustion is lower which results in a reduced rate of pressure rise and lower peak temperature because less energy is released in a smaller compressed volume.

Brake power is directly proportional to the indicated power and thermal efficiency. As CR decreases, efficiency and in-cylinder pressure diminish, resulting in lower brake power output. Previous studies suggest that maximum efficiency in APC is achieved at CR 7 to 9. However, this investigation identifies optimal efficiency for the W20 engine at CR 12.3 and 11.90, this discrepancy can be explained by several factors specific to the hydrogen argon mixture for this specific engine as this specific engine is optimized at 12.3 compression ratio. Moreover, the closed-loop configuration allows precise control over intake conditions, stabilizing combustion at a higher compression ratio. The

controlled environment reduces variability and optimizes performance-enhancing efficient operation at CR of 12.3 and CR 11.90. Furthermore, hydrogen's high flame speed ensures fast complete combustion. Its wide flammability range compliments argon's stabilizing effects enhancing overall engine performance at a high compression ratio as well.

Following this investigation, it can be concluded that the highest engine performance was observed at a compression ratio of 12.3 and CR 11.9, due to the specific thermodynamic properties of the hydrogen-argon mixture and optimized closed-loop configuration of the W20 engine. However, at CR 11.90, the engine demonstrated the targeted design specifications and achieved the desired performance outcomes, including the maximum in-cylinder pressure and temperature range of 230 bar and 3000 K, as well as the engine power output of 900KW for 75.2% load. These results fulfill the key requirements for the development of the HAPC. Therefore, a CR of 11.90 is an optimal choice for the further optimization of the HAPC in the W20 engine.

Effect of Exhaust Pressure

The results indicate higher back pressure forces the engine to expend more energy during the exhaust stroke to overcome resistance in the exhaust system leading to increased pumping losses. The losses directly reduce the IMEP and the net power output. Additionally, argon's high specific heat capacity exacerbates the problem by retaining more heat within the cylinder. This trapped heat reduces thermal gradients which are crucial for efficient combustion and lower exhaust temperatures indicating incomplete energy conversion. Moreover, the simulation result confirms a decline in indicated efficiency caused by slower frame propagation and incomplete combustion. Reducing oxygen availability coupled with argon's inert nature diminishes the reactivity of the mixture. Higher residual argon also reduces volumetric efficiency by occupying chamber space that could otherwise be filled with fresh reactants. This challenge particularly occurs in a closed-loop system where the working fluid is continuously recycled without the introduction of fresh air. Over time the accumulation of argon compounds the thermal load of the

engine while contributing nothing to energy release further reducing efficiency and performance.

The closed loop configuration introduces additional thermal and dynamic challenges which are observed by the in-cylinder pressure and temperature curve. Elevated back pressure can hinder complete exhaust gas expulsion, reducing volumetric efficiency, so increasing residual gas content and elevating cylinder temperatures which may adversely impact combustion quality. Addressing this issue may require refinement of valve timing exhaust system design or turbocharger operation. While the overall pressure profile appears consistent with typical engine cycles and shows increment this is the reason for boosting pressure increment as well.

From this discussion, it could be concluded that high exhaust back pressure reduces efficiency and power output which is against the targeted required engine design specification. Mitigation strategies should focus on minimizing back pressure and optimizing backflow to improve overall efficiency for that reason the baseline exhaust pressure which is 3.23 bar is suggested for the closed loop W20-HAPC engine which can be provided by turbocharger as found in the reference engine. Moreover, an exhaust back pressure of 3.32 bar could be another option but advanced exhaust design such as larger diameter pipes or multiple runners could reduce flow resistance through compromising efficiency. Variable valve timing (VVT) optimization could be implemented to optimize scavenging and limit the effect of residual gases, particularly under varying load and back pressure conditions. Another significant effect of back pressure was observed, showing that an increase in boost pressure can lead to a reduction in exhaust gas temperature. This result constitutes a key finding from the simulation and presents a valuable area for further investigation, particularly in optimizing exhaust gas management for improved engine performance.

4.7 Sweep 5: Effects of Impurities in Hydrogen Fuel on Engine Performance

4.7.1 Design of Experiments and results in continuing operation

This sub-section provides a comprehensive analysis of the final sweep, with a focused examination of the feasibility and implications of utilizing hydrogen impurities as a fuel source in the integration of industrial-grade hydrogen. The simulations performed in the previous tasks considered only pure hydrogen and oxygen are introduced in the system resulting in H_2O as a combustion product. In reality, small amounts of N_2, CO, CO_2, and other trace gases might be accommodated in the streams. These gases and the products of their oxidation will lead to a gradual reduction of the ratio of the specific heat and the mixture which reduces thermodynamic efficiency over time. An impurity steam will also come from the lubricating oil contributing to particulate formation. The design of the experimental inputs is captured in Table 17.

Table 17 The design of experiment inputs.

Reference load	75.25%
Reference mixture composition	90% Argon + 10% Oxygen
Injected fuel mass (mg/c)	300
Fuel composition	(H_2 -98% + N_2- 2%)
Combustion parameters	As in table 13 (75.25% Load)
Test condition	Simulation Time (min.)
CR	12.3

To analyse these effects in hydrogen as a fuel that is directly injected at low pressure into the combustion chamber in the formation of 98% hydrogen and 2% nitrogen impurities. Two methods were available for analysing these to comprehend the impact of impurities on this engine and the time-lapse or multiple cycle running of the model. For this analysis, the simulation has run over time differently to observe the difference of how impurities

in hydrogen fuel affect engine performance, and how quickly they cause a noticeable drop in efficiency.

Performance results

In Figure 56, the presented data illustrates the performance characteristics of the specific engine using pure hydrogen and its diluted mixture. The result reveals that pure hydrogen (which is denoted as 0 min) delivers the highest performance metrics including a net indicated mean effective pressure of 22.90 bar, net indicator divisions of 56%, and thermal efficiency of 57.78% while the peak temperature and pressure were 238.59 bar and 2740.36 K with the brake power of 902.70 kW and indicated power of 996.49 kW. When hydrogen is diluted the engine performance progressively declines.

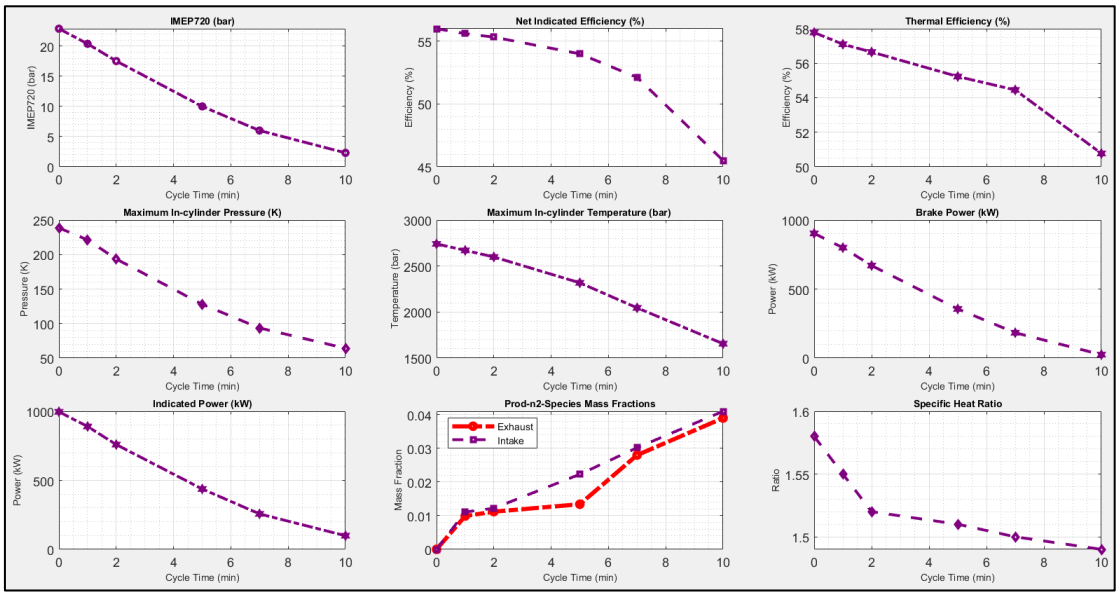

Figure 56 Engine performance vs. effect of impurities of hydrogen as fuel in the system.

For instance, after 10 minutes the IMEP decreases significantly to 2.31 bar with indeed indicated and thermal efficiency of 43.55% and 50.77% respectively. Similarly, maximum pressure and temperature drops to 59.42 bar and 1589.78 K. The dilution also reduces power output, brake power, and indicated power declining to 24.58 kW and 98.70 kW respectively. The highest fraction of nitrogen species (N_2) both exhaust and intake increase as the hydrogen is injecting in the cycles, so the impurities also increasing

according to time duration as well, reaching 0.039 and 0.041 respectively after 10 minutes, compared to zero for pure hydrogen. Note that for this six-cylinder engine, 500 cycles take one minute to complete, but in software it takes longer to run the simulation. Additionally, the specific heat ratio decreases from 1.58 to 1.48 for the time run, reflecting changes in the thermodynamic behaviour of the working fluid. It is also noticed that after 10 minutes the indicated efficiency of the engine and the fuel injection becomes zero.

4.7.2 Discussion

The simulation data presented indicates that impurities in hydrogen fuel have a significant impact on the thermodynamics properties of the fuel-mixture, leading to a noticeable degradation in engine performance. For instance, IMEP decreases after 10 minutes of operations when impurities accumulated in the hydrogen, particularly in the absence of a membrane separation system. Similarly, thermal efficiency declines, highlighting the negative effect of impurities on combustion effectiveness. This can be attributed to the buildup of impurities, which leads to a reduction in both the maximum in-cylinder pressure and temperature during combustion, ultimately affecting the overall combustion dynamics. Additionally, the specific heat ratio diminishes from 1.58 for pure hydrogen to 1.48 after prolonged exposure to impurities which reflect the nitrogen species in both intended exhaust streams increased reflecting the accumulation of non-reactive components that further dilute the reactive fuel mixture compromising combustion and energy release.

The engine's ability to operate continuously without intervention is also limited by impurity accumulation. The data illustrates a decline in engine performance after 10 minutes of operation, indicating the initial minimal impact of impurity buildup gradually intensified, eventually leading to a complete loss of performance. Moreover, engines operation with low impurity levels such as 2% may achieve longer duration but require higher boost pressure, a higher impurity level necessitates frequent intervention to prevent performance degradation. This highlights the need for strategies to extend

operating time by requiring mixture separators. Implementing a robust purification strategy is critical to mitigating the impact of impurities and maintaining engine performance. A combination of gas phase flash-off and in-cycle gas separator offers an effective solution. Gas phase flashes off removes the volatile impurities by heating the gas mixtures allowing non-combustible components to separate from the fuel (Senda et al., 2008). On the other hand, in-cycle gas separators continuously extract selective gases such as nitrogen and argon during the engine operation preventing their accumulation in the combustion chamber (Randolph et al., 2019). These methods ensure the fuel retains high purity enabling sustained efficiency and power output while minimizing engine wear and reducing maintenance requirements.

Finally, impurities in hydrogen fuel adversely affect both the thermodynamic properties and performance of the hydrogen-fuelled engine. They reduced the calorific value of the mixture of lower combustion temperatures and pressures and degraded engine power and efficiency. Without effective purification the engine's operating time becomes limited and performance declines significantly over time. Therefore, a feasible purification strategy as suggested combining gas phase flash-off and in-cycle gas separation is essential to ensure optimum engine performance efficiency and longevity by separating membrane. Such measures are critical and suggested for the reliable and sustainable use of hydrogen as a clean energy source for the W20 engine.

4.8 Summary of the Results

In summary, this thesis investigated the HAPC in a medium-speed W20 engine through 1D simulations, focusing on key parameters that influence engine performance. The analysis identified optimal mixture composition, the selection of inert gas as working fluid, the oxygen-to-fuel ratio, the effects of exhaust back pressure, and fuel impurities. A comprehensive summary of the thesis, alongside the effects of these key parameters on engine performance, derived from both simulations and the literature is presented in Table 18. The table classified their influence on performance using descriptors such as

"strong influence", "high influence", and "low or negative influence", providing a clear and structured overview of the results.

Table 18 Thesis Summary and Key Parameters Influence on Engine Performance Metrics

Parameter	***IMEP720***	***Indicated Efficiency***	***Thermal Efficiency***	***P_{max}***	***T_{max}***	***Brake Power***	***Indicated Power***	***EGT***
Engine Speed	↓	↓	↓	↓	↓	↑↑	↑	↓
Optimized Mixture of Noble Gases	↑↑	↑↑	↑↑	↑↑	↑↑	↑↑	↑↑	↑↑
Working Fluid	↑↑	↑↑	↑↑	↑↑	↑	↑	↑	↑
Oxygen-to-Fuel Ratio	↑	↑	↑	↑	↑↑	↑	↑	↑
Compression Ratio (CR)	↑↑	↑↑	↑↑	↑↑	↑	↑	↑	↑
Exhaust Back Pressure	↓	↓	↓	↓	↓	↓	↓	↓
Impurities in Hydrogen Fuel	↓	↓	↓	↓	↓	↓	↓	↓
Variable Valve Timings	↑	↑	↑	↑	↑	↑	↑	↑
Injection Timing	↑	↑	↑	↑	↑	↑	↑	↑
Fuel Injection Strategy	↑	↑	↑	↑	↑	↑	↑	↑
Recycling Ar & Separating H_2O	↑↑	↑↑	↑↑	↑	↑	↑	↑	↑
Start of Cycle	↑	↑	↑	↑	↑	↑	↑	↑
Condenser Efficiency	↑	↑	↑	↑	↑	↑	↑	↑
Coolant Temperature	↓	↓	↓	↓	↓	↓	↓	↓
Membrane Separation	↑	↑	↑	↑	↑	↑	↑	↑
Engine performance metrics Key: ↑↑ Strong influence, ↑ High influence, ↓ Low or negative influence								

5 Conclusions

5.1 Specific conclusions addressing individual research questions

To draw a conclusion, the investigation into the performance of the W20 engines adopted for the closed-loop GT-power model-based simulations of HAPC has provided valuable insights into optimizing combustion efficiency, engine performance, and operational sustainability. Each sweep explored specific design parameters, addressing the constraints of performance, thermal efficiency, and long-term durability while ensuring the feasibility of implementing the Nobel power cycle into this medium-speed engine.

In **RQ1,** the effect of gas mixture composition analysed for varying argon to oxygen ratios revealed a significant influence on inert gas composition on both combustion dynamics and engine efficiency. The mixture of 90% to 88% argon with 10% to 12% oxygen emerged as optimal and, striking balance between maintaining high thermal efficiency and preventing excessive thermal stress with the same engine configuration as the reference dual-fuel engine. Under this condition, the maximum in-cylinder pressure and temperature remained closer to borderline limits while maximizing combustion efficiency. Where in **RQ2**, it has been found that argon is the optimal inert gas for hydrogen combustion in the W20 engine, offering superior efficiency and combustion stability due to its high density, thermal insulation, and favourable specific heat ratio. Alternatives like helium, neon, and xenon face challenges such as less availability, higher thermal losses, low density, poor diffusivity, instability, or impractical operation requirements making argon the most effective and practical choice.

In **RQ3**, the influence of stoichiometric oxygen ratios analysed of varying Lambda values illuminated the trade-off between combustion intensity, fuel efficiency, and exhaust gas composition. The stoichiometric to slightly lean mixture provided the most favourable results achieving peak indicated efficiency while maintaining combustion completeness and minimizing the formation of undesirable by-products. Richer mixtures resulted in higher in-cylinder pressure but posed to risk of increased thermal stress and incomplete

combustion. These findings show the importance of adjusting the oxygen-to-fuel ratio based on engine loads to maintain optimal performance and fuel efficiency.

In **RQ4**, compression ratio and exhaust back pressure before condenser analysis has been conducted where it is found that higher composition ratio maximizes the thermal efficiency and power output. However, it is suggested to use a compression ratio of 11.9 or 12 which is attributed to the thermodynamic advantages inherent in the hydrogen argon mixture, including its specific heat ratio and stable combustion properties. On the other hand, increasing exhaust pressure was found to negatively affect scavenging efficiency, thereby increasing pumping losses and reducing the engine's net power output. However, it is found that high boost pressure reduces exhaust gas temperature. The optimal baseline exhaust back pressure was identified as 3.23 bar which can be effectively managed by a turbocharger. Furthermore, mitigation strategies such as variable valve timing (VVT) and exhaust system optimization is suggested to reduce the negative impact of exhaust pressure on engine performance.

In the last sweep at **RQ5** impurities in hydrogen as fuel were analysed where it was found that the presence of impurities in hydrogen fuel such as nitrogen or other particles significantly diminished combustion efficiency and power output. Impurities dilute the hydrogen content, reducing the calorific value of the fuel mixture, which leads to lower combustion temperatures and pressure. Overtime this accumulation of impurities in closed-loop results in declining engine performance, as evidenced by the reduction of indicated mean effective pressure and thermal efficiency after 10 minutes of operation. It has been also noticed that with slightly higher boost pressure the engine might operate a bit longer but effectively it has shown the same performance drop. To counter this a robust fuel purification strategy incorporating both gas phase flash-off and in-cylinder gas separation could be considered effectively to maintain fuel purity ensuring sustained engine performance and minimizing maintenance requirements.

In essence, the result of this study underscores the feasibility of employing the closed-loop hydrogen argon power cycle in the W20 engine, with certain design constraints. This demonstrates that the closed-loop HAPC offers a viable pathway toward achieving near zero exhaust emissions and high efficiency in a medium-speed engine thereby paving a way for future developments in clean engine technology.

5.2 Contribution to the Field of Research

The study contributes significantly to the advancement of the integrated hydrogen argon power cycle (iHAPC) in the context of medium-speed engines, particularly the W20 engines. It is systematically investigating the role of various factors throughout theory and simulation data the role of various factors, such as mixture composition, and various inert gas analyses to provide superior efficiency, compression ratios, Exhaust back pressure, and influence of impurities in hydrogen fuel. This is the primary and performance level-based simulation. Through this comprehensive analysis, the research provides detailed insights into the complex interplay between these parameters and their impact on combustion efficiency, power output, and emission. A key contribution is the identification of optimal operating conditions such as idle Lambda range for achieving balanced performance in the closed loop system. Moreover, the study highlights the thermal and dynamic challenges posed by exhaust back pressure and other parameters emphasizing the critical need for advanced design consideration in managing thermal load and scavenging efficiency with hardware utilization. This work lays a foundation for future experimental validation and further optimization for HAPC in pilot testing, fostering deeper understanding of these promising technologies in sustainable engine development.

5.3 Outlook

From a research perspective, further investigation into the thermodynamic properties of the hydrogen argon mixture under varying operational conditions is essential for deepening the understanding of the underlying mechanism governing combustion behaviour. A full cycle efficiency analysis is needed to figure out the required minimum efficiency

of the condenser, and turbocharger and how it affects engine efficiency. The effect of Miller timing for two stage turbochargers for gas exchange therefore excess energy outcome consumption should be analysed. Moreover, multi-parameter optimization of the HAPC, along with strategies to mitigate oil residues in the exhaust, requires thorough investigation. In addition to addressing knock phenomena, thermal stress analysis is crucial to understanding the underlying mechanism behind pre-ignition and autoignition. Furthermore, while this study provides foundational insights into the effect of fuel impurities, advanced research is essential to evaluate their impact on the combustion efficiency and performance degradation. Another crucial thing is injection timing, and it is recommended to optimize variable valve timing parameters in early or late IVC and late EVO/EVC to enhance engine performance and efficiency. Lastly, for this thesis, the imposed burn rate with a non-predictive combustion object has been used to do the system level analysis but for more advanced study predictive Wiebe combustion model is suggested with full cycle system analysis.

This finding of the study highlights strategic approaches to enhance the performance and durability of hydrogen-powered engines for industrial applications. Simulated data analysis underscores the importance of maintaining oxygen levels above 12% and managing exhaust pipe temperatures to avoid material degradation. The observed higher in-cylinder pressure and temperature of hydrogen fuelled engines compared to natural gas-based system suggests cylinder coatings and further material investigations are recommended to prevent in cylinder damage. Experimental setups, such as Rapid Compression Expansion Machines (RCEM) and optically accessible chambers, are essential for bridging theoretical insights and practical applications. Additionally, mitigating inert gas accumulation, such as argon, is critical to sustaining fuel reactivity and optimising combustion dynamics, especially in the presence of impurities in hydrogen as fuel. These strategies, coupled with academia-industry collaboration, are vital for ensuring the efficiency, reliability, and is capability of HAPC engine technology.

References

Ahlström, J. M. (2020). *RENEWABLE HYDROGEN PRODUCTION FROM BIOMASS 2 Renewable Hydrogen Production from Biomass*.

Ahmad, Z. (2022). *Experimental Studies on Fuel Effects in Dual-Fuel Combustion*.

Bich, E., Millat, J., & Vogel, E. (1990). The viscosity and thermal conductivity of pure monatomic gases from their normal boiling point up to 5000 K in the limit of zero density and at 0.101325 MPa. *Journal of Physical and Chemical Reference Data*, *19*(6), 1289–1305. https://doi.org/10.1063/1.555846

Bimmertips, T. (2021). *BMW DIRECT INJECTION VS. PORT INJECTION EXPLAINED*.

Bounaceur, R., Glaude, P. A., Sirjean, B., Fournet, R., Montagne, P., Vierling, M., & Moliere, M. (2016). Prediction of Auto-Ignition Temperatures and Delays for Gas Turbine Applications. *Journal of Engineering for Gas Turbines and Power*, *138*(2). https://doi.org/10.1115/1.4031264

Clements, R. M., & Smy, P. R. (1976). The variation of ionization with air/fuel ratio for a spark-ignition engine. *Journal of Applied Physics*, *47*(2), 505–509. https://doi.org/10.1063/1.322651

Dibble, R. W., Sierra Aznar, M., Timothy, B. S., & Jyh-Yuan, C. (2015). *RECIRCULATING NOBLE GAS INTERNAL COMBUSTION POWER CYCLE*.

Ding, W., Deng, J., Wang, C., Deng, R., Yang, H., Tang, Y., Ma, Z., & Li, L. (2023). Operating and Thermal Efficiency Boundary Expansion of Argon Power Cycle Hydrogen Engine. *Processes*, *11*(6). https://doi.org/10.3390/pr11061850

Dong, G., Du, Q., Li, L., Atkins, A., & Morgan, R. (2022). A high efficiency zero-emission argon split cycle engine. *International Journal of Engine Research*, *23*(5), 865–875. https://doi.org/10.1177/14680874221076098

Donohoe, N., Heufer, K. A., Aul, C. J., Petersen, E. L., Bourque, G., Gordon, R., & Curran, H. J. (2015). Influence of steam dilution on the ignition of hydrogen, syngas and natural gas blends at elevated pressures. *Combustion and Flame*, *162*(4), 1126–1135. https://doi.org/10.1016/j.combustflame.2014.10.005

Energy Agency. (2011). *World energy outlook 2011*. IEA, International Energy Agency : OECD.

Energy Agency, I. (2018). *World Energy Balances 2018*.

Energy Agency, I. (2024). *Net Zero by 2050 - A Roadmap for the Global Energy Sector*. www.iea.org/t&c/

Energy Information Administration (EIA). (2023). *IEO2023_Narrative*.

Falfari, S., Cazzoli, G., Mariani, V., & Bianchi, G. M. (2023). Hydrogen Application as a Fuel in Internal Combustion Engines. *Energies*, *16*(6). https://doi.org/10.3390/en16062545

Gamma Technologies. (2023). *Engine Performance Analysis Modeling*. www.gtisoft.com

Gamma Technologies. (2024a). *Engine Performance Application Manual GT-SUITE 2 Engine Performance Application Manual*.

Gamma Technologies. (2024b). *Flow Theory Manual GT-SUITE*.

Gamma Technologies. (2024c). *Gamma Technologies and GT-SUITE: Pioneering the Future of Simulation*.

Gamma Technologies. (2024d). *Mechanics Theory Manual GT-SUITE 2 Mechanics Theory Manual*.

Gracki, J. A., Flynn, G. P., & Ross, J. (1969). Viscosity of nitrogen, helium, hydrogen, and argon from -100 to 25°C up to 150-250 atm. *The Journal of Chemical Physics*, *51*(9), 3856–3863. https://doi.org/10.1063/1.1672602

Hamarashid, L. (2009). *GT-Power Modeling of a 6-Cylinder Natural Gas Engine and Investigation of the Possible Performance Improvements by Studying the Miller Cycle*.

Heywood, J. B. (1988). *Internal combustion engine fundamentals*.

Hodgson, M., Roy, S., Roskilly, A. P., & Smallbone, A. (2021a). The performance and efficiency of novel oxy-hydrogen-argon gas power cycles for zero emission power generation. *Energy Conversion and Management*, *244*. https://doi.org/10.1016/j.enconman.2021.114510

Hodgson, M., Roy, S., Roskilly, A. P., & Smallbone, A. (2021b). The performance and efficiency of novel oxy-hydrogen-argon gas power cycles for zero emission power generation. *Energy Conversion and Management*, *244*. https://doi.org/10.1016/j.enconman.2021.114510

Jan, S. M., Mohammed, A., Elkhazraji, A., Masurier, J. B., & Dibble, R. (2020). The Road Towards High Efficiency Argon SI Combustion in a CFR Engine: Cooling the Intake to Sub-Zero Temperatures. *SAE Technical Papers*, *2020-April*(April). https://doi.org/10.4271/2020-01-0550

Jin, S., Deng, J., Wang, C., Ding, W., Deng, R., Yang, H., & Li, L. (2023, April 11). Knock Inhibition in Hydrogen Fueled Argon Power Cycle Engine with a Higher Compression Ratio by Water Direct Injection at Late Exhaust Stroke. *SAE Technical Paper 2023-01-0227*. https://doi.org/10.4271/2023-01-0227

Jin, S., Deng, J., Xie, K., Liang, X., Wang, C., Ding, W., & Li, L. (2023). Knock control in hydrogen-fueled argon power cycle engine with higher compression ratio by water port injection. *Applied Energy*, *349*. https://doi.org/10.1016/j.apenergy.2023.121664

Jin, S., Huang, X., Deng, J., Gong, Y., Zhong, H., & Li, L. (2021). Initiation characteristics of spark-ignited premixed hydrogen-oxygen flames with diluents of argon/nitrogen/carbon dioxide. *International Journal of Hydrogen Energy*, *46*(40), 21212–21221. https://doi.org/10.1016/j.ijhydene.2021.03.234

Jin, S., Shu, B., He, X., Fernandes, R., & Li, L. (2021). A study on autoignition characteristics of H2-O2 mixtures with diluents of Ar/N2 in rapid compression machine for argon power cycle engines. *Fuel*, *303*. https://doi.org/10.1016/j.fuel.2021.121291

Killingsworth, N. J., Rapp, V. H., Flowers, D. L., Aceves, S. M., Chen, J. Y., & Dibble, R. (2011). Increased efficiency in SI engine with air replaced by oxygen in argon mixture. *Proceedings of the Combustion Institute*, *33*(2), 3141–3149. https://doi.org/10.1016/j.proci.2010.07.035

Kim, J., Scarcelli, R., Beardsell, G., Strickland, T., Nilsen, C., & Sierra Aznar, M. (2024, April 9). Modeling Pre-Chamber Assisted Efficient Combustion in an Argon Power Cycle Engine. *SAE Technical Papers*. https://doi.org/10.4271/2024-01-2690

Kim, N., Cho, S., & Min, K. (2015). A study on the combustion and emission characteristics of an SI engine under full load conditions with ethanol port injection and gasoline direct injection. *Fuel*, *158*, 725–732. https://doi.org/10.1016/j.fuel.2015.06.025

Kosarev, I. N., Starikovskaia, S. M., & Starikovskii, A. Y. (2007). The kinetics of autoignition of rich N2O-H2-O2-Ar mixtures at high temperatures. *Combustion and Flame*, *151*(1–2), 61–73. https://doi.org/10.1016/j.combustflame.2007.06.009

Kulkarni, D., Patil, A., Wagh, J., & Chougule, S. D. (2019). *Modelling of Internal Combustion Engine using GT Power*. www.ijert.org

Lee, D., Quarme Gbadago, D., Jo, Y., Hwang, G., Jo, Y., Smith, R., & Hwang, S. (2021). Integrating hydrogen liquefaction with steam methane reforming and CO2 liquefaction processes using techno-economic perspectives. *Energy Conversion and Management*, *245*. https://doi.org/10.1016/j.enconman.2021.114620

Li, L., Gong, Y., Deng, J., & Gong, X. (2018a). CO 2 Reduction Request and Future High-Efficiency Zero-Emission Argon Power Cycle Engine. *Automotive Innovation*, *1*(1), 43–53. https://doi.org/10.1007/s42154-018-0007-y

Li, L., Gong, Y., Deng, J., & Gong, X. (2018b). CO 2 Reduction Request and Future High-Efficiency Zero-Emission Argon Power Cycle Engine. *Automotive Innovation*, *1*(1), 43–53. https://doi.org/10.1007/s42154-018-0007-y

Li, W., Liu, Z., Wang, Z., & Dou, H. (2015). Experimental and theoretical analysis of effects of atomic, diatomic and polyatomic inert gases in air and EGR on mixture properties, combustion, thermal efficiency and NOx emissions of a pilot-ignited NG engine. *Energy Conversion and Management*, *105*, 1082–1095. https://doi.org/10.1016/j.enconman.2015.08.052

Luo, Q. H., & Sun, B. G. (2016). Effect of the Miller cycle on the performance of turbocharged hydrogen internal combustion engines. *Energy Conversion and Management*, *123*, 209–217. https://doi.org/10.1016/j.enconman.2016.06.039

Mansor, M. R. A., Nakagami, K., Kondo, Y., & Shioji, M. (2022). Study of heat loss mechanism in argon-circulated hydrogen engine combustion chamber wall surface conditions. *Energy Reports*, *8*, 815–826. https://doi.org/10.1016/j.egyr.2022.07.076

Margot, X., Quintero, P., Gomez-Soriano, J., & Escalona, J. (2021). Implementation of 1D–3D integrated model for thermal prediction in internal combustion engines. *Applied Thermal Engineering*, *194*. https://doi.org/10.1016/j.applthermaleng.2021.117034

Martinez, I. (2020). *FUEL PROPERTIES*.

Mat Taib, N., Abu Mansor, M. R., & Faizal Wan Mahmood, W. M. (2020). Simulation of hydrogen combustion in neon-oxygen compression ignition engine. *CFD Letters*, *12*(12), 1–16. https://doi.org/10.37934/cfdl.12.12.116

Mikulski, M. (2024). *Project Proposal: iHAPC-Integrated Hydrogen-Argon Power Cycle, Status : (University of Vaasa Internal Material, Confidential)*.

Mohammed, A. M. (2018). *A path towards high efficiency using Argon in an HCCI engine*.

Morovatiyan, M., Shahsavan, M., Aguilar, J., Baghirzade, M., & Mack, J. H. (2022). An Assessment of Hydrogen Addition to Methane Combustion with Argon as a Working Fluid in a Constant Volume Combustion Chamber. *Combustion Science and Technology*, *194*(12), 2395–2413. https://doi.org/10.1080/00102202.2020.1870454

Nabi, M. N., Rasul, M., & Gudimetla, P. (2019). Modelling and simulation of performance and combustion characteristics of diesel engine. *Energy Procedia*, *160*, 662–669. https://doi.org/10.1016/j.egypro.2019.02.219

Ngwaka, U., Wu, D., Happian-Smith, J., Jia, B., Smallbone, A., Diyoke, C., & Roskilly, A. P. (2021). Parametric analysis of a semi-closed-loop linear joule engine generator using argon and oxy-hydrogen combustion. *Energy*, *217*. https://doi.org/10.1016/j.energy.2020.119357

Peterson, J. N., Hahn, T. F., Comings, E. W., & -kiP, kci. (1971). Thermal Conductivity of Mixtures of Argon-Helium, Argon-Nitrogen, and Argon-Neon The variance of the estimate. In *AlChE Journal* (Vol. 17, Issue 2).

Pochari, C. (2019). *CLOSED CYCLE HYDROGEN ENGINE TECHNOLOGY*.

Pröll, T., Bolhàr-Nordenkampf, J., Kolbitsch, P., & Hofbauer, H. (2010). Syngas and a separate nitrogen/argon stream via chemical looping reforming - A 140 kW pilot plant study. *Fuel*, *89*(6), 1249–1256. https://doi.org/10.1016/j.fuel.2009.09.033

Randolph, E., Graham Conway, Jason Herrera, Terrence Alger, Nishant Thakral, & Christopher Chadwell. (2019). A Gas Separation Membrane Highly Selective to CO2 in the Exhaust of Internal Combustion Engines. *2019 JSAE/SAE Powertrains, Fuels and Lubricants*.

Rapp, V. H. (2011). *Investigation of Alternative Fuels and Advanced Engine Technology: Improving Engine Efficiency and Reducing Emissions*.

Renewable Energy Agency, I. (2019). *TRANSFORMING THE ENERGY SYSTEM-AND HOLDING THE LINE ON RISING GLOBAL TEMPERATURES 2*. www.irena.org

Saidu Arah, A., & Audu, R. (2020). *Internal Combustion Engines: Theory and Calculation*. https://www.researchgate.net/publication/366020563

Samimi-Abianeh, O., Piehl, J. A., Zyada, A., Al-Sadoon, M., & Bravo, L. (2019). Effect of Diluents on the Autoignition of Propane Mixtures Using a Rapid Compression Machine. *Energy and Fuels*, *33*(4), 3529–3538. https://doi.org/10.1021/acs.energyfuels.8b04100

Sánchez, A. L., & Williams, F. A. (2014). Recent advances in understanding of flammability characteristics of hydrogen. In *Progress in Energy and Combustion Science* (Vol. 41, Issue 1, pp. 1–55). Elsevier Ltd. https://doi.org/10.1016/j.pecs.2013.10.002

Senda, J., Wada, Y., Kawano, D., & Fujimoto, H. (2008). Improvement of combustion and emissions in diesel engines by means of enhanced mixture formation based on flash boiling of mixed fuel. *International Journal of Engine Research*, *9*(1), 15–27. https://doi.org/10.1243/14680874JER02007

Shahsavan, M., Morovatiyan, M., & Mack, J. H. (2018a). A computational investigation of non-premixed combustion of natural gas injected into mixture of argon and oxygen. *ASME 2018 Internal Combustion Engine Division Fall Technical Conference, ICEF 2018*, *1*. https://doi.org/10.1115/ICEF2018-9618

Shahsavan, M., Morovatiyan, M., & Mack, J. H. (2018b). A numerical investigation of hydrogen injection into noble gas working fluids. *International Journal of Hydrogen Energy*, *43*(29), 13575–13582. https://doi.org/10.1016/j.ijhydene.2018.05.040

Shahsavan, M., Morovatiyan, M., & Mack, J. H. (2018c). A numerical investigation of hydrogen injection into noble gas working fluids. *International Journal of Hydrogen Energy*, *43*(29), 13575–13582. https://doi.org/10.1016/j.ijhydene.2018.05.040

Shi, S., Tomomatsu, Y., Chaturvedi, B., Sierra Aznar, M., & Chen, J. Y. (2021). Engine efficiency enhancement and operation range extension by argon power cycle using natural gas. *Applied Energy*, *281*. https://doi.org/10.1016/j.apenergy.2020.116109

Sierra Aznar, M. (2018a). *Numerical and experimental investigation of the Argon Power Cycle for power generation efficiency improvement and emissions reduction*.

Sierra Aznar, M. (2018b). *Numerical and experimental investigation of the Argon Power Cycle for power generation efficiency improvement and emissions reduction*.

Stępień, Z. (2021). A comprehensive overview of hydrogen-fueled internal combustion engines: Achievements and future challenges. In *Energies* (Vol. 14, Issue 20). MDPI. https://doi.org/10.3390/en14206504

Tingting, L. (2022). *Using Simulation to Model Closed-Cycle Argon Hydrogen Engines*.

Van Den Brink, H. S. (2022a). *Where innovation starts Exploring injection strategies for the Argon Power Cycle in CONVERGE CFD Where innovation starts Exploring injection strategies for the Argon Power Cycle*. www.tue.nl

Van Den Brink, H. S. (2022b). *Where innovation starts Exploring injection strategies for the Argon Power Cycle in CONVERGE CFD Where innovation starts Exploring injection strategies for the Argon Power Cycle*. www.tue.nl

Van Oijen, J. A. (2019a). *Argon Power Cycle*.

Van Oijen, J. A. (2019b). *Argon Power Cycle*.

Wang, C., Deng, J., Ding, W., Tang, Y., Cui, W., Su, X., & Li, L. (2024). Efficiency and power enhancement strategies for methane direct injection argon power cycle engines. *Fuel*, *363*. https://doi.org/10.1016/j.fuel.2023.130808

Wang, C., Deng, J., Su, X., Cui, W., Tang, Y., & Li, L. (2023, October 31). Efficiency Enhancement and Lean Combustion Performance Improvement by Argon Power Cycle in a Methane Direct Injection Engine. *SAE Technical Paper*. https://doi.org/10.4271/2023-01-1618

Wang, C., Jin, S., Deng, J., Ding, W., Tang, Y., & Li, L. (2023a). *International Journal of Automotive Manufacturing and Materials Future High-Efficiency and Zero-Emission Argon Power Cycle Engines: A Review*. https://www.sciltp.com/journals/ijamm

Wang, C., Jin, S., Deng, J., Ding, W., Tang, Y., & Li, L. (2023b). *International Journal of Automotive Manufacturing and Materials Future High-Efficiency and Zero-Emission Argon Power Cycle Engines: A Review*. https://www.sciltp.com/journals/ijamm

Wang, C., Yue, Z., Zhao, Y., Ye, Y., Liu, X., & Liu, H. (2023). Numerical Simulation of the High-Boosting Influence on Mixing, Combustion and Emissions of High-Power-

Density Engine. *Journal of Thermal Science*, *32*(3), 933–946. https://doi.org/10.1007/s11630-023-1796-9

Wärtsilä. (2020). *Wärtsilä 20 Product Guide*.

Wu, Z., Yu, Y., Xie, W., Liu, Z., Li, L., & Deng, J. (2021). Optimization of the flame characteristics of H2–O2 coaxial injection applied to hydrogen-fueled argon cycle engines. *International Journal of Hydrogen Energy*, *46*(27), 14780–14789. https://doi.org/10.1016/j.ijhydene.2021.01.197

Xie, K., Deng, J., Jin, S., & Li, L. (2021). Numerical Study on Flammability Limit and Performance of Compression-Ignition Argon Power Cycle Engine with Fuel of Hydrogen. *SAE Technical Papers*, *2021*. https://doi.org/10.4271/2021-01-0391

Xinyu, L., Ales, S., Ho Lung, Y., & Evatt, H. (2020). *Comparison of hydrogen port injection and direct injection (DI) in a single-cylinder dual-fuel diesel engine*.

Zhang, E., Gong, Y., Deng, J., Hu, Z., Jiang, C., Wu, Z., & Li, L. (2017). Cyclic Variations of Argon Power Cycle Engine with Fuel of Hydrogen. *SAE Technical Papers*, *2017-October*. https://doi.org/10.4271/2017-01-2409

Zhang, Q., Zuo, Z., & Liu, J. (2013). Failure analysis of a diesel engine cylinder head based on finite element method. *Engineering Failure Analysis*, *34*, 51–58. https://doi.org/10.1016/j.engfailanal.2013.07.023

Appendices

Appendix 1. GT Suite Model Development Flow Chart

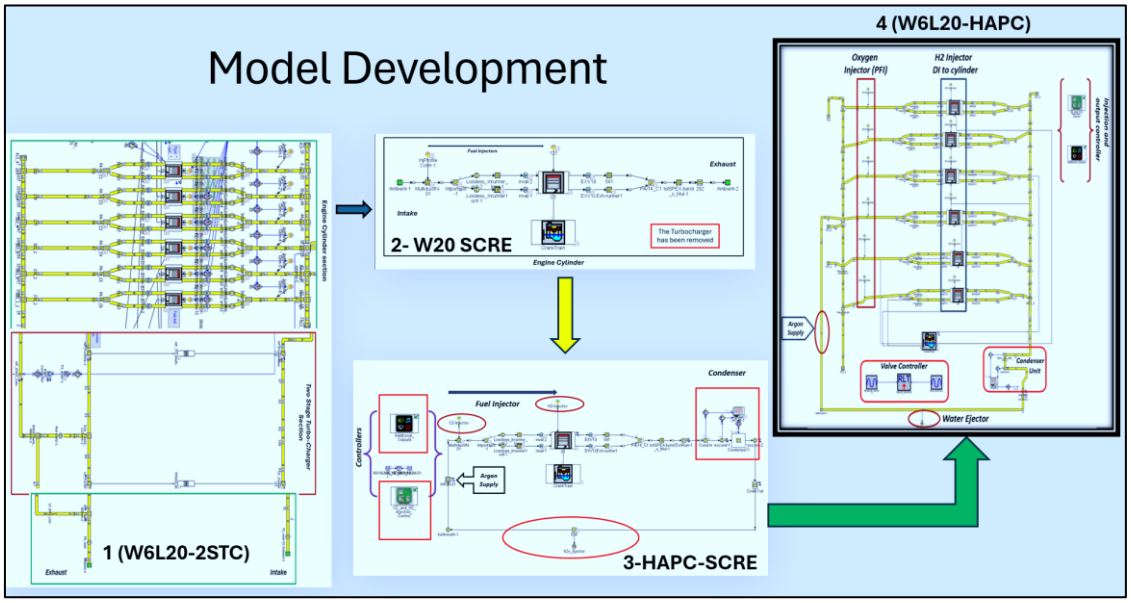

Appendix 2. An Overview of Simulation Dashboard